



ISBN: 978-90-393-6018-7

Printing: Flyeralarm.nl

Design: Gijs Briët and Wouter Karthaus

The research described in this thesis was performed at the Hubrecht Institute of the Royal Netherlands Academy of Arts and Sciences (KNAW), within the framework of the Graduate School of Cancer Genomics and Developmental Biology in Utrecht, The Netherlands

Financial support by the J.E. Jurriaanse stichting for the publication of this thesis is gratefully acknowledged

Financial support by PeproTech<sup>®</sup> is for the publication of this thesis is gratefully acknowledged

Copyright © by W.R.Karthaus. All rights reserved. No part of this book may be reproduced, stored in a retrieval system or transmitted in any form or by any means, without prior permission of the author.

# **Generation and exploitation of stem cell derived organoid cultures**

Ontwikkeling en toepassing van stamcel gederiveerde organoid culturen  
(met een samenvatting in het Nederlands)

Proefschrift

ter verkrijging van de graad doctor aan de Universiteit Utrecht op gezag aan de rector magnificus, prof.dr. G.J. van der Zwaan, ingevolge het besluit van het college voor promoties in het openbaar te verdedigen op donderdag 12 september 2013 des middags te 2.30 uur

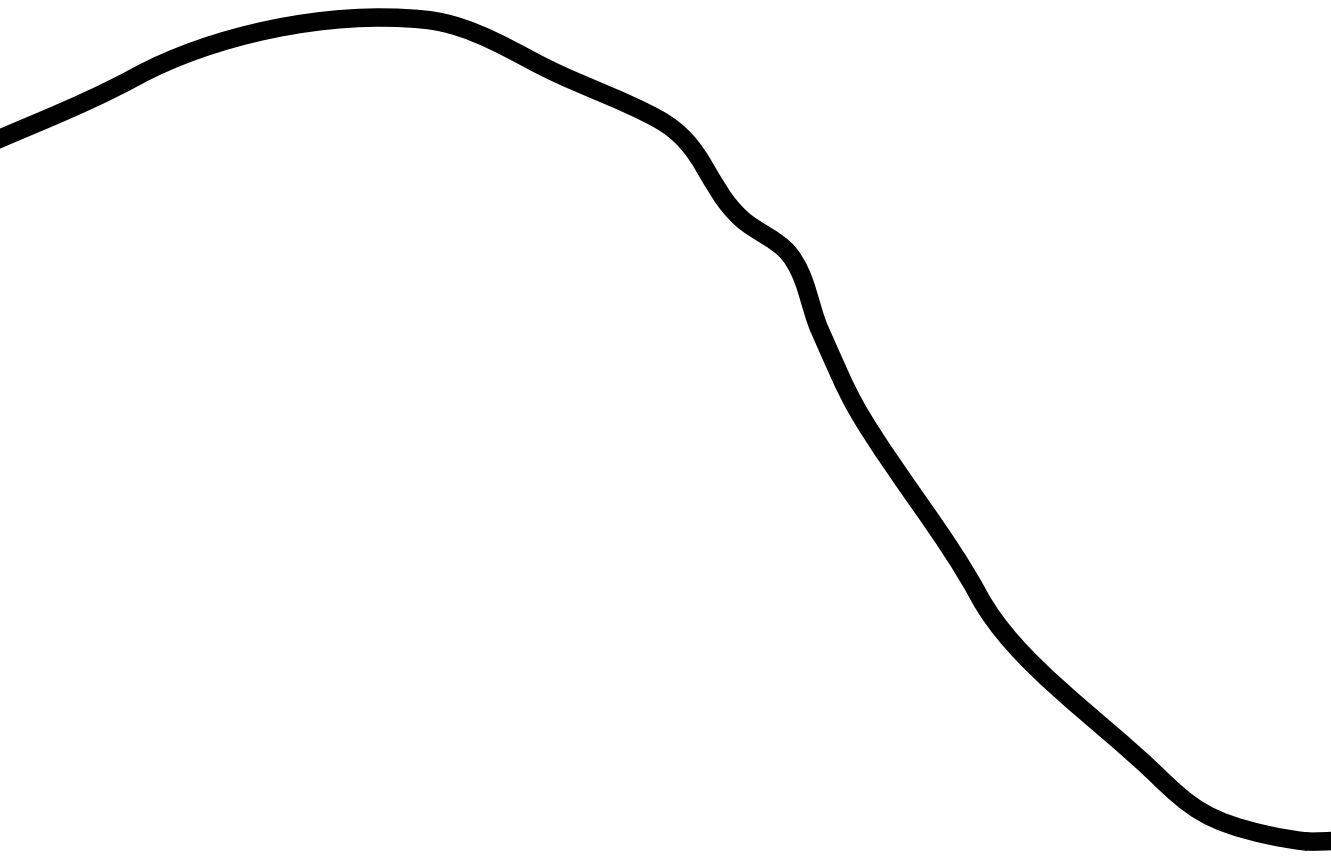
door

Wouter Richard Karthaus  
geboren 31 mei 1985 te Nijmegen

Promotor: Prof. dr. H.C. Clevers

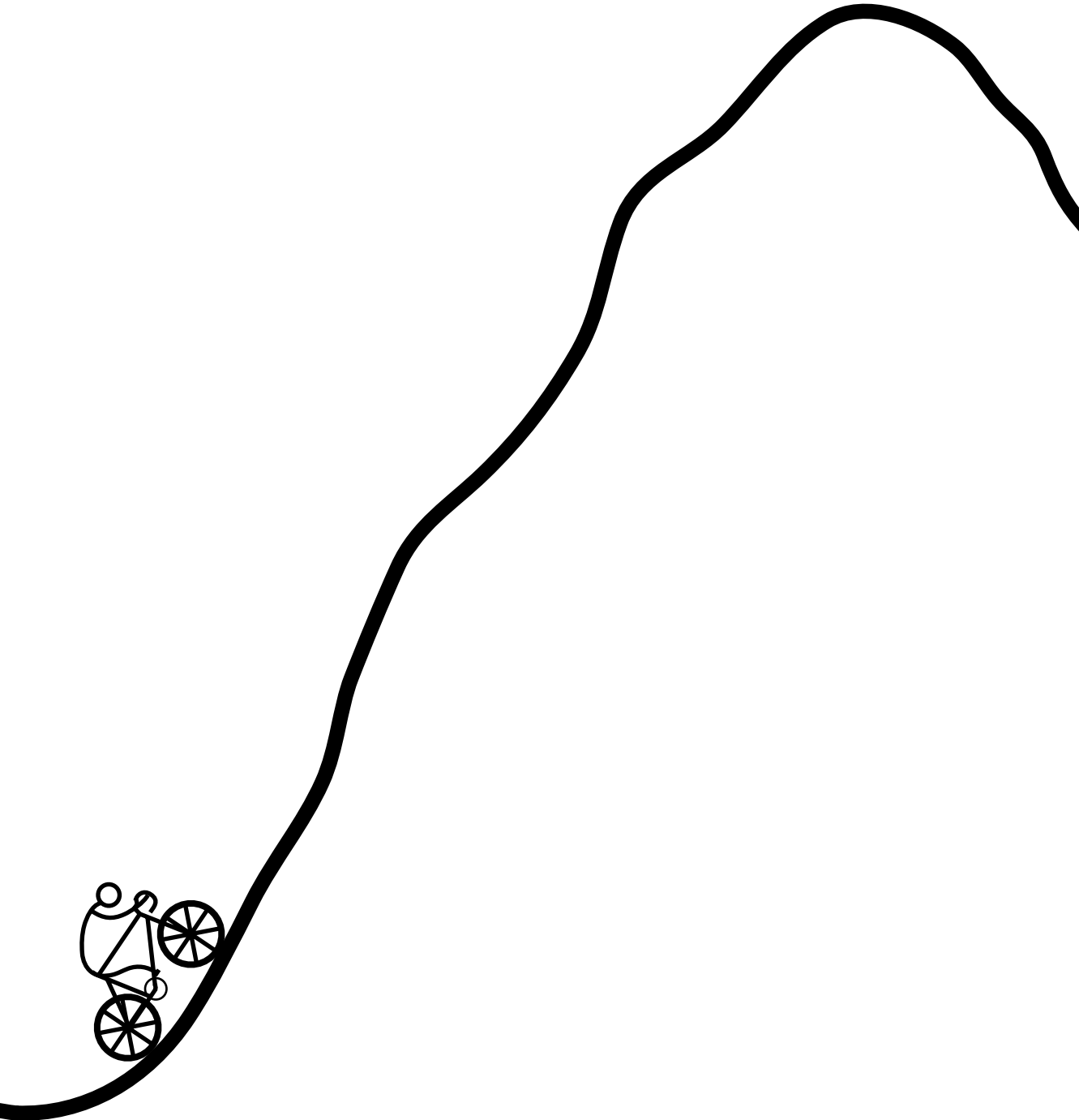
Contents:

<b>Chapter 1:</b>	LGR protein family members as stem cells markers	pg. 8
<b>Thesis outline</b>		pg.26
<b>Chapter 2:</b>	Generation and characterization of Nr2e3 eGFP/ CreERT2 reporter mice.	pg. 30
<b>Chapter 3:</b>	Role of the regenerating gene family in the intestine	pg. 44
<b>Chapter 4:</b>	Secretion of antimicrobial Paneth cell products is directly controlled by immune cell-derived Interferon- $\gamma$	pg. 54
<b>Chapter 5:</b>	A novel epithelial culture system reveals ligand-independent Androgen Receptor signaling in prostate	pg. 82
<b>Chapter 6:</b>	Tnfrsf19 marks luminal progenitor cells in the prostate	pg. 112
<b>Chapter 7:</b>	Summarizing discussion	pg. 128
<b>Addendum:</b>	Samenvatting	pg. 136
	Dankwoord	pg. 140
	Curriculum Vitae	pg. 142
	List of publications	pg. 143



# Chapter 1: LGR protein family members as stem cells markers

Wouter R. Karthaus and Hans C. Clevers



# LGR protein family members as stem cells markers

**Wouter R. Karthaus and Hans C. Clevers**

Hubrecht Institute, KNAW and University Medical Center Utrecht,  
Uppsalalaan 8, 3584 CT Utrecht, The Netherlands

**Adult stem cells drive homeostasis of self-renewing tissues and mediate tissue repair upon damage. It is believed that each organ contains one or more unique classes of stem cells. In this review, we describe the identification of Leucine-Rich G-protein coupled (LGR) receptor family members as molecular markers of adult stem cells. Using lineage tracing as a strategy, Lgr family members have been identified on novel stem cell types of the intestine, colon, stomach, liver and skin. We discuss the function of Lgr proteins in stem cell biology and the advances that have been made in understanding biology of Lgr stem cells after their original discovery.**

## Introduction

In 1908, the Russian histologist Aleksandr Maximow first used the term 'stem cell' in his Unitarian theory of hematopoiesis to describe the cell, which gives rise to all other blood cells. It is believed that tissue homeostasis and regeneration of all organs relies on dedicated, organ-specific stem cells. However, with the notable exception of the hematopoietic system, identifying stem cells and unraveling their characteristics has proven to be challenging.

The minimal definition of a stem cell is 1) a stem cell has the capacity to self-renew i.e. upon mitosis at least one of the daughter cells remains as a stem cell, and 2) a stem cell is multipotent i.e. it possesses the capacity to give rise to every cell type of the corresponding tissue. Other characteristics of stem cells are heavily debated, including the mode of mitosis and quiescence.

During mitosis, stem cells either divide symmetrically, i.e. both daughter cells are intrinsically equal to each other and their fates are stochastically determined post mitosis. Alternatively, stem cells divide asymmetrically, where a pre-mitotic decision of cell fate has been made either by cell intrinsic asymmetric distribution of stemness signals<sup>1</sup> or by extrinsic regulation in which during



mitosis one daughter cell is predetermined to be forced out of the stem cell niche<sup>2</sup>.

It is often assumed that stem cells are invariably quiescent, i.e. that stem cells divide infrequently. It is also generally believed that stem cells always divide asymmetrically, giving rise to one stem cell and one rapidly dividing transit-amplifying (TA) cell. The TA cell subsequently differentiates into the various specialized cell types. There is indeed good evidence for quiescent stem cell pools, for instance in the hair follicle<sup>3</sup> and the bone marrow. Additionally, quiescent and actively cycling stem cells may co-exist in the same tissue<sup>4</sup>. A special case of asymmetric stem cell division was postulated as the 'immortal strand hypothesis' by Cairns in 1975<sup>5</sup>. He hypothesized that stem cells would segregate their genome asymmetrically, retaining an "immortal strand" to protect genomic integrity, while distributing the newly synthesized DNA strands to the daughter cells. Although some stem cell populations are indeed found to be label-retaining because of asymmetric DNA strand segregation<sup>6</sup>, in other well-described stem cell systems such DNA label retention is not an intrinsic feature of stem cells<sup>7,8</sup>. Of note, post-mitotic differentiated cells also retain DNA labels, complicating data interpretation.

Several assays have been developed to identify stem cells. Isolation of cell populations using molecular markers like CD133, CD117, Nestin and/or CD34, followed by transplantation into immune-deficient animals or by analysis in cell culture, has been widely applied. However, in these experiments the stem cells as well as their natural environment, the niche, are manipulated significantly, complicating interpretation. The most powerful strategy for stem cell identification is to genetically label putative stem cells and visually follow their progeny over time *in vivo*, a strategy known as lineage tracing. The sole requirement for lineage tracing is a single molecular marker that allows specific marking of stem cells.

Using this lineage tracing strategy, two members of the leucine-rich repeat-containing G-protein-coupled receptor (Lgr) family have been identified as stem cell markers. Several recent studies have provided a theoretical underpinning for the stem cell-specificity of the Lgr molecules, as it turns out that the Lgr genes encode the receptors for Roof plate specific (R)-spondins, Wnt pathway agonists that are potent stem cell growth factors<sup>9-14</sup>.

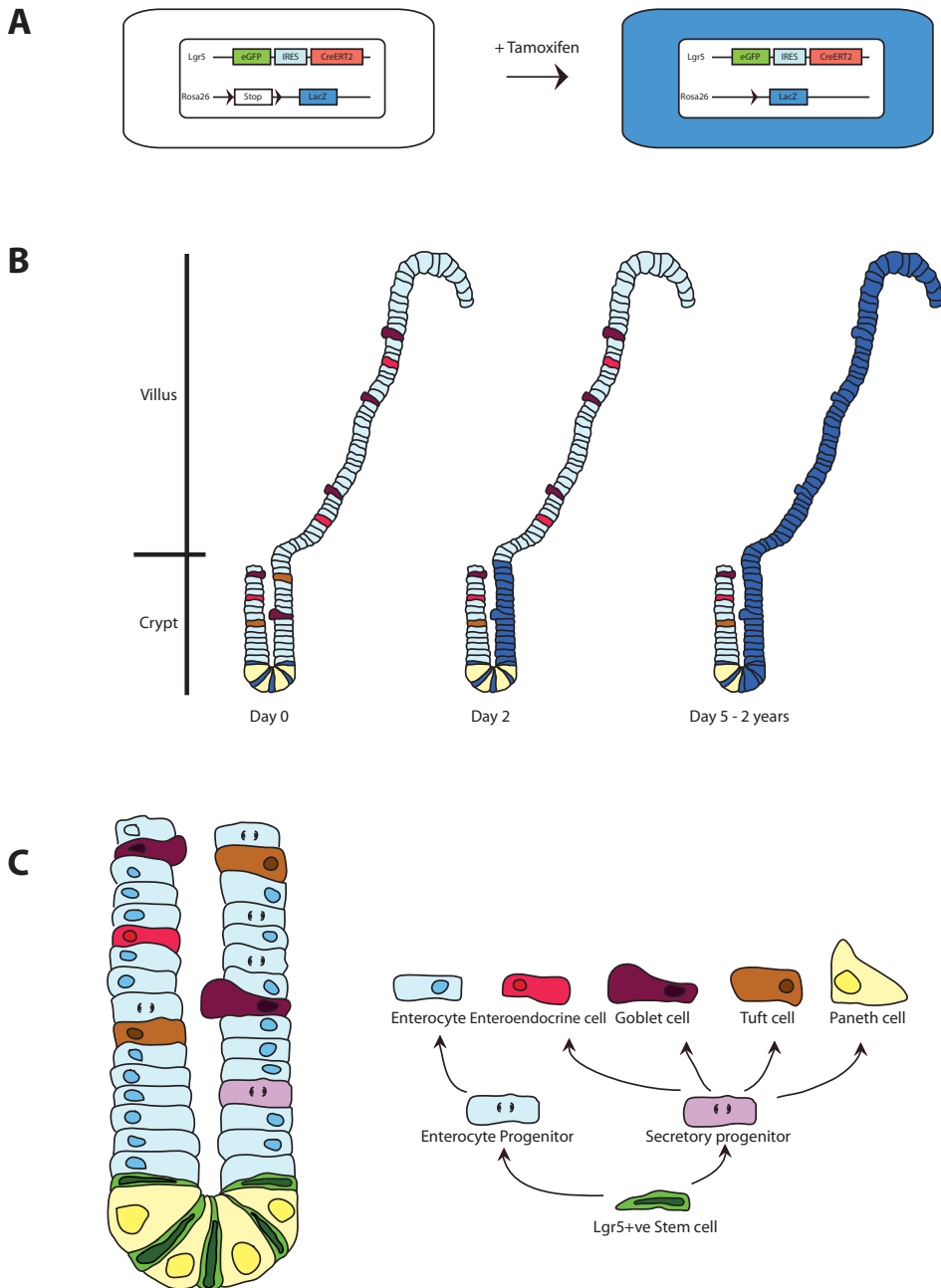


### Figure 1: Lgr5+ve stem cells give rise to all cells in the intestine.

A: Lineage tracing strategy from Lgr5+ve cells. eGFP and CreERT2 are specifically expressed in Lgr5+ve stem cells. Upon tamoxifen induction the CreERT2 is activated and the roadblock sequence is removed from the Rosa26 Cre reporter allele resulting the expressing of lacZ (Blue). B: At day 0 post injection (PI) single lacZ expressing Lgr5+ve stem cells are found in the crypt. Overtime lacZ expressing cells migrate towards the villus, forming a blue ribbon of lacZ expressing cells derived from Lgr5+ve stem cells. LacZ-labeled cells are found 2 years PI C: schematic overview of the lineage hierarchy and cell types generated by Lgr5+ve stem cells in the small intestine

## Identification of *Lgr5* as a stem cell marker in the small intestine & colon

The small intestinal epithelium is composed of numerous protrusions in the lumen named villi and small invaginations at the base of the villi termed the crypts of Lieberkühn (Figure 1b). Driven by rapid proliferation, the intestinal epithelium is completely renewed within 4-5 days<sup>15</sup>. All proliferation takes place in the crypts, where stem cells give rise to rapidly dividing TA cells. TA cells move up toward the villus domain where they eventually terminally differentiate. The rapid proliferation in the crypts is dependent on several signaling pathways, the most prominent being the canonical Wnt signaling pathway. Wnt signaling is activated upon binding of Wnt ligands to their Lrp5/6-Frizzled receptor complexes at the cell surface. Subsequently, Lrp5/6 is phosphorylated, and in turn the key regulated component of the pathway,  $\beta$ -catenin, is stabilized. The accumulated  $\beta$ -catenin translocates to the nucleus where it complexes with a member of the Tcf/Lef transcription factor family and subsequently activates transcription of Tcf target genes. (For an extensive review on Wnt signaling, readers are referred to Nusse and Clevers 2012 Cell). Hyperactivation of the Wnt Pathway (by loss of function mutations of the tumor suppressors *Apc* and *Axin2* or by activating point mutations in  *$\beta$ -catenin* that prevent its degradation) leads to the formation of adenomas in the intestine<sup>16-18</sup>. In the healthy adult gut, abrogating Wnt signaling by expressing the Wnt inhibitor Dickkopf1 or deletion of  *$\beta$ -catenin* or *Tcf4* leads to a complete stop in proliferation<sup>19-21</sup>. Thus, the Wnt pathway is essential for physiological self-renewal of the intestinal epithelium, while its inappropriate activation causes intestinal cancer.

By microarraying, the Wnt-driven target gene program in human colon cancer was determined and was found to closely resemble the normal gene program of proliferative crypt progenitor cells<sup>22</sup>. Further studies revealed that this Wnt signaling module consists of approximately 80 genes<sup>23</sup>, which can roughly be divided into 3 groups: genes expressed in post-mitotic Paneth cells; genes expressed in the proliferative TA compartment; and genes of which the expression is restricted to the crypt bottom in so called crypt base columnar cells (CBC cells). This cell type identified by Leblond and colleagues over 4 decades ago<sup>24</sup>. CBC cells are slender cells located at the base of the crypt and are intermingled with Paneth cells. One of the genes with restricted expression in CBC cells is *Lgr5/Gpr49*.

The *Lgr5* gene encodes a 7-transmembrane G-protein coupled receptor and has two close homologs, *Lgr4* and *Lgr6*. The closest relatives of the Lgr receptors in the large 7 transmembrane G-protein

coupled receptors are the thyroid-stimulating hormone (TSH) follicle-stimulating hormone (FSH) and luteinizing hormone (LH) receptors <sup>25,26</sup>.

To enable lineage tracing from Lgr5 positive (Lgr5+ve) cells, Barker and colleagues generated a mice where Green Fluorescent Protein (GFP) followed by an internal ribosomal entry site (IRES) and a tamoxifen inducible variant of the Cre recombinase enzyme (CreERT2) (Lgr5<sup>GFP-IRES-CreERT2</sup>) was knocked into the Lgr5 locus<sup>27</sup>. In mice harboring the Lgr5<sup>GFP-IRES-CreERT2</sup> allele, Lgr5-expressing (Lgr5+ve) cells are recognized by GFP expression. CreERT2 expression enables genetic labeling of Lgr5+ve cells when Lgr5<sup>GFP-IRES-CreERT2</sup> mice are crossed to mice harboring the Rosa26-LacZ reporter allele. In the Rosa26 allele, a transcriptional roadblock sequence flanked by loxP sites is followed by a lacZ coding sequence <sup>28</sup>. Upon tamoxifen injection in these compound mice, the CreERT2 protein is activated and Lgr5+ve cells are genetically marked by the expression of lacZ (Figure 1A). Cells expressing the lacZ reporter gene, i.e. Lgr5 progeny, can be stained blue, allowing lineage tracing (Figure 1B).

These mice showed that, in the small intestine and colon, Lgr5+ve cells are actively cycling and give rise to all different cell types: including Paneth cells, Goblet cells, Enteroendocrine cells, absorptive enterocytes <sup>27</sup>Tuft cells <sup>29</sup>and M cells <sup>30</sup>(figure 1C). Moreover, lineage tracing from Lgr5+ve cells was maintained for over 2 years, thus Lgr5 marks long-lived multipotent stem cells in the small intestine and the colon <sup>31</sup>. It has been reported by several groups that Lgr5+ve ISC randomly segregate their genome, and are not label-retaining <sup>32,33</sup>. Using the Confetti multicolor lineage tracing allele, Snippert and colleagues showed that Lgr5+ve ISC divide symmetrically and are subject to neutral drift i.e. cell fate is stochastically determined post-mitosis <sup>34,35</sup>.

Using a similar lineage tracing approach, *Bmi1*, *Hopx*, *mTERT*, and *Lrig* have been proposed to mark an alternative, quiescent stem cell population in the small intestine <sup>36-39</sup>, the +4 stem cell originally proposed by Chris Potten <sup>40</sup>. Cells marked by either of these markers show roughly the same kinetics of lineage tracing as Lgr5+ve cells. It is also shown for the markers Lrig and Hopx that the +4 and CBC stem cell populations are interconnected <sup>38,39</sup>. Detailed expression analysis of Lgr5+ve cells implies that these four proposed stem cell markers are robustly expressed in Lgr5+ve cells, suggesting that +4 cells and CBC cells may represent overlapping -if not identical- populations of stem cells <sup>41</sup>. In a mouse model generated by Tian and colleagues, expression of the diphtheria toxin receptor (DTR) is controlled by the Lgr5 promoter <sup>42</sup>. By feeding mice with diphtheria toxin (DT), all Lgr5-expressing stem cells were

killed, yet the crypts remained functional. The authors were able to initiate lineage tracing from *Bmi1* expressing (*Bmi1*+ve) cells in mice in which the *Lgr5*+ cells were killed. Upon DT withdrawal, *Lgr5*+ cells reappeared, and lineage tracing demonstrated that they were derived from *Bmi1*+ve cells, indicative of stem cell plasticity in the crypt.

Recently Buczacki and colleagues show that within the *Lgr5*+ve stem cells a label retaining quiescent population exists<sup>43</sup>. Under homeostatic conditions these cells differentiate into secretory lineage. However when the intestine is injured these label retaining can revert back to actively cycling state and give rise to all cell types. Showing that both actively cycling and quiescent stem cells reside in the crypt.

### **Paneth cells constitute part of the intestinal stem cell niche**

Paneth cells are mainly known for their antimicrobial function<sup>44</sup>, but also closely associate with CBC cells. Ablation of Paneth cells, either by deletion of *Gfi1*<sup>45</sup>, or *Sox9*<sup>46</sup> or expression of DTR under a Paneth cell specific promoter<sup>47</sup> leads to a significant decrease in stem cell number and proliferation<sup>48</sup>. In an in vitro 'mini-gut' culture system (described later in this review) *Lgr5*+ve cells are strongly dependent on Paneth cells<sup>48</sup>. Analysis of the Paneth cell transcriptome revealed expression of putative niche factors such as *Tgfa* and *Egf*, *Wnt3* and Notch ligands *Dll1* and *-4*, signals that also are key constituents of the 'mini-gut' culture system. Indeed, in vitro deletion of *Wnt3* from Paneth cells blocks the proliferation of the mini-gut stem cells<sup>49</sup>.

Notch signaling plays a crucial role in specialization and differentiation in the intestine. Inhibition of notch signaling drives all cells towards a secretory fate<sup>50</sup>, whereas deletion of the key target gene of Notch signaling, *Math1*/*Atoh1*, turns all cells to the opposite fate, the enterocyte. Indeed, mice lacking epithelial *Math1* have no Paneth cells. Surprisingly ISC in these mice proliferate normally<sup>51</sup>. This might be due to the fact that the loss of *Math1* makes stem cells refractory to the loss of Notch signaling<sup>52</sup>.

### ***Lgr5*+ve cells serve as cancer-initiating cells and cancer stem cells**

Stem cells are likely candidates for cancer-initiating cells (CIC). Deleting the tumor suppressor *Apc* specifically in *Lgr5*+ve ISC led to adenoma formation in the small intestine and colon within 3-5 weeks<sup>53</sup>. Deleting *Apc* in non-stem cells using another Cre protocol, did not lead to progressively growing adenomas. Transformed villus cells were lost in 4-5 days. Transformed crypt cells were capable of forming microadenomas but these did not progress.

Zhu and colleagues obtained similar results with another CBC specific Cre driver CD133<sup>54</sup>.

Despite the hyperactivation of the Wnt-pathway in all cells in APC-mutant adenomas, it has appeared that a cellular hierarchy is maintained. In adenomas in mouse small intestine, *Lgr5* expression is restricted to a small cell population at the base of the adenomas. These *Lgr5*<sup>+</sup> cells alternate with APC-mutant Paneth cells, much like the situation of a normal crypt. Multicolor lineage tracing within established adenomas revealed that *Lgr5*<sup>+</sup> cells were able to give rise to all cell types in the adenoma, implying that *Lgr5* marks cancer stem cells<sup>55</sup>. A similar anatomy has been observed in full-blown human colon cancers<sup>56</sup>.

### **Lgr5 marks other cell stem cell populations**

Following the discovery of *Lgr5* as an ISC marker, restricted populations of *Lgr5*<sup>+</sup> cells have been identified in other tissues where Wnt signaling is active. The murine pylorus, the caudal part of the stomach, is composed of glands. At the base of these glands, a restricted cell population was found that expresses *Lgr5*. Resembling *Lgr5*<sup>+</sup> ISC, pyloric *Lgr5*<sup>+</sup> cells are actively cycling and are capable of self-renewal and differentiating to all different cell types. Thus *Lgr5*<sup>+</sup> cells represent the stem cells of the pylorus of the stomach<sup>11</sup>.

Hair growth is mediated by Wnt-signaling<sup>57,58</sup>. *Lgr5* marks a restricted, actively cycling cell population in the hair follicle capable of generating hairs throughout life<sup>59</sup>. *Lgr5*<sup>+</sup> cells represent a subset of CD34 cells, a previously proposed stem cell marker. In a hair transplantation assay, sorted *Lgr5*<sup>+</sup> cells are transplanted to immunocompromised mice and can give rise to hairs. In this assay, *Lgr5*<sup>+</sup> cell outperformed CD34<sup>+</sup> cells. As for other *Lgr5*<sup>+</sup> stem cells, *Lgr5*<sup>+</sup> cells in the hair follicle are rapidly cycling, especially in anagen (the growth phase of hairs).

### **Lgr6, an Lgr5 relative, marks stem cells in the skin**

*Lgr6*, like *Lgr5*, is expressed in rare cell populations in various tissues. In the skin, *Lgr6* is expressed in the isthmus of the hair follicle. These cells are distinct from the *Lgr5*<sup>+</sup> cells of the hair follicle<sup>60</sup>. Lineage tracing initiated at e17.5 showed that *Lgr6* positive (*Lgr6*<sup>+</sup>) cells contribute to the sebaceous gland, epidermis and the hair. In adults, when lineage tracing was initiated before wounding, *Lgr6*<sup>+</sup> cells were able to contribute to newly generated

epidermis as well as newly formed hair follicles. Thus, Lgr6 marks a population of primitive stem cells in the skin.

### Function of Lgr receptors: Mouse Genetics

Using a mouse model in which a LacZ/placental alkaline phosphatase cassette is inserted in the Lgr4 locus, Van Schoore *et al.* found a broad expression pattern of Lgr4, with strong expression in the heart, kidneys, reproductive tracts, nervous system cells, cartilage and hair follicles<sup>61</sup>. Also, Lgr4 is expressed broadly in several proliferative compartments including the adult small intestinal crypt<sup>9,62</sup>. Thus, Lgr4 is not restricted to stem cell compartments.

Analysis of a Lgr4 knock out mouse model, in which LacZ was knocked in the Lgr4 locus, showed that only 40% of Lgr4-null mice are born. Several organs were growth-retarded in utero, including kidneys and liver, leading to prenatal death<sup>63</sup>. In a different genetic background (CD1) Lgr4-null mice were capable of surviving to adulthood. However, these mice displayed severe defects in the male reproductive tract.<sup>64</sup> These effects were ascribed to loss of Lgr4 regulation of cAMP-dependent estrogen receptor activity<sup>65</sup>. Lgr4-null mice also have severe defects in the anterior segment of the eye<sup>66</sup> and display abnormal definitive erythropoiesis<sup>67</sup> and a delay in osteoblast differentiation and mineralization<sup>68</sup>.

For a hypomorphic allele generated by Hoshii *et al.*<sup>69</sup>, Lgr4 mRNA levels are approximately 10% of normal. 60% of these mice develop to adulthood. Defects similar to the Lgr4-null mice were found in the male reproductive tract. Furthermore, hypomorphic embryos develop a gall bladder bud, but from mid gestation are unable to develop a gall bladder or cystic duct. No effects on pancreas or liver were observed in these mice.

Nishimori and colleagues created an inducible allele of Lgr4, which enables deletion of the exon encoding the 7TM domain<sup>70</sup>. Embryonic deletion of Lgr4 by crossing to mice ubiquitously expressing Cre, leads to embryonic/perinatal lethality. Lgr4-null mice showed renal hypoplasia with a notable decrease in numbers of glomeruli. Also, these mice are born with open eyes, possibly a result of decreased keratinocyte motility. This hypothesis was later confirmed using a skin-specific Cre line (Keratin5 Cre)<sup>71</sup>. Taken together, Lgr4 plays a pleiotropic role in the development of various tissues.

Little was known about Lgr5 before its discovery as a stem cell marker. Lgr5 is a Wnt target<sup>22</sup> and is upregulated in tumors of the colon, ovary and liver, which often have mutations in the Wnt pathway<sup>72-74</sup>.

Morita *et al.* generated an Lgr5-null allele via insertion of a lacZ reporter allele N-terminal of the transmembrane domain <sup>75</sup>. Homozygous disruption of Lgr5 results in neonatal lethality. Lgr5-null mice suffer from a condition named ankyloglossia i.e. a fusion of the tongue to the floor of the oral cavity in newborns, which results in ingestion of air at birth, dilation of the gastrointestinal tract and absence of milk in the stomach. Interestingly, accelerated Paneth cell maturation has been observed in the developing intestine of these Lgr5 null embryos <sup>76</sup>.

In the adult intestine deletion of Lgr4 leads to a 50% decrease in proliferation in the crypts, moreover in these mice differentiation towards Paneth cell lineage was strongly decreased <sup>62</sup>. In recent studies, the role of Lgr5 in adults has been addressed using a floxed allele. Deletion of Lgr5 in the small intestinal epithelium using a specific Cre did not yield on obvious phenotype. Combined deletion of Lgr4 and -5 aggravated the proliferation phenotype observed in Lgr4 knock out mice process, leading to complete loss of proliferative crypts and death of the animal <sup>9</sup>. Lgr6 knockout mice are viable and do not have any notable developmental defects <sup>60</sup>.

### **Function of Lgr Receptors: Molecular function**

Lgr4, -5 and -6 are part of a large family of 7 transmembrane G-protein coupled receptors and are closely related to TSH-, FSH- and LH- receptors <sup>26</sup>. The ectodomains of Lgr receptors consist of multiple leucine-rich repeats that are flanked by cysteine-rich regions on the C-terminal side. The protein sequence connecting the ectodomain to the first transmembrane domain is highly conserved suggesting a functional role <sup>77</sup>. The ligands and the downstream signaling pathway of Lgr4, 5 and 6 were unknown until recently. G-protein coupled receptors often signal through cAMP and/or calcium pathways.

In humans, the R-spondin family consists of 4 paralogs. All members contain a leader peptide, two cysteine-rich furin-like domains and a thrombospondin type 1 domain (More extensively reviewed by de Lau & Clevers <sup>78</sup>). In *Xenopus*, R-spondins act as activators of canonical Wnt signaling and play a pivotal role in Wnt-dependent myogenesis <sup>79</sup>. Indeed, all members of the R-spondin family synergize with secreted Wnts to increase downstream signaling <sup>80,81</sup>. Transgenic overexpression of human R-spondin1 led to hyper proliferation of the intestinal epithelium. Similar results were obtained with systemic administration of R-spondin <sup>10</sup>.

Several independent studies reported that the Lgr receptors bind to members



of the Roof plate specific Spondins (R-spondin) family and synergize with the Wnt pathway receptors (Figure 2). By immunoprecipitating a tagged version of Lgr4 and Lgr5 from stably expressing cells, de Lau and colleagues showed that Lgr4 and Lgr5 are associated with the Lrp5/6-Frizzled complex, the membrane receptors for Wnt ligands. Next, by immunoprecipitating a tagged version of human R-spondin1 bound to HEK293 cells followed by mass-spectrometry of associated membrane proteins, it was shown that Lgr receptors bind R-spondin. Close relatives Lgr1, Lgr7 and Lgr8 were also tested and found to not interact with R-spondin. Using a TOPFLASH Wnt reporter assay, it was shown that Wnt3a and R-Spondin/Lgr synergize in activating the Wnt-pathway, confirming the interaction. Similar results were found by Carmon and colleagues and<sup>82</sup> later by Niehrs and colleagues<sup>83</sup>.

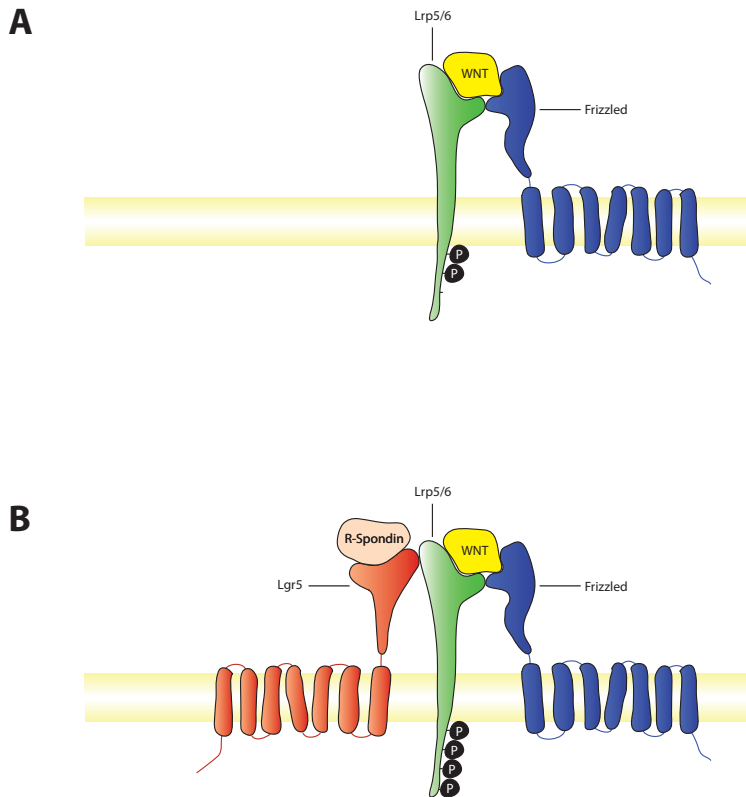


### Figure 2: Lgr5 receptor associates with a Lrp-Frizzled complex.

A model for the interaction between Lgr5 and Frizzled-Lrp proteins that synergizes downstream Wnt activation. Wnt ligands bind to a Frizzled-Lrp5/6 protein complex on the cell membrane, activating downstream Wnt signaling. Upon binding of R-spondin by Lgr5, an interaction is established between the Lgr5-R-spondin complex and the Wnt-Frizzled-Lrp complex, boosting downstream signaling.

## Organoids: Promise for regenerative medicine

Lgr5+ve cells can be isolated on the basis of GFP expression using FACS sorting. Single sorted Lgr5+ve cells of the intestine are capable of forming mini-guts or organoids in a matrigel-based 3-Dimensional culture system. Organoids can grow indefinitely in serum-free defined medium containing Epidermal Growth Factor (EGF), the Bmp inhibitor Noggin and R-spondin sato<sup>14</sup>. Small intestinal organoids are composed of small buds, which represent proliferative crypt compartments, and flank a central lumen, which is lined by a differentiated villus compartment. In SI organoids, all cell types are present and the epithelial cells are properly polarized and can fully differentiate. The organization in the crypt structures resembles the *in vivo* situation, Lgr5+ve cells are wedged between Paneth cells and a rapidly proliferating TA-compartment fills the remainder of these buds (Figure 3A).

Based on this discovery, culture conditions have been developed for murine colon, liver and stomach<sup>11-13</sup>. Also epithelium of human small intestine and colon can be cultured in a similar fashion with the addition of nicotinamide, Prostaglandin E2, Wnt3a, Alk4/5/7 inhibitor (a83-01) and a p38 inhibitor (SB202190)<sup>13</sup>.

In an effort to apply these cultures to regenerative medicine, murine colonic organoids, derived from a single Lgr5+ve cell, were transplanted into immunocompromised mice (Rag2-null) in which the colonic epithelium was damaged by dextran sodium sulphate<sup>84</sup>. The clonal colon organoids were capable of engraftment and aided in the regeneration of the damaged colon (Figure 3B). 25 weeks post engraftment cells were still contributing to the epithelial layer and showed no signs of (adenomatous) change.

## Discussion

Intensive study of the Wnt signaling pathway has led to the identification of Lgr5 and its family members as stem cell markers. Using the Lgr family as tools, several novel stem cell populations have been identified and new insights into stem cell biology have been obtained. Most notably, stem cells can be proliferative throughout life, they do not have to divide asymmetrically or retain DNA labels, and they can be readily expanded *in vitro* while remaining fully functional.

The recently uncovered molecular function of the Lgr receptors can be exploited for regenerative medicine purposes. Indeed, with development of the organoid culture system and the successful transplantation of colonic

organoids cultures, the first exciting steps have been made towards a regenerative medicine-based application of these insights. In all, Lgr family members play a central role in the biology of multiple adult stem cells. The developed tools and technology are expected to lead to novel insights in stem cell biology and to clinical applications.

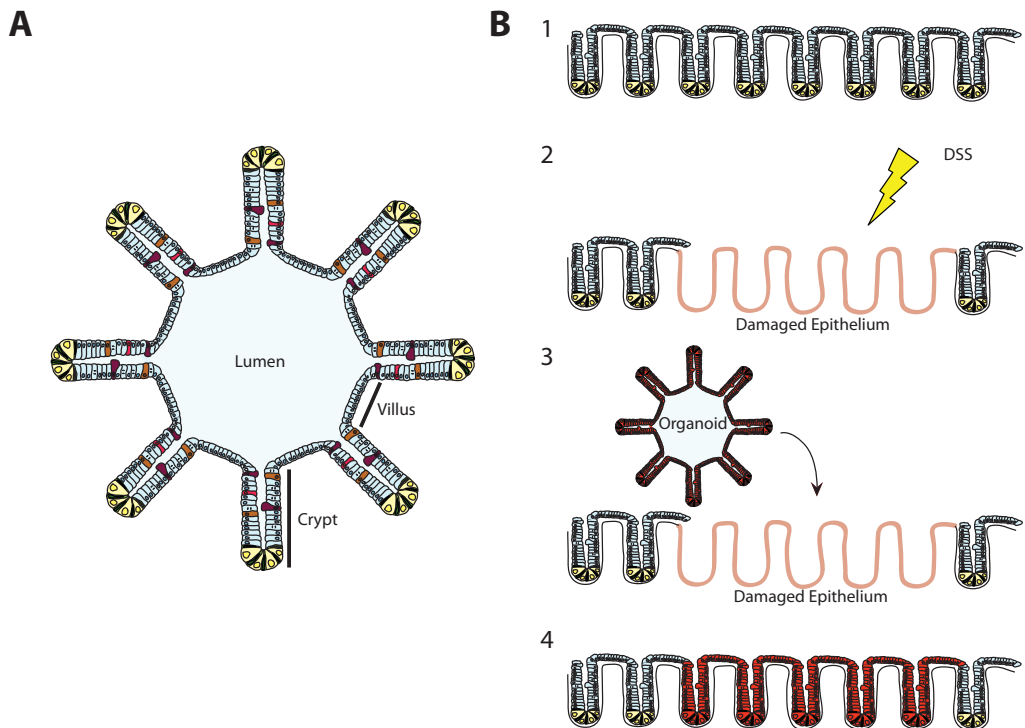


### Figure 3: Organoids functionally engraft in vivo.

A: Schematic view of a small intestinal organoid showing distinct crypt and villus regions and containing all celltypes found in vivo. B: Schematic overview of organoid engraftment in DSS injured tissue. 1) Healthy epithelium, 2) DSS treatment damages the epithelial integrity, leaving holes in the epithelium 3) Organoids migrate towards the damage site and 4) engraft in the holes, restoring the epithelial function and contribute over a prolonged period of time to the epithelium

## References:

- 1 Neumüller, R. & Knoblich, J. Dividing cellular asymmetry: asymmetric cell division and its implications for stem cells and cancer. *Genes & development* **23**, 2675-2699, doi:10.1101/gad.1850809 (2009).
- 2 Fuller, M. & Spradling, A. Male and female Drosophila germline stem cells: two versions of immortality. *Science (New York, N.Y.)* **316**, 402-404, doi:10.1126/science.1140861 (2007).
- 3 Tumber, T. *et al.* Defining the epithelial stem cell niche in skin. *Science (New York, N.Y.)* **303**, 359-363, doi:10.1126/science.1092436 (2004).
- 4 Li, L. & Clevers, H. Coexistence of quiescent and active adult stem cells in mammals. *Science (New York, N.Y.)* **327**, 542-545, doi:10.1126/science.1180794 (2010).
- 5 Cairns, J. Mutation selection and the natural history of cancer. *Nature* **255**, 197-200 (1975).
- 6 Shinin, V., Gayraud-Morel, B., Gomès, D. & Tajbakhsh, S. Asymmetric division and cosegregation of template DNA strands in adult muscle satellite cells. *Nature cell biology* **8**, 677-687, doi:10.1038/ncb1425 (2006).
- 7 Kiel, M. *et al.* Haematopoietic stem cells do not asymmetrically segregate chromosomes or retain BrdU. *Nature* **449**, 238-242, doi:10.1038/nature06115 (2007).
- 8 Waghmare, S. *et al.* Quantitative proliferation dynamics and random chromosome segregation of hair follicle stem cells. *The EMBO journal* **27**, 1309-1320, doi:10.1038/emboj.2008.72 (2008).
- 9 de Lau, W. *et al.* Lgr5 homologues associate with Wnt receptors and mediate R-spondin signalling. *Nature* **476**, 293-297, doi:10.1038/nature10337 (2011).
- 10 Kim, K.-A. *et al.* Mitogenic influence of human R-spondin1 on the intestinal epithelium. *Science (New York, N.Y.)* **309**, 1256-1259, doi:10.1126/science.1112521 (2005).
- 11 Barker, N. *et al.* Lgr5(+ve) stem cells drive self-renewal in the stomach and build long-lived gastric units in vitro. *Cell stem cell* **6**, 25-36, doi:10.1016/j.stem.2009.11.013 (2010).
- 12 Huch, M. *et al.* In vitro expansion of single Lgr5+ liver stem cells induced by Wnt-driven regeneration. *Nature* **494**, 247-250, doi:10.1038/nature11826 (2013).
- 13 Sato, T. *et al.* Long-term expansion of epithelial organoids from human colon, adenoma, adenocarcinoma, and Barrett's epithelium. *Gastroenterology* **141**, 1762-1772, doi:10.1053/j.gastro.2011.07.050 (2011).
- 14 Sato, T. *et al.* Single Lgr5 stem cells build crypt-villus structures in vitro without a mesenchymal niche. *Nature* **459**, 262-265, doi:10.1038/nature07935 (2009).
- 15 Cheng, H. & Leblond, C. Origin, differentiation and renewal of the four main epithelial cell types in the mouse small intestine. V. Unitarian Theory of the origin of the four epithelial cell types. *The American journal of anatomy* **141**, 537-561, doi:10.1002/aja.1001410407 (1974).
- 16 Korinek, V. *et al.* Constitutive transcriptional activation by a beta-catenin-Tcf complex in APC-/- colon carcinoma. *Science (New York, N.Y.)* **275**, 1784-1787 (1997).
- 17 Morin, P. *et al.* Activation of beta-catenin-Tcf signaling in colon cancer by mutations in beta-catenin or APC. *Science (New York, N.Y.)* **275**, 1787-1790 (1997).
- 18 Liu, W. *et al.* Mutations in AXIN2 cause colorectal cancer with defective mismatch repair by activating beta-catenin/TCF signalling. *Nature genetics* **26**, 146-147, doi:10.1038/79859 (2000).
- 19 Pinto, D., Gregorieff, A., Begthel, H. & Clevers, H. Canonical Wnt signals are essential for homeostasis of the intestinal epithelium. *Genes & development* **17**, 1709-1713,

- doi:10.1101/gad.267103 (2003).
- 20 van Es, J. *et al.* A critical role for the Wnt effector Tcf4 in adult intestinal homeostatic self-renewal. *Molecular and cellular biology* **32**, 1918-1927, doi:10.1128/MCB.06288-11 (2012).
- 21 Ireland, H. *et al.* Inducible Cre-mediated control of gene expression in the murine gastrointestinal tract: effect of loss of beta-catenin. *Gastroenterology* **126**, 1236-1246, doi:10.1053/j.gastro.2004.03.020 (2004).
- 22 van de Wetering, M. *et al.* The beta-catenin/TCF-4 complex imposes a crypt progenitor phenotype on colorectal cancer cells. *Cell* **111**, 241-250 (2002).
- 23 Van der Flier, L. *et al.* The Intestinal Wnt/TCF Signature. *Gastroenterology* **132**, 628-632, doi:10.1053/j.gastro.2006.08.039 (2007).
- 24 Cheng, H. & Leblond, C. Origin, differentiation and renewal of the four main epithelial cell types in the mouse small intestine. I. Columnar cell. *The American journal of anatomy* **141**, 461-479, doi:10.1002/aja.1001410403 (1974).
- 25 Hsu, S. *et al.* The three subfamilies of leucine-rich repeat-containing G protein-coupled receptors (LGR): identification of LGR6 and LGR7 and the signaling mechanism for LGR7. *Molecular endocrinology (Baltimore, Md.)* **14**, 1257-1271, doi:10.1210/me.14.8.1257 (2000).
- 26 Hsu, S., Liang, S. & Hsueh, A. Characterization of two LGR genes homologous to gonadotropin and thyrotropin receptors with extracellular leucine-rich repeats and a G protein-coupled, seven-transmembrane region. *Molecular endocrinology (Baltimore, Md.)* **12**, 1830-1845, doi:10.1210/me.12.12.1830 (1998).
- 27 Barker, N. *et al.* Identification of stem cells in small intestine and colon by marker gene Lgr5. *Nature* **449**, 1003-1007, doi:10.1038/nature06196 (2007).
- 28 Soriano, P. Generalized lacZ expression with the ROSA26 Cre reporter strain. *Nature genetics* **21**, 70-71, doi:10.1038/5007 (1999).
- 29 Gerbe, F. *et al.* Distinct ATOH1 and Neurog3 requirements define tuft cells as a new secretory cell type in the intestinal epithelium. *The Journal of cell biology* **192**, 767-780, doi:10.1083/jcb.201010127 (2011).
- 30 de Lau, W. *et al.* Peyer's patch M cells derived from Lgr5(+) stem cells require SpiB and are induced by RankL in cultured "miniguts". *Molecular and cellular biology* **32**, 3639-3647, doi:10.1128/MCB.00434-12 (2012).
- 31 Barker, N. *et al.* Very long-term self-renewal of small intestine, colon, and hair follicles from cycling Lgr5+ve stem cells. *Cold Spring Harbor symposia on quantitative biology* **73**, 351-356, doi:10.1101/sqb.2008.72.003 (2008).
- 32 Schepers, A., Vries, R., van den Born, M., van de Wetering, M. & Clevers, H. Lgr5 intestinal stem cells have high telomerase activity and randomly segregate their chromosomes. *The EMBO journal* **30**, 1104-1109, doi:10.1038/emboj.2011.26 (2011).
- 33 Escobar, M. *et al.* Intestinal epithelial stem cells do not protect their genome by asymmetric chromosome segregation. *Nature communications* **2**, 258, doi:10.1038/ncomms1260 (2011).
- 34 Snippert, H. *et al.* Intestinal crypt homeostasis results from neutral competition between symmetrically dividing Lgr5 stem cells. *Cell* **143**, 134-144, doi:10.1016/j.cell.2010.09.016 (2010).
- 35 Lopez-Garcia, C., Klein, A., Simons, B. & Winton, D. Intestinal stem cell replacement follows a pattern of neutral drift. *Science (New York, N.Y.)* **330**, 822-825, doi:10.1126/science.1196236 (2010).
- 36 Sangiorgi, E. & Capecchi, M. Bmi1 is expressed in vivo in intestinal stem cells. *Nature*

- 37 *genetics* **40**, 915-920, doi:10.1038/ng.165 (2008).
- 38 Breault, D. *et al.* Generation of mTert-GFP mice as a model to identify and study tissue progenitor cells. *Proceedings of the National Academy of Sciences of the United States of America* **105**, 10420-10425, doi:10.1073/pnas.0804800105 (2008).
- 39 Powell, A. *et al.* The pan-ErbB negative regulator Lrig1 is an intestinal stem cell marker that functions as a tumor suppressor. *Cell* **149**, 146-158, doi:10.1016/j.cell.2012.02.042 (2012).
- 40 Takeda, N. *et al.* Interconversion between intestinal stem cell populations in distinct niches. *Science (New York, N.Y.)* **334**, 1420-1424, doi:10.1126/science.1213214 (2011).
- 41 Potten, C., Owen, G. & Booth, D. Intestinal stem cells protect their genome by selective segregation of template DNA strands. *Journal of cell science* **115**, 2381-2388 (2002).
- 42 Muñoz, J. *et al.* The Lgr5 intestinal stem cell signature: robust expression of proposed quiescent '+4' cell markers. *The EMBO journal* **31**, 3079-3091, doi:10.1038/emboj.2012.166 (2012).
- 43 Tian, H. *et al.* A reserve stem cell population in small intestine renders Lgr5-positive cells dispensable. *Nature* **478**, 255-259, doi:10.1038/nature10408 (2011).
- 44 Buczaccki, S. *et al.* Intestinal label-retaining cells are secretory precursors expressing Lgr5. *Nature* **495**, 65-69, doi:10.1038/nature11965 (2013).
- 45 Ayabe, T. *et al.* Secretion of microbicidal alpha-defensins by intestinal Paneth cells in response to bacteria. *Nature immunology* **1**, 113-118, doi:10.1038/77783 (2000).
- 46 Shroyer, N., Wallis, D., Venken, K., Bellen, H. & Zoghbi, H. Gfi1 functions downstream of Math1 to control intestinal secretory cell subtype allocation and differentiation. *Genes & development* **19**, 2412-2417, doi:10.1101/gad.1353905 (2005).
- 47 Bastide, P. *et al.* Sox9 regulates cell proliferation and is required for Paneth cell differentiation in the intestinal epithelium. *The Journal of cell biology* **178**, 635-648, doi:10.1083/jcb.200704152 (2007).
- 48 Garabedian, E., Roberts, L., McNevin, M. & Gordon, J. Examining the role of Paneth cells in the small intestine by lineage ablation in transgenic mice. *The Journal of biological chemistry* **272**, 23729-23740, doi:10.1074/jbc.272.38.23729 (1997).
- 49 Sato, T. *et al.* Paneth cells constitute the niche for Lgr5 stem cells in intestinal crypts. *Nature* **469**, 415-418, doi:10.1038/nature09637 (2011).
- 50 Farin, H., Van Es, J. & Clevers, H. Redundant sources of Wnt regulate intestinal stem cells and promote formation of Paneth cells. *Gastroenterology* **143**, 1518, doi:10.1053/j.gastro.2012.08.031 (2012).
- 51 van Es, J. *et al.* Notch/gamma-secretase inhibition turns proliferative cells in intestinal crypts and adenomas into goblet cells. *Nature* **435**, 959-963, doi:10.1038/nature03659 (2005).
- 52 Durand, A. *et al.* Functional intestinal stem cells after Paneth cell ablation induced by the loss of transcription factor Math1 (Atoh1). *Proceedings of the National Academy of Sciences of the United States of America* **109**, 8965-8970, doi:10.1073/pnas.1201652109 (2012).
- 53 van Es, J., de Geest, N., van de Born, M., Clevers, H. & Hassan, B. Intestinal stem cells lacking the Math1 tumour suppressor are refractory to Notch inhibitors. *Nature communications* **1**, 18, doi:10.1038/ncomms1017 (2010).
- 54 Barker, N. *et al.* Crypt stem cells as the cells-of-origin of intestinal cancer. *Nature* **457**, 608-611, doi:10.1038/nature07602 (2009).
- 55 Zhu, L. *et al.* Prominin 1 marks intestinal stem cells that are susceptible to neoplastic transformation. *Nature* **457**, 603-607, doi:10.1038/nature07589 (2009).

- 55 Schepers, A. *et al.* Lineage tracing reveals Lgr5+ stem cell activity in mouse intestinal adenomas. *Science (New York, N.Y.)* **337**, 730-735, doi:10.1126/science.1224676 (2012).
- 56 Merlos-Suárez, A. *et al.* The intestinal stem cell signature identifies colorectal cancer stem cells and predicts disease relapse. *Cell stem cell* **8**, 511-524, doi:10.1016/j.stem.2011.02.020 (2011).
- 57 Gat, U., DasGupta, R., Degenstein, L. & Fuchs, E. De Novo hair follicle morphogenesis and hair tumors in mice expressing a truncated beta-catenin in skin. *Cell* **95**, 605-614 (1998).
- 58 Nguyen, H., Rendl, M. & Fuchs, E. Tcf3 governs stem cell features and represses cell fate determination in skin. *Cell* **127**, 171-183, doi:10.1016/j.cell.2006.07.036 (2006).
- 59 Jaks, V. *et al.* Lgr5 marks cycling, yet long-lived, hair follicle stem cells. *Nature genetics* **40**, 1291-1299, doi:10.1038/ng.239 (2008).
- 60 Snippert, H. *et al.* Lgr6 marks stem cells in the hair follicle that generate all cell lineages of the skin. *Science (New York, N.Y.)* **327**, 1385-1389, doi:10.1126/science.1184733 (2010).
- 61 Van Schoore, G., Mendive, F., Pochet, R. & Vassart, G. Expression pattern of the orphan receptor LGR4/GPR48 gene in the mouse. *Histochemistry and cell biology* **124**, 35-50, doi:10.1007/s00418-005-0002-3 (2005).
- 62 Mustata, R. *et al.* Lgr4 is required for Paneth cell differentiation and maintenance of intestinal stem cells ex vivo. *EMBO reports* **12**, 558-564, doi:10.1038/embor.2011.52 (2011).
- 63 Mazerbourg, S. *et al.* Leucine-rich repeat-containing, G protein-coupled receptor 4 null mice exhibit intrauterine growth retardation associated with embryonic and perinatal lethality. *Molecular endocrinology (Baltimore, Md.)* **18**, 2241-2254, doi:10.1210/me.2004-0133 (2004).
- 64 Mendive, F. *et al.* Defective postnatal development of the male reproductive tract in LGR4 knockout mice. *Developmental biology* **290**, 421-434, doi:10.1016/j.ydbio.2005.11.043 (2006).
- 65 Li, X.-Y. *et al.* G protein-coupled receptor 48 upregulates estrogen receptor alpha expression via cAMP/PKA signaling in the male reproductive tract. *Development (Cambridge, England)* **137**, 151-157, doi:10.1242/dev.040659 (2010).
- 66 Weng, J. *et al.* Deletion of G protein-coupled receptor 48 leads to ocular anterior segment dysgenesis (ASD) through down-regulation of Pitx2. *Proceedings of the National Academy of Sciences of the United States of America* **105**, 6081-6086, doi:10.1073/pnas.0708257105 (2008).
- 67 Song, H. *et al.* Inactivation of G-protein-coupled receptor 48 (Gpr48/Lgr4) impairs definitive erythropoiesis at midgestation through down-regulation of the ATF4 signaling pathway. *The Journal of biological chemistry* **283**, 36687-36697, doi:10.1074/jbc.M800721200 (2008).
- 68 Luo, J. *et al.* Regulation of bone formation and remodeling by G-protein-coupled receptor 48. *Development (Cambridge, England)* **136**, 2747-2756, doi:10.1242/dev.033571 (2009).
- 69 Hoshii, T. *et al.* LGR4 regulates the postnatal development and integrity of male reproductive tracts in mice. *Biology of reproduction* **76**, 303-313, doi:10.1095/biolreprod.106.054619 (2007).
- 70 Mohri, Y., Kato, S., Umezawa, A., Okuyama, R. & Nishimori, K. Impaired hair placode formation with reduced expression of hair follicle-related genes in mice lacking Lgr4. *Developmental dynamics : an official publication of the American Association of Anatomists* **237**, 2235-

- 2242, doi:10.1002/dvdy.21639 (2008).
- 71 Jin, C. *et al.* GPR48 regulates epithelial cell proliferation and migration by activating EGFR during eyelid development. *Investigative ophthalmology & visual science* **49**, 4245-4253, doi:10.1167/iovs.08-1860 (2008).
- 72 McClanahan, T. *et al.* Identification of overexpression of orphan G protein-coupled receptor GPR49 in human colon and ovarian primary tumors. *Cancer biology & therapy* **5**, 419-426 (2006).
- 73 Yamamoto, Y. *et al.* Overexpression of orphan G-protein-coupled receptor, Gpr49, in human hepatocellular carcinomas with beta-catenin mutations. *Hepatology (Baltimore, Md.)* **37**, 528-533, doi:10.1053/jhep.2003.50029 (2003).
- 74 Zucman-Rossi, J. *et al.* Differential effects of inactivated Axin1 and activated beta-catenin mutations in human hepatocellular carcinomas. *Oncogene* **26**, 774-780, doi:10.1038/sj.onc.1209824 (2007).
- 75 Morita, H. *et al.* Neonatal lethality of LGR5 null mice is associated with ankyloglossia and gastrointestinal distension. *Molecular and cellular biology* **24**, 9736-9743, doi:10.1128/MCB.24.22.9736-9743.2004 (2004).
- 76 Garcia, M. *et al.* LGR5 deficiency deregulates Wnt signaling and leads to precocious Paneth cell differentiation in the fetal intestine. *Developmental biology* **331**, 58-67, doi:10.1016/j.ydbio.2009.04.020 (2009).
- 77 Vassart, G., Pardo, L. & Costagliola, S. A molecular dissection of the glycoprotein hormone receptors. *Trends in biochemical sciences* **29**, 119-126, doi:10.1016/j.tibs.2004.01.006 (2004).
- 78 de Lau, W., Snel, B. & Clevers, H. The R-spondin protein family. *Genome biology* **13**, 242, doi:10.1186/gb-2012-13-3-242 (2012).
- 79 Kazanskaya, O. *et al.* The Wnt signaling regulator R-spondin 3 promotes angioblast and vascular development. *Development (Cambridge, England)* **135**, 3655-3664, doi:10.1242/dev.027284 (2008).
- 80 Binnerts, M. *et al.* R-Spondin1 regulates Wnt signaling by inhibiting internalization of LRP6. *Proceedings of the National Academy of Sciences of the United States of America* **104**, 14700-14705, doi:10.1073/pnas.0702305104 (2007).
- 81 Kim, K.-A. *et al.* R-Spondin family members regulate the Wnt pathway by a common mechanism. *Molecular biology of the cell* **19**, 2588-2596, doi:10.1091/mbc.E08-02-0187 (2008).
- 82 Carmon, K., Gong, X., Lin, Q., Thomas, A. & Liu, Q. R-spondins function as ligands of the orphan receptors LGR4 and LGR5 to regulate Wnt/beta-catenin signaling. *Proceedings of the National Academy of Sciences of the United States of America* **108**, 11452-11457, doi:10.1073/pnas.1106083108 (2011).
- 83 Glinka, A. *et al.* LGR4 and LGR5 are R-spondin receptors mediating Wnt/ $\beta$ -catenin and Wnt/PCP signalling. *EMBO reports* **12**, 1055-1061, doi:10.1038/embor.2011.175 (2011).
- 84 Yui, S. *et al.* Functional engraftment of colon epithelium expanded in vitro from a single adult Lgr5 stem cell. *Nature medicine* **18**, 618-623, doi:10.1038/nm.2695 (2012).





## Outline of this thesis

The work summarized in this thesis is focused on the understanding of stem cell function during homeostasis, cancer and regeneration in the intestine and the prostate.

Following the identification of the intestinal epithelium stem cell (ISC) Barker *et al.* 2007 by *Lgr5*, the transcriptome of the ISC was defined using microarray technology. One of the genes specifically expressed by ISC's is *Nr2e3*. Originally *Nr2e3* was identified as a retinal specific gene, where it fulfills a crucial function in cone and rod photoreceptor progenitor cells. We postulated that *Nr2e3* might mark novel stem cell populations in different organs and has a function in stem cell maintenance. Therefore we generated a mouse model where eGFP and the recombinase CreERT2 are controlled by endogenous DNA sequences of *Nr2e3* (*Nr2e3<sup>KI</sup>*). The *Nr2e3<sup>KI</sup>* mouse model allows detection and isolation of *Nr2e3*+ve cells by eGFP expression, and enabled us to perform lineage-tracing studies when crossed with a Cre reporter line (**Chapter 2**). Analysis of eGFP expression revealed restricted *Nr2e3*+ve cell populations in a variety of organs, including the Small intestine, lung, eye and stomach. Lineage tracing revealed that none of the novel *Nr2e3*+ve populations represent stem cells. Moreover we show *Nr2e3* is indispensable for retinal progenitor cells.

How disturbances in the intestinal milieu i.e. commensal bacteria influence *Lgr5*+ve stem cells function is not well understood. In **chapter 3** we describe the generation of a mouse model where the whole regenerating gene family is knocked-out. The regenerating (Reg) gene family, is composed of highly homologous, secreted proteins containing a c-type lectin binding domain and are known to have a bactericidal function. Several members of the regenerating gene family are expressed in the small intestine. Future studies will elucidate the role of these proteins in the intestine and their influence of homeostasis and stem cell function.

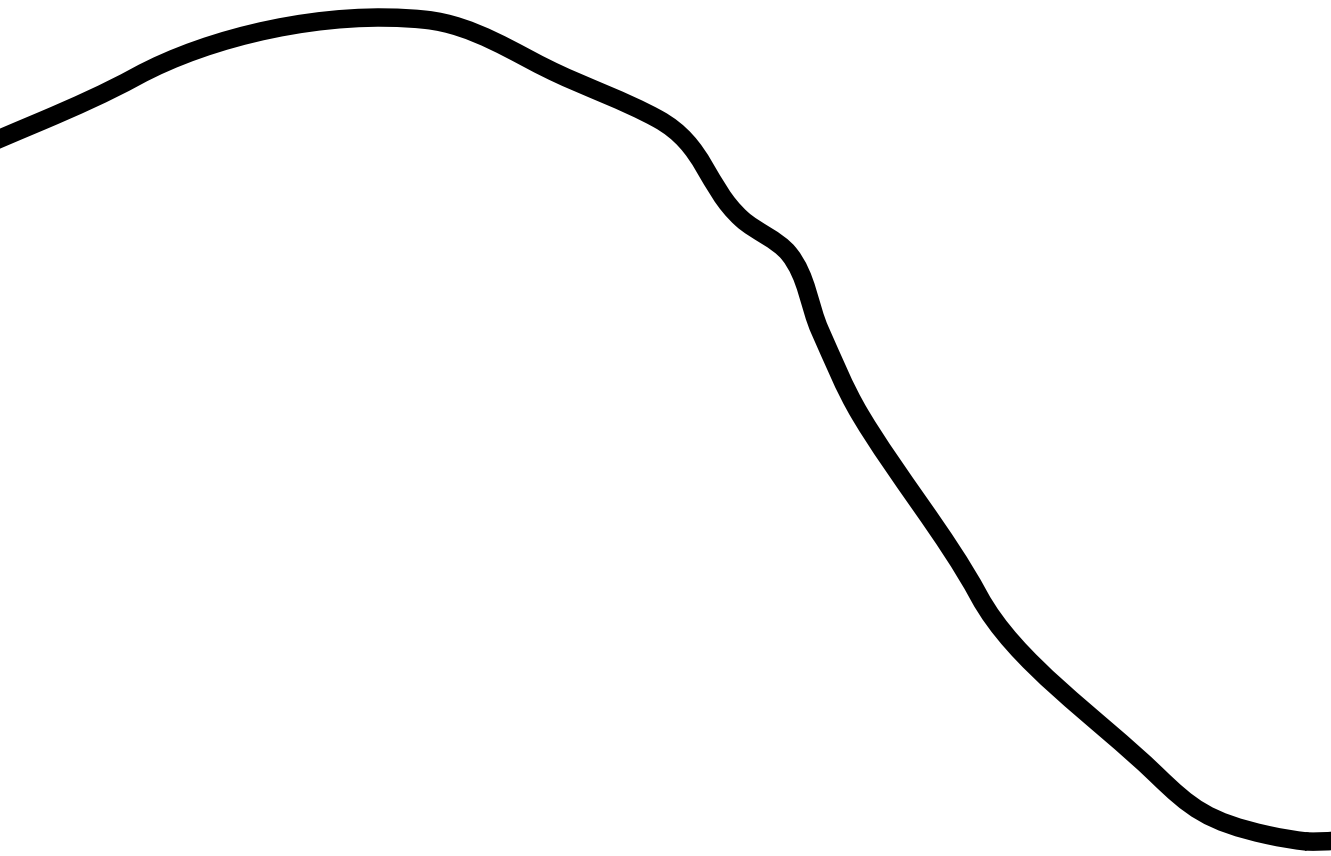
Based on the requirements of *Lgr5*+ve ISC, a novel culture method for intestinal epithelium was developed by Sato *et al.* called organoid culture. In organoid culture the small intestinal epithelium is composed of a defined crypt and villus region and contains all intestinal epithelial celltypes that exist in vivo (Stem cells, Paneth cells, Goblet cells, Enteroendocrine cells and tuft cells). This system allows for the study of the epithelium in an isolated fashion, which could lead to novel insights into diseases with a complex etiology like inflammatory bowel disease. In **chapter 4** we study the effects

of a key inflammatory factor interferon gamma (Ifny) on the intestinal epithelium using the organoid culture. We found that Ifny uniquely acts as a degranulation agent for Paneth cells in the intestine. In contrast to prior findings we find that pathogen associated molecular patterns (PAMPs) do not induce Paneth cell degranulation. We find that PAMP activated immune cells act as a critical mediator in Ifny induced degranulation of Paneth cells.

Based on the small intestinal organoid system, similar culture methods were developed for other gastrointestinal organs. In **chapter 5** we describe the development of the first non-gastrointestinal organoid culture, one of the prostate. Organoids derived from the murine prostate can be cultured in the presence or androgens and are composed of the two distinct epithelial lineages, luminal and basal, that are also present *in vivo*. Moreover murine organoids mimicked *in vivo* phenotypes of murine models of prostate cancer (PCa) and are easily manipulated with chemical compounds and lentiviruses, enabling future studies for novel PCa genes. Next we developed a culture system that allows for the growth for human prostate epithelium. Human prostate organoids are also composed of distinct luminal and basal epithelial cells.

We show that prostate organoids are responsive to clinically approved anti-androgens, Casodex and Enzalutamide. Surprisingly we find that in the absence of androgens, anti-androgen treatment still was effective on organoids, suggesting a ligand independent function of the Androgen Receptor.

Next we tried to identify stem cell populations in the prostate (**Chapter 6**). From the transcriptome of Lgr5+ve ISC, Tnfrsf19 was found to be expressed specifically by ISC. Using the *Tnfrsf19<sup>KI</sup>* mouse generated by Stange *et al.*, where eGFP and CreERT2 are controlled by endogenous Tnfrsf19 DNA sequences, we defined the expression pattern of Tnfrsf19 in the murine prostate. Tnfrsf19 is expressed in distinct luminal and basal cell populations. By crossing the *Tnfrsf19<sup>KI</sup>* mouse with a Cre reporter line, we show that *in vivo* luminal Tnfrsf19+ve serve as unipotent progenitor cells for the luminal lineage. But when single luminal Tnfrsf19+ve cells are bipotent (i.e. capable of generating both luminal and basal lineage) when placed in organoid culture conditions.



# Chapter 2: Generation and characterization of Nr2e3 eGFP/CreERT2 reporter mice.

Wouter R. Karthaus, Johan H. van Es, Maaïke van den Born and Hans C. Clevers.



## Generation and characterization of Nr2e3 eGFP/ CreERT2 reporter mice.

**Wouter R. Karthaus, Johan H. van Es, Maaïke van den Born and Hans C. Clevers.**

Hubrecht Institute, Royal Netherlands Academy of Arts and Sciences &  
University Medical Center Utrecht, 3584 CT, Utrecht<sup>1</sup>

### **Abstract:**

Identification and study of adult stem cells is crucial to understand how tissues are maintained during homeostasis. Recently we have shown that Lgr5 marks the stem cells of the intestine, stomach, skin and liver. Using microarray profiling we found that *Nr2e3* is specifically expressed in the Lgr5+ve stem cells of the small intestine. *Nr2e3* was originally identified as an essential transcription factor in cone and rod progenitors in the retina. To investigate whether *Nr2e3* might mark novel stem cell populations we generated an *Nr2e3<sup>Ki</sup>* mouse, where GFP and CreERT2 were inserted into the *Nr2e3* genomic locus by homologous recombination. Using the *Nr2e3<sup>Ki</sup>* mouse we found that GFP-reporter expression marks several restricted cell populations in a variety of tissues, including lung, small intestine and stomach. Cre mediated lineage tracing however, revealed that none of these cells represent novel stem cell populations during homeostasis. In the stomach the neck mucus cells are labeled, and we find that the lifespan of these cells is 2-4 weeks. Moreover we find that *Nr2e3* is only indispensable for the function of retinal progenitors. In all we conclude that the *Nr2e3<sup>Ki</sup>* mouse is a model for studying the dynamics of the neck mucus cells and *Nr2e3* function in the retina.

### **Introduction:**

Tissue homeostasis and regeneration are dependent on resident stem cells. In various organs Wnt signaling has been associated closely with stem cell function <sup>1-5</sup>. In the small intestine disruption of Wnt signaling pathway, either by genetic ablation of the final effector *Tcf7l2* <sup>1</sup> or of the essential cofactor  $\beta$ -Catenin (*Ctnnb1*) <sup>6</sup> results in a complete proliferation stop in the intestinal epithelium. Conversely hyperactivation of the Wnt-pathway, by deletion of the tumor suppressors *Apc* <sup>7</sup>, *Axin2* <sup>8</sup> or by expressing a mutated form of  $\beta$ -Catenin <sup>9</sup>, results in accumulation of  $\beta$ -Catenin in the nucleus and leads to intestinal hyperplasia and eventually adenoma formation.

Detailed study of the Wnt signaling transcriptome in the intestine resulted in the identification of various Wnt target genes <sup>10,11</sup>. Analysis of the Wnt

transcriptome in the crypt revealed that one gene *Lgr5* was expressed specifically in the crypt base columnar cells, slender cells wedged between the Paneth cells in at the base of the crypts. Cheng and Leblond suggested CBC's to be the stem cells of the small intestine in the 1970's <sup>12,13</sup>.

Using a mouse model where an eGFP and the recombinase CreERT2 are placed under the control of the endogenous *Lgr5* promoter. Analysis of eGFP expression revealed that *Lgr5* expression was localized in CBC cells <sup>14</sup>. By crossing *Lgr5*Ki mice with *Rosa26 lacZ* reporter mice, it was shown via lineage tracing that *Lgr5* marks stem cells of the small intestine and the colon <sup>14</sup>. In following studies it was shown that *Lgr5* also marks stem cells of the hair follicle <sup>15</sup>, stomach <sup>2</sup> and recently the liver <sup>3</sup>. By analyzing the transcriptome of the various *Lgr5*+ve stem cell populations we identified multiple stem cell specific genes. One of these genes is *Nr2e3*. Here we use a novel mouse model for *Nr2e3* to study the contribution of *Nr2e3* expressing cells during homeostasis and study the function of *Nr2e3* in these cells.

## Results:

### Generation of *Nr2e3*-KI mouse (figure 1)

Following the identification of *Lgr5* as stem cell marker for the small intestine, colon <sup>14</sup>, skin <sup>15</sup> and stomach <sup>2</sup>, we subsequently identified transcriptional profiles of all stem cell populations <sup>2,3,16</sup>. In the small intestine expression of, Nuclear receptor, class 2, subfamily E, member 3 (*Nr2e3*) also known as photoreceptor-specific nuclear receptor (PNR) closely followed the expression pattern of *Lgr5* with restricted expression in the crypt base columnar cells (Figure 1). Moreover we found that *Nr2e3* was expressed broadly in the small intestine at E16.5 as was described previously <sup>17</sup>.

Originally the orphan nuclear receptor *Nr2e3* has been identified in the retina, with its expression restricted to the outer neuroblast layer (ONBL) <sup>18</sup>, the progenitor pool for cones and rods. Given the restricted expression of *Nr2e3* in the ISC stem cell compartment and the retinal progenitors we hypothesized that *Nr2e3* might mark novel stem cell populations. To identify further *Nr2e3* positive cells in various tissues and simultaneously allow lineage tracing from *Nr2e3*+ve cells we generated mice, where the expression of eGFP and CreERT2 was inserted into the Start codon of the *Nr2e3* gene (*Nr2e3<sup>KI</sup>*)(Figure 1). This strategy introduces a Stop codon 5' thus representing a null allele.

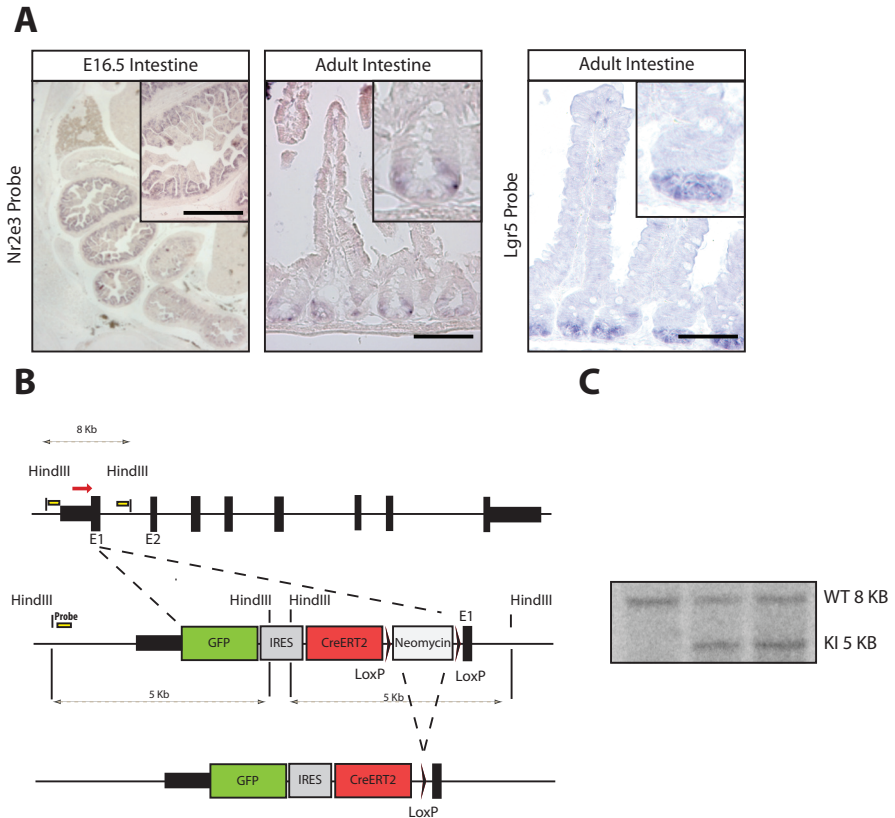


### Figure 1: Generation of Nr2e3<sup>KI</sup> mouse.

A: In situ hybridization of Nr2e3 and Lgr5 showing restricted expression in CBC's of the small intestine in adult mice. Broader expression of Nr2e3 is detected in the intestine at E16 B: Schematic overview of targeting strategy for the Nr2e3 locus C: Southernblot of targeted ES-cells showing specific homologous recombination in the Nr2e3 locus. All scale bars represent 50  $\mu$ m

### Nr2e3 expressing cells identified by eGFP.

Using the Nr2e3<sup>KI</sup> mouse model we screened for eGFP expression in a variety of tissues. As expected we found restricted expression of eGFP in the CBC cells of the small intestine as well as in the ONBL in the retina (Figure 2). Moreover we found eGFP expression in restricted cell populations in the lung and stomach (Figure 2). In the lung eGFP expression was confined to dome-shaped cells in the bronchioles, that might represent Clara or club cells (Figure 2). Clara cells are known to contribute during homeostasis and the regeneration of the bronchiole epithelium.<sup>19,20</sup> In the stomach we found restricted eGFP expression at the base of the glands in the corpus and pylorus (Figure 2). Recently we identified stem cell populations in the gland base in both the corpus and the pylorus. Could Nr2e3 mark these cells?



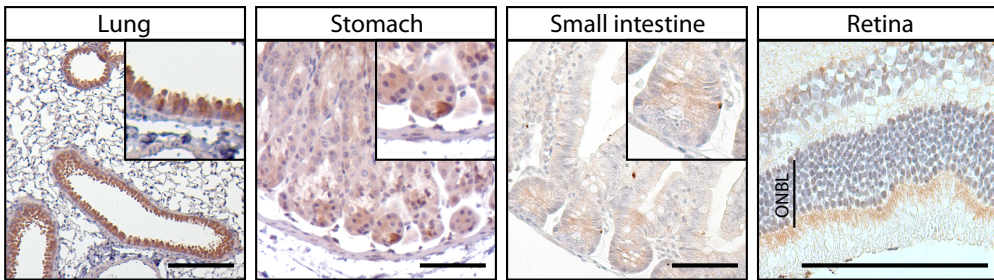


**Figure 2: Restricted cell populations expressing eGFP in the Nr2e3KI mouse.**

In the lung eGFP expression was observed in dome-shaped Clara cells in the bronchioles. In the stomach eGFP expression was observed in single cells at the base of the glands. In the small intestine restricted eGFP expression was observed in the crypts. In the retina eGFP expression was observed in the outer neuroblast layer. All scale bars represent 50  $\mu\text{m}$

### Lineage tracing from Nr2e3/GFP+ve cells.

To examine the contribution of the eGFP+ve/Nr2e3 expressing cells during homeostasis in the various tissues, we crossed the Nr2e3<sup>KI</sup> mouse with the Rosa26lacZ Cre reporter mouse <sup>21</sup>. In the Rosa26lacZ mice, a transcriptional roadblock flanked by loxP sites precedes the coding sequence of  $\beta$ -galactosidase (lacZ) (Figure 3). Upon tamoxifen induction of Cre activity,  $\beta$ -galactosidase expression is stably induced in Nr2e3 expressing cells. Thus Nr2e3 expressing cells and their progeny are genetically labeled and can be visualized by  $\beta$ -galactosidase staining. CreERT2 recombinase activity was induced by 5 consecutive injections with 5mg/kg tamoxifen. At 1-day post injection (Day 6) Nr2e3 expressing cells were observed in the base and pit of the glands in the corpus. We found at 7 and 14 days PI that LacZ positive cells remained as single cells in the base (Figure 3). 1-month PI we did not detect any remaining  $\beta$ -galactosidase activity in the corpus glands (Figure 3). Thus Nr2e3 expressing cells do not represent the stem cells of the stomach epithelium. Recently we observed that tumor necrosis factor receptor super family member 19 (Tnfrsf19) also marks cells in the base of the corpus glands that were identified as both parietal and chief cells (Stange et al. unpublished data). Tnfrsf19+ve parietal cells were able to act as facultative stem cells of the corpus. Therefore we postulated that the  $\beta$ -galactosidase expressing cells in Nr2e3<sup>KI</sup> mice might represent the chief cells or neck mucus cells cell types found in the base. Co-staining of lacZ positive cells with trefoil factor 2 (Tff2) revealed that Nr2e3 expressing/recombined cells represent the neck mucus cells. We found no overlap with markers of Chief cells (H-K-ATPase) and parietal cells (pepsinogen). From our

data we conclude that *Nr2e3* specifically labels pit mucus cells and that this cell type in the stomach epithelium is short lived (> 1 month) and does not contribute to self-renewal during homeostasis. Unfortunately we did not find any recombination events in other eGFP positive domains in the small intestine, lung and retina arguing that the *Nr2e3* promoter activity is too low to drive sufficient levels of CreErt2 expression (Supplementary figure 3).

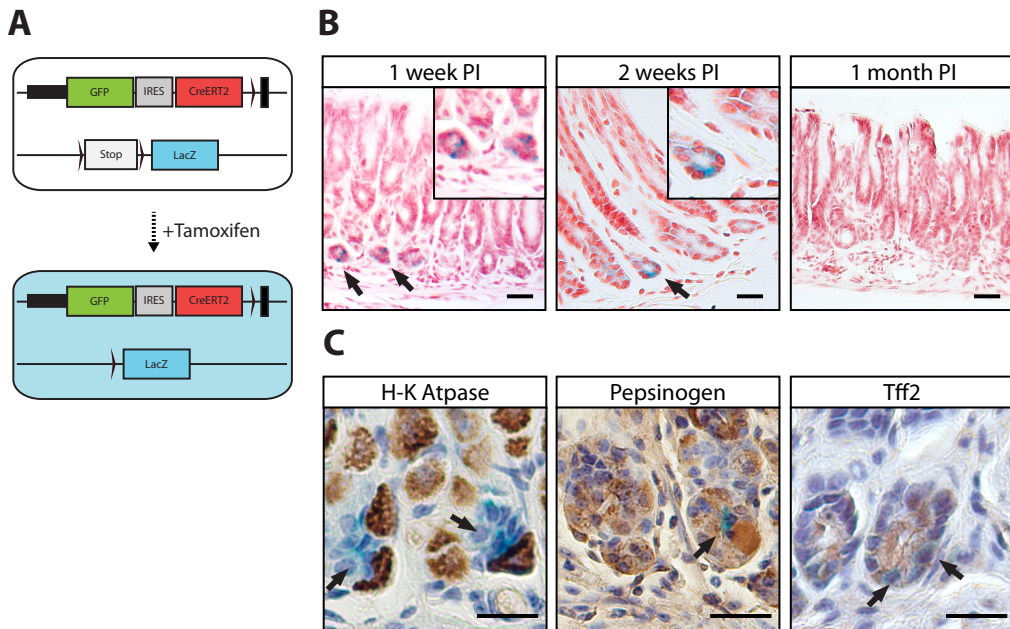


### Figure 3: Lineage tracing of *Nr2e3*+ve cells in the stomach.

A: Schematic overview of lineage tracing strategy from *Nr2e3*+ve cells. Upon Tamoxifen injection CreERT2 removed the roadblock sequence from the R26 allele, allowing expression of lacZ and lineage tracing. B: In the stomach blue lacZ expressing cells in the glandbase are observed 1 week and 2 weeks post tamoxifen induction, but are absent after 1 month. C: LacZ+ve cells stain negative for the parietal cell marker pepsinogen and the chief cell marker H-K-ATPase, but positive for Tff2 revealing that lacZ+ve cells represent neck mucus cells. All scale bars represent 50  $\mu$ M

### *Nr2e3* is only essential for retinal progenitors.

In humans, mutations in *Nr2e3* coding sequence have been associated with Enhanced S-Cone Sensitivity Syndrome (ESCS), Goldmann-Favre Syndrome (GFS), Clumped Pigmentary Retinal Degeneration (CPRD) and Retinitis Pigmentosa (RP)<sup>22,23</sup>. There are several mice models mimicking retinal degeneration (RD). In the *rd7/rd7* mouse model the expression of *Nr2e3* is disrupted by insertion of a long interspaced nuclear element (LINE) retrotransposon after exon 5<sup>24-26</sup>. In *rd7/rd7* mice mRNA splicing efficiency is greatly reduced, resulting in strongly diminished protein levels<sup>24,27</sup>. However,

the development of RD is dependent on the genetic background and only fully penetrates in C57BL/6 mice and not on a mixed genetic background,<sup>24,26,28</sup>. In contrast to the *rd7* allele homozygous mice carrying the *Nr2e3<sup>Kl</sup>* null allele developed RD also on a mixed IB10/Ola - C57BL/6 background, demonstrating a dose sensitivity of phenotype manifestation (Figure 4). We found that the pathology developed in a similar fashion as the *rd7/rd7* mice, with the presence of distinct waves in the ONBL at 4 weeks of age and signs of severe retinal degeneration in adults (Figure 4). We found no phenotypes in other *Nr2e3*+ve tissues (Supplementary Figure 2) demonstrating that *Nr2e3* expression is dispensable for normal homeostasis of stomach, lung and intestine.

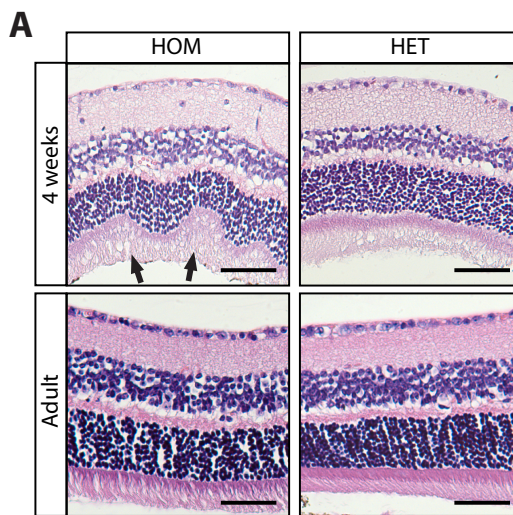


#### Figure 4: *Nr2e3* is indispensable for retinal development.

A: In the retina of 4-week old *Nr2e3<sup>Kl/Kl</sup>* mice distinct wave like patterns are observed. *Nr2e3<sup>Kl/+</sup>* is shown as a control. In retina of 8-week old (adult) *Nr2e3<sup>Kl/Kl</sup>* mice retinal degeneration is observed, but the distinct wavelike patterns are lost. *Nr2e3<sup>Kl/+</sup>* is shown as a control. All scale bars represent 50  $\mu$ m

#### Discussion:

Using a novel mouse model, the *Nr2e3<sup>Kl</sup>* allele, we show that the retinal specific marker *Nr2e3* marks a several restricted cell populations in a variety of organs including, Clara cells in the lung, CBC's in the intestine and neck mucus cells in the stomach. Using lineage tracing we show that *Nr2e3* specifically labels neck mucus cells in the stomach epithelium. We have found that these cells have a turnover of 2-4 weeks and do not form other cell types during homeostasis. In future experiments *Nr2e3<sup>Kl</sup>* mice can be used for specific deletions in neck

mucus cells and add to the understanding of neck mucus cell function. In other organs *Nr2e3*+ve cell populations did not undergo CreERT2 mediated recombination. Most likely this is due to the low expression level of *Nr2e3* in the cell populations.

Homozygous *Nr2e3*<sup>KI</sup> mice are a model for Retinal Degeneration, with distinct waves in the retina at 4 weeks of age and signs of degeneration of the retina. In contrast to the *rd7/rd7* mice, where RD only fully penetrates in a C57Bl/6 background<sup>28</sup>, *Nr2e3*<sup>KI</sup> mice develop RD in a mixed genetic background. Given the increased *Nr2e3* mRNA expression levels in the *rd7/rd7* mouse<sup>22,26</sup> it is likely that it is a hypomorph, whereas the *Nr2e3*<sup>KI</sup> represents a full knock out.

Therefore we conclude that the *Nr2e3*<sup>KI</sup> mouse is a model for studying the dynamics of the neck mucus cells and *Nr2e3* function in the retina.

## Materials & Methods:

### Generation and treatments of mice:

All mice work was done in accordance with rules and regulations of the Dutch animal welfare laws of the Netherlands and was approved by the animal welfare committee of the royal Dutch academy of sciences. *Nr2e3*<sup>eGFP-IRES-CreERT2</sup> mice (*Nr2e3* -KI) were generated using the KI construct depicted in figure 1. All DNA fragments were sequence verified. 100 µg of targeting construct was linearized and electroporated (800V, 3 µF) in male 129/Ola-derived IB-10 embryonic stem cells. Recombined ES-cell clones expressing the neomycin resistance gene were selected with G418 (200 µg/ml). Clones were screened for homologous recombination by Southern blotting. The sequences of all oligonucleotides used are given in Supplementary Table 1. Positive clones were injected in C57Bl/6 blastocysts using standard procedures.

By crossing *Nr2e3*<sup>KI</sup> mice with the *PGK-Cre* mouse strain<sup>29</sup> Neomycin resistance cassette was excised. Subsequently *Nr2e3*<sup>KI</sup> mice were crossed with *Rosa26-LacZ Cre* reporter mice<sup>21</sup>. 8 week and older mice were analyzed for GFP expression and or injected intraperitoneal with 200 µl Tamoxifen in sunflower oil at 5 mg/ml. Mice were sacrificed using standard CO<sub>2</sub>/O<sub>2</sub>-CO<sub>2</sub> asphyxiation.

### Immunohistochemistry, In situ Hybridization and B-galactosidase assay

Murine tissues were fixed using 4% Paraformaldehyde at 4°C, paraffin embedded and sectioned at 4-10 µm. Mouse ESTs were obtained from imaGenes, berlin, Germany. 0.5 kB *Nr2e3* ISH probe was generated from

BC017521 (cDNA clone MGC:27652 IMAGE:4512088, Imagenes) by KpnI digest. *Lgr5* probe was generated as described previously<sup>30</sup>. Probe synthesis was and in situ hybridization was performed as described previously<sup>31</sup>. In short slides were deparaffinized, rehydrated, proteinase K digested and blocked using hybridization mix. Hybridization was performed at 65°C degrees in blocking buffer for 72 hours. Slides were washed at 65°C in 50% formamide/2x SSC and incubated with anti-digoxenin antibody overnight at 4°C. Probes were visualized using NBT/BCIP precipitation reaction. Immunohistochemical staining of eGFP was performed as described previously<sup>32</sup>.

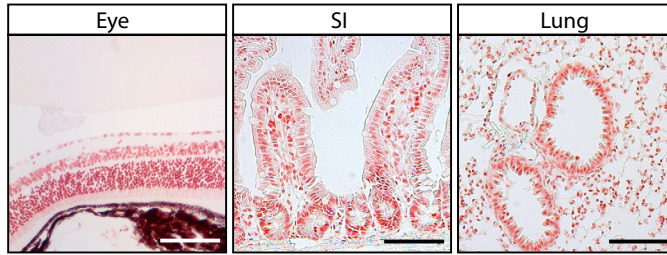
H-K-ATPase was stained using anti H-K-ATPase antibody (1:1000, MBL) for 48 hours at 4 °C degrees. Pepsinogen was stained using anti-Pepsinogen antibody (1:50000, Abcam) for 48 hours at 4°C degrees. Trefoil factor 2 or SP19 was stained overnight using Goat-anti-SP (P-19) antibody (1:750, Santa Cruz) at 4°C degrees. Stainings were visualized using standard DAB solution. LacZ staining was performed as described previously<sup>14</sup>. In short, Tissues were fixed for 2 hours in ice in 1% PFA, 0,2% Glutaraldehyde and 0,02% NP-40 in PBS0. Subsequently tissues were washed twice in PBS0 and stained overnight in 5 mM K3Fe(CN)6, 5 mM K4Fe(CN)6 3 H2O, 2 mM MgCl2, 0.02% NP-40, 0.1% sodium deoxycholate and 1 mg/ml X-Gal in PBS0. The next day tissues were washed using PBS0 and fixed overnight in 4% PFA overnight. Tissues were processed using standard histological techniques. 4 µM slides of LacZ stained tissue were counterstained using neutral red. At least 2 mice were analyzed per time point.

## References:

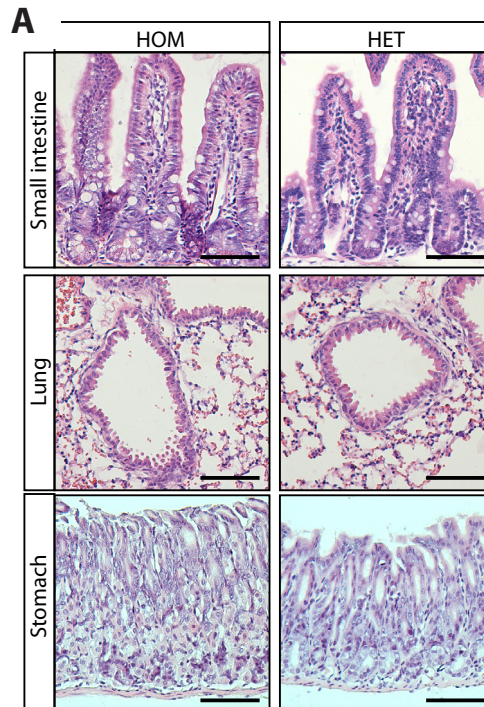
- 1 Korinek, V. *et al.* Depletion of epithelial stem-cell compartments in the small intestine of mice lacking Tcf-4. *Nature genetics* 19, 379-383, doi:10.1038/1270 (1998).
- 2 Barker, N. *et al.* *Lgr5*(+ve) stem cells drive self-renewal in the stomach and build long-lived gastric units in vitro. *Cell stem cell* 6, 25-36, doi:10.1016/j.stem.2009.11.013 (2010).
- 3 Huch, M. *et al.* In vitro expansion of single *Lgr5*+ liver stem cells induced by Wnt-driven regeneration. *Nature* 494, 247-250, doi:10.1038/nature11826 (2013).
- 4 van Amerongen, R., Bowman, A. & Nusse, R. Developmental stage and time dictate the fate of Wnt/ $\beta$ -catenin-responsive stem cells in the mammary gland. *Cell stem cell* 11, 387-400, doi:10.1016/j.stem.2012.05.023 (2012).
- 5 Willert, K. *et al.* Wnt proteins are lipid-modified and can act as stem cell growth factors. *Nature* 423, 448-452, doi:10.1038/nature01611 (2003).
- 6 Ireland, H. *et al.* Inducible Cre-mediated control of gene expression in the murine gastrointestinal tract: effect of loss of beta-catenin. *Gastroenterology* 126, 1236-1246, doi:10.1053/j.gastro.2004.03.020 (2004).
- 7 Korinek, V. *et al.* Constitutive transcriptional activation by a beta-catenin-Tcf complex in APC-/- colon carcinoma. *Science (New York, N.Y.)* 275, 1784-1787 (1997).

- 8 Liu, W. *et al.* Mutations in AXIN2 cause colorectal cancer with defective mismatch repair by activating beta-catenin/TCF signalling. *Nature genetics* 26, 146-147, doi:10.1038/79859 (2000).
- 9 Morin, P. *et al.* Activation of beta-catenin-Tcf signaling in colon cancer by mutations in beta-catenin or APC. *Science (New York, N.Y.)* 275, 1787-1790 (1997).
- 10 van de Wetering, M., de Lau, W. & Clevers, H. WNT signaling and lymphocyte development. *Cell* 109 Suppl, 9 (2002).
- 11 Van der Flier, L. *et al.* The Intestinal Wnt/TCF Signature. *Gastroenterology* 132, 628-632, doi:10.1053/j.gastro.2006.08.039 (2007).
- 12 Cheng, H. & Leblond, C. Origin, differentiation and renewal of the four main epithelial cell types in the mouse small intestine. V. Unitarian Theory of the origin of the four epithelial cell types. *The American journal of anatomy* 141, 537-561, doi:10.1002/aja.1001410407 (1974).
- 13 Cheng, H. & Leblond, C. Origin, differentiation and renewal of the four main epithelial cell types in the mouse small intestine. I. Columnar cell. *The American journal of anatomy* 141, 461-479, doi:10.1002/aja.1001410403 (1974).
- 14 Barker, N. *et al.* Identification of stem cells in small intestine and colon by marker gene Lgr5. *Nature* 449, 1003-1007, doi:10.1038/nature06196 (2007).
- 15 Jaks, V. *et al.* Lgr5 marks cycling, yet long-lived, hair follicle stem cells. *Nature genetics* 40, 1291-1299, doi:10.1038/ng.239 (2008).
- 16 Muñoz, J. *et al.* The Lgr5 intestinal stem cell signature: robust expression of proposed quiescent '+4' cell markers. *The EMBO journal* 31, 3079-3091, doi:10.1038/emboj.2012.166 (2012).
- 17 Choi, M. *et al.* A dynamic expression survey identifies transcription factors relevant in mouse digestive tract development. *Development (Cambridge, England)* 133, 4119-4129, doi:10.1242/dev.02537 (2006).
- 18 Kobayashi, M. *et al.* Identification of a photoreceptor cell-specific nuclear receptor. *Proceedings of the National Academy of Sciences of the United States of America* 96, 4814-4819, doi:10.1073/pnas.96.9.4814 (1999).
- 19 Rawlins, E. *et al.* The role of Scgb1a1+ Clara cells in the long-term maintenance and repair of lung airway, but not alveolar, epithelium. *Cell stem cell* 4, 525-534, doi:10.1016/j.stem.2009.04.002 (2009).
- 20 Zheng, D. *et al.* Regeneration of alveolar type I and II cells from Scgb1a1-expressing cells following severe pulmonary damage induced by bleomycin and influenza. *PloS one* 7, doi:10.1371/journal.pone.0048451 (2012).
- 21 Soriano, P. Generalized lacZ expression with the ROSA26 Cre reporter strain. *Nature genetics* 21, 70-71, doi:10.1038/5007 (1999).
- 22 Haider, N. *et al.* Mutation of a nuclear receptor gene, NR2E3, causes enhanced S cone syndrome, a disorder of retinal cell fate. *Nature genetics* 24, 127-131, doi:10.1038/72777 (2000).
- 23 Schorderet, D. & Escher, P. NR2E3 mutations in enhanced S-cone sensitivity syndrome (ESCS), Goldmann-Favre syndrome (GFS), clumped pigmentary retinal degeneration (CPRD), and retinitis pigmentosa (RP). *Human mutation* 30, 1475-1485, doi:10.1002/humu.21096 (2009).
- 24 Akhmedov, N. *et al.* A deletion in a photoreceptor-specific nuclear receptor mRNA causes retinal degeneration in the rd7 mouse. *Proceedings of the National Academy of Sciences of the United States of America* 97, 5551-5556, doi:10.1073/pnas.97.10.5551 (2000).
- 25 Cheng, H., Khan, N., Roger, J. & Swaroop, A. Excess cones in the retinal degeneration

- rd7 mouse, caused by the loss of function of orphan nuclear receptor Nr2e3, originate from early-born photoreceptor precursors. *Human molecular genetics* 20, 4102-4115, doi:10.1093/hmg/ddr334 (2011).
- 26 Haider, N., Naggert, J. & Nishina, P. Excess cone cell proliferation due to lack of a functional NR2E3 causes retinal dysplasia and degeneration in rd7/rd7 mice. *Human molecular genetics* 10, 1619-1626, doi:10.1093/hmg/10.16.1619 (2001).
- 27 Chen, J., Rattner, A. & Nathans, J. Effects of L1 retrotransposon insertion on transcript processing, localization and accumulation: lessons from the retinal degeneration 7 mouse and implications for the genomic ecology of L1 elements. *Human molecular genetics* 15, 2146-2156, doi:10.1093/hmg/ddl138 (2006).
- 28 Haider, N. *et al.* Mapping of genetic modifiers of Nr2e3 rd7/rd7 that suppress retinal degeneration and restore blue cone cells to normal quantity. *Mammalian genome : official journal of the International Mammalian Genome Society* 19, 145-154, doi:10.1007/s00335-008-9092-2 (2008).
- 29 Lallemand, Y., Luria, V., Haffner-Krausz, R. & Lonai, P. Maternally expressed PGK-Cre transgene as a tool for early and uniform activation of the Cre site-specific recombinase. *Transgenic research* 7, 105-112, doi:10.1023/A:1008868325009 (1998).
- 30 Tian, H. *et al.* A reserve stem cell population in small intestine renders Lgr5-positive cells dispensable. *Nature* 478, 255-259, doi:10.1038/nature10408 (2011).
- 31 Gregorieff, A. *et al.* Expression pattern of Wnt signaling components in the adult intestine. *Gastroenterology* 129, 626-638, doi:10.1016/j.gastro.2005.06.007 (2005).
- 32 van der Flier, L. *et al.* Transcription factor achaete scute-like 2 controls intestinal stem cell fate. *Cell* 136, 903-912, doi:10.1016/j.cell.2009.01.031 (2009).

**Supplementary Figure S1:**

No recombination events were found in other the Nr2e3+ve cell populations in the retina, lung and small intestine. All scale bars represent 50  $\mu$ M

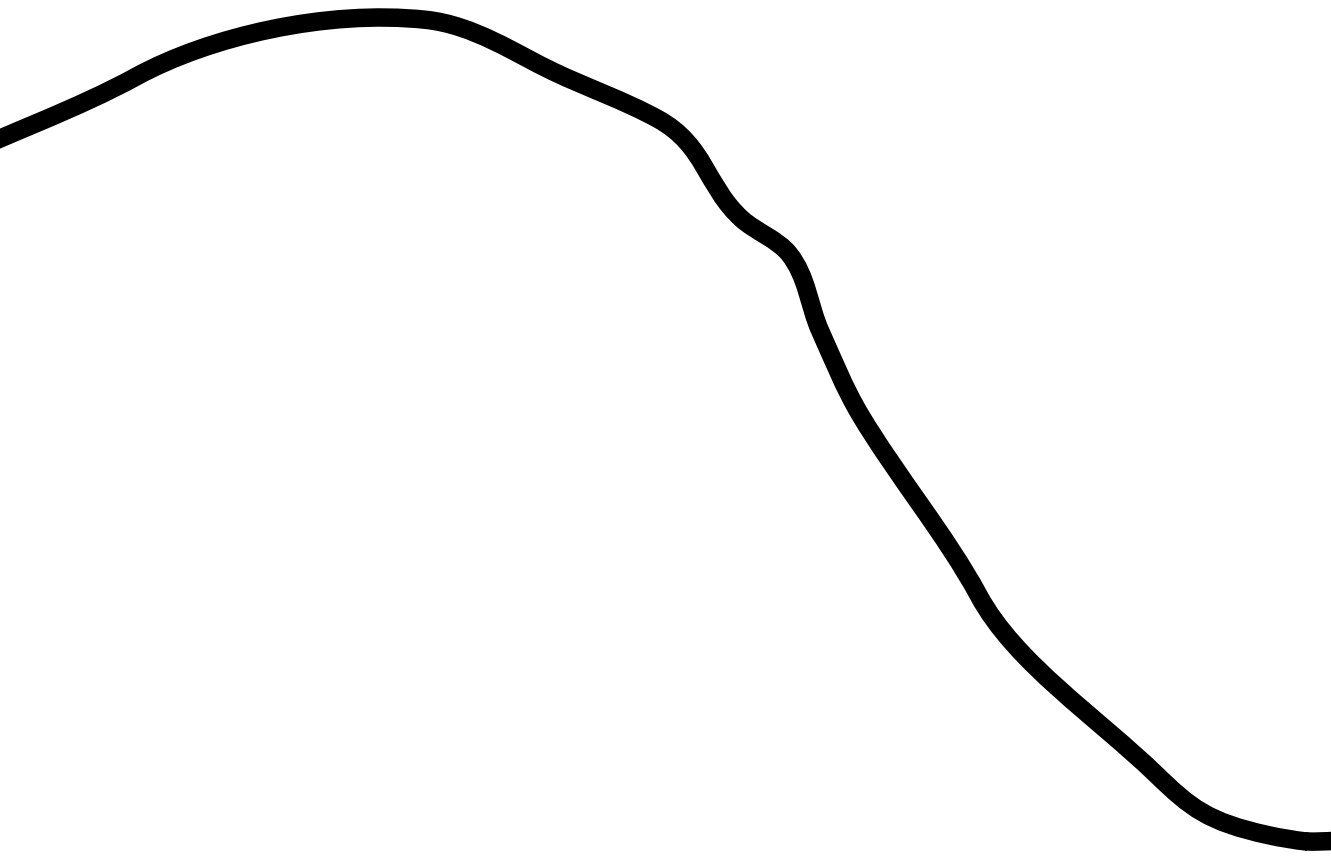
**Supplementary Figure S2:**

No abnormalities were found in other tissues with Nr2e3+ve cell populations. All scale bars represent 50  $\mu$ M



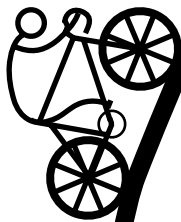
## Supplementary table 1

Oligo name	Oligo sequence
Nr2e35armfor1	ATCTCGAGACGCCCCATGGGGAAGGGATTGC
Nr2e35armrev1	ATCTCGAGCGGATATGGATGGTCCTAAGGG
Nr2e35armintrev1	GGGCTGAAGGACATAGCCTGG
Nr2e35armintFor2	CGGGGCATAGATCTTAGGTG
Nr2e35armintFor3	GGGACAGGAAAGGATGTTCC
Nr2e35armintFor4	GTGAACAAGCAACAGAGGCAG
Nr2e35armintFor5	GCTGTGCTGGCAGAAGTCTG
Nr2e33armfor1	TTGCGGCCGCCTACAGTGGCTGCCTCCACTATG
Nr2e33armrev1	TTGCGGCCGCCTGTGATCAGAGAGGGCTCAAG
Nr2e33armintrev1	GCTCAAGCTCGCTCGTGGCTC
Nr2e33armintfor2	GGCAGATCTAGTTTGAGGAACG
Nr2e33armintfor3	GTGCTTACAAGCAGGCATGAAC
Nr2e33armintfor4	GACCCCGAGTTCCCCGCATCC
Nr2e33armintfor5	AAGGAAGTGGTTGACTGTGAG
nr2e3southern5forward	CTAGCACGCACTAGATTTTCATTC
nr2e3southern5reverse	GAACAGTGCATGCAGCACTGC
Nr2e3ssouthern3forward	CCACTGCTGGCACCACCTGAG
nr2e3southern3reverse	GTAGCCAGGCTGTCTTGAAC
Nr2e3southernint5	ACCCCCACAAAGTCAAATG
Nr2e3southernint3	GCCTGAAGGATCCTGAGCACG



# Chapter 3: Role of the regenerating gene family in the intestine

Wouter R. Karthaus \*, Laurens G. van der Flier \*, Johan H. van Es, Maaïke van den Born and Hans C. Clevers.



# Role of the regenerating gene family in the intestine

**Wouter R. Karthaus \***, **Laurens G. van der Flier \***, **Johan H. van Es**, **Maaïke van den Born** and **Hans C. Clevers**.

Hubrecht Institute, Royal Netherlands Academy of Arts and Sciences & University Medical Center Utrecht, 3584 CT, Utrecht<sup>1</sup>

*\*Equal contribution*

## Abstract:

The regenerating (Reg) gene family is composed of highly homologous, secreted proteins containing a c-type lectin-binding domain. With the exception of Reg4, all Reg genes are located within a single locus. Several members of the regenerating gene family are expressed in the small intestine. In the intestine, the bactericidal Reg3g protein plays a role in innate immunity. To study the function of the Reg family, we generated a mouse model where the entire Reg locus is flanked by loxP sites (Reg<sup>FAM</sup>), allowing Cre-mediated DNA recombination. A Reg4 allele where exon2 is flanked by loxP sites was generated independently. By crossing the Reg<sup>FAM</sup> and Reg4<sup>loxP/loxP</sup> mice with PGK-Cre mice and Villin-Cre, we will delete the complete Reg family and study their exact function.

## Introduction

The regenerating (Reg) gene family encompasses a group of highly homologous secreted proteins, containing a C-type lectin-binding domain. In humans, five Reg genes are identified and in mouse seven, which are further subdivided into subclasses I, II, III and IV <sup>1</sup>. In both human and mice, the Reg genes are clustered in one locus <sup>2,3</sup>, with the exception of Reg4. During homeostasis, the Reg genes are expressed predominantly in the pancreas and small intestine. However, in several pathologies such as cancer and inflammatory bowel disease <sup>4,5</sup>, as well as during regeneration of various tissues, *Reg* genes are often strongly upregulated<sup>1,6</sup>.

The first member of the Reg family, Reg1, was identified from a regenerating islet-derived cDNA library screen in rats <sup>7</sup>. Reg genes were thought to play a role during regeneration. Single knockout mice have been generated for Reg1, Reg3b and Reg3g with only mild somatic phenotypes <sup>8-10</sup>.

Surprisingly, it was shown by Cash *et al.* that the Reg3b and Reg3g have bactericidal properties <sup>11</sup>, that are dependent on the c-type lectin domain <sup>12</sup>. In a recent study, it was shown that the spatial segregation of the

commensal bacteria and the intestinal epithelium is dependent on Reg3g<sup>10</sup>. The role of the other Reg family members is unclear, but is probably similar. To study the function of the complete Reg gene family in the intestine, we decided to generate an inducible knockout mouse model for the entire Reg gene family. We generated two alleles, one where the whole cluster is flanked by loxP sites and a separate floxed Reg4 allele.

## Results:

### Reg family member expression patterns in the intestine and pancreas

To study the Reg expression pattern in the small intestine, we performed in situ hybridization on APC<sup>min</sup> intestines and pancreas. *Reg1* is expressed at the crypt-villus junction in the duodenum of the intestine (Figure 1A). In the pancreas, *Reg1* is expressed in the acinar cells (Figure 1B). *Reg2* expression pattern is similar in the pancreas, whereas the intestine is negative for *Reg2* (Figure 1C-D). *Reg3a* is expressed at low levels in the crypts and acinar cells (Figure 1E-F). In the intestine, *Reg3b* expression is strong at the crypt-villus junction, in the pancreas, expression is confined to the acinar cells (Figure 1G-H). *Reg3d* expression was absent in the small intestine and found at low levels in the pancreas (Figure 1I-J). *Reg3g* expression was similar to that of *Reg3b*, with strong expression at the crypt-villus junction, but also expression in Paneth cells, albeit at lower levels (Figure 1K). In the pancreas, *Reg3g* is absent (Figure 1L). In the intestine *Reg4* expression is confined to the Paneth cells and enteroendocrine cells (Figure 1M). *Reg4* is also the only member expressed in the colon (Figure 1O). In the pancreas, *Reg4* is absent (Figure 1N). Results were verified by analysis of Reg expression in freshly isolated crypts from the duodenum, jejunum, ileum and colon using RT-PCR. Interestingly, *Reg1* expression is strongest in the duodenum. The expression of other Reg family members was not significantly different among different intestinal regions (Figure 1O).

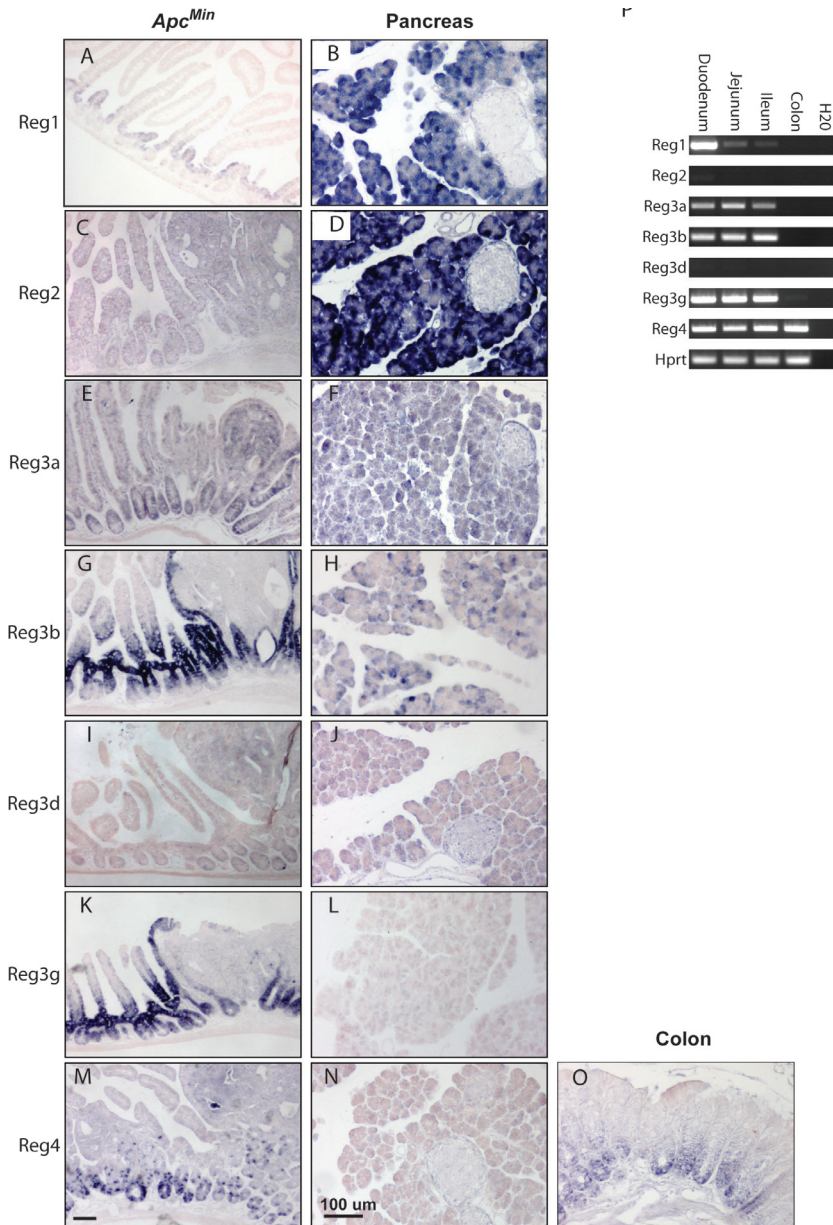


**Figure 1: Expression pattern of the Reg gene family in the intestine & Pancreas.**

A, B: Reg1 is expressed at the crypt/villus junction in the small intestine and in the acinar cells of the pancreas C, D: Reg2 is not expressed in the small intestine, but strongly in the acinar cells of the pancreas E, F: Reg3a expression is expressed in the crypts of the small intestine and the acinar cells of the pancreas G, H: Reg3b is expressed at the crypt/villus junction in the small intestine and in the acinar cells of the pancreas I, J: Reg3d is not expressed in the small intestine and at low levels in the pancreas K, L: Reg3g is expressed at the crypt/villus junction in the small intestine but not in the pancreas M, N, O: Reg4 is expressed by single cells at the bottom of the crypts of the small intestine and colon and in the small intestine sporadic cells on the villus. Reg4 expression is absent in the pancreas. P: Confirmation

of the Reg expression patterns in the intestine via RT-PCR. Reg1 is predominantly expressed in the duodenum, whereas expression of the remainder of the reg family is not significantly different among intestinal regions. Reg4 is the only family member expressed in the colon. Scale bars represent 100  $\mu$ M.

### **Generation of Reg<sup>FAM</sup> conditional allele:**

In mice, six of the seven Reg family members are located on a 100 kB locus on chromosome 6<sup>3</sup> (Figure 2A). To generate a full knock out for the Reg family (Reg<sup>FAM</sup>), we introduced two loxP sites in the outermost Reg genes in the locus by successive homologous recombination.

One of the flanking genes is Reg3b. Via homologous recombination, we replaced exon2 by a CreERT and a loxP site. For selection of recombined ES-Cells a Hygromycin resistance cassette was introduced. Via southern blotting homologous recombination was confirmed (Figure 2B). Subsequently, a second loxP site was introduced at the opposing end of the Reg cluster. Via homologous recombination a neomycin resistance cassette flanked by loxP sites was introduced into the *Reg3g* locus (Figure 2C). Homologous recombination was confirmed by southern blotting (Figure 2B-C).

After dual targeting, two outcomes are possible 1) Both homologous recombinations occurred on the same chromosome copy (Cis) 2) Homologous recombination occurred on different chromosome copies (Trans) (Figure 3A).

To distinguish Cis and Trans recombination, double-targeted ES-cells were transfected with a Cre expressing plasmid, allowing transient expression of Cre-recombinase. When recombination takes place in Cis, the entire Reg<sup>FAM</sup> locus will be deleted (Figure 3B).

2 days post-transfection, DNA was isolated from ES-cells and was analyzed via PCR for a recombined allele. Non-transfected clones were used as a control. We found that 4 clones harbored a recombined allele (Figure 3C). We interpreted that in these clones homologous recombination took place in Cis. Chimeric mice were generated from a Cis Reg<sup>FAM</sup> clone 1.

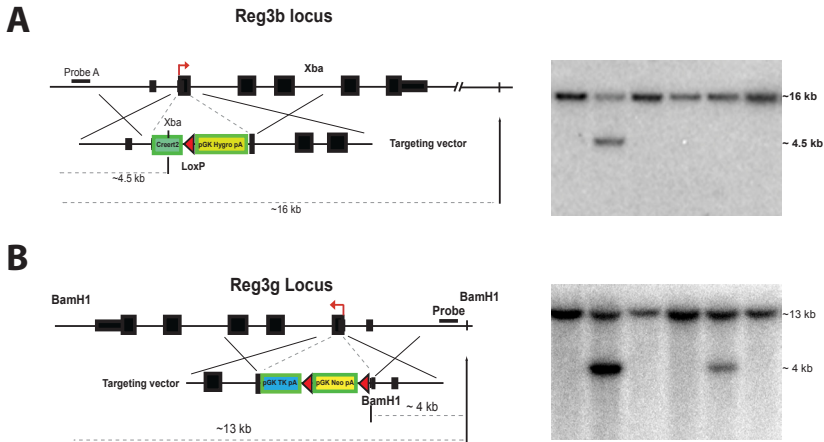


**Figure 2: Reg3b & Reg3g targeting strategies.**

A: Genomic organization of the Reg family locus on chromosome 6 B: Targetting strategy for the Reg3b locus. C: Targetting strategy for the Reg3g locus. Homologous recombination was confirmed with Southern blotting

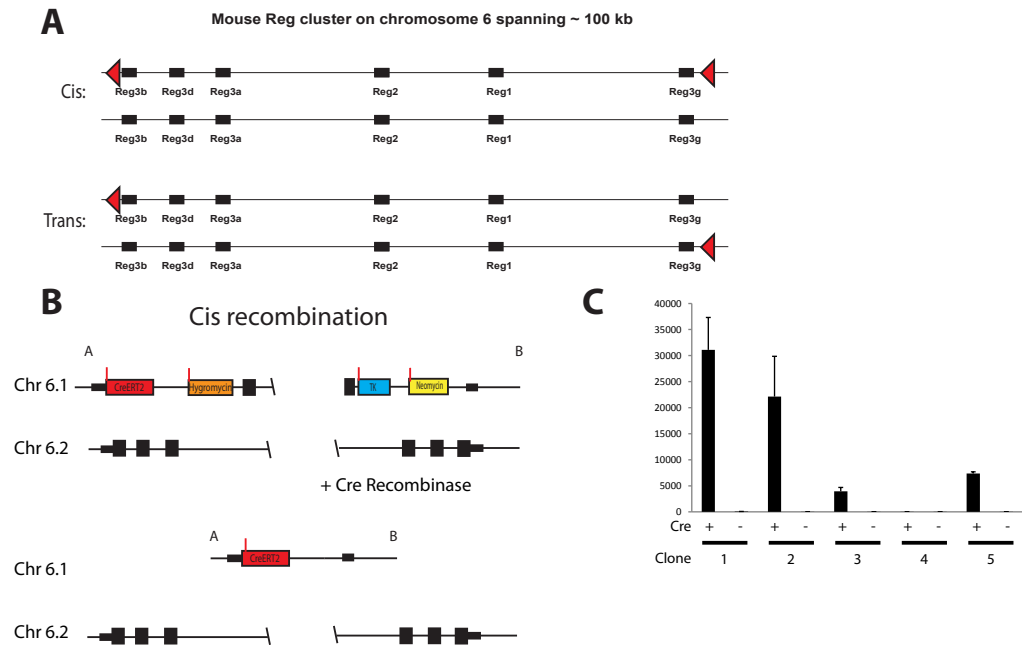


**Figure 3: Cis & Trans recombination of the Reg<sup>FAM</sup> locus.**

A: Schematic overview of the possible homologous recombinations in the Reg locus. In Cis both recombination events took place on the same chromosome copy. During trans recombination both events occurred on different chromosome copies. B: Schematic overview of Cre mediated deletion of the Reg locus. PCR strategies is based on the deleted Reg locus C: QPCR analysis of the double targeted ES-cell clones reveal that 4 clones are in Cis. Results are presented as mean  $\pm$  standard deviation.



## Reg4 is dispensable for epithelial function

For Reg4, a separate targeting strategy was designed. Via homologous recombination two loxP were introduced around the second exon, allowing Cre-mediated recombination. A neomycin flanked by Frt sites was introduced for selection. Homologous recombination was confirmed via Southern blot (Figure 4). After removal of the Neomycin<sup>R</sup> cassette by crossing with a FLPeR deleter strain <sup>13</sup>, Reg4<sup>loxP/loxP</sup> mice were crossed to a mouse harboring the PGKCre allele <sup>14</sup>. In the PGKCre strain, the Cre recombination takes place in the zygote, creating a null mouse. We found that Reg4<sup>del/del</sup> developed normally and in the adult we found no epithelial phenotype (Figure 4).

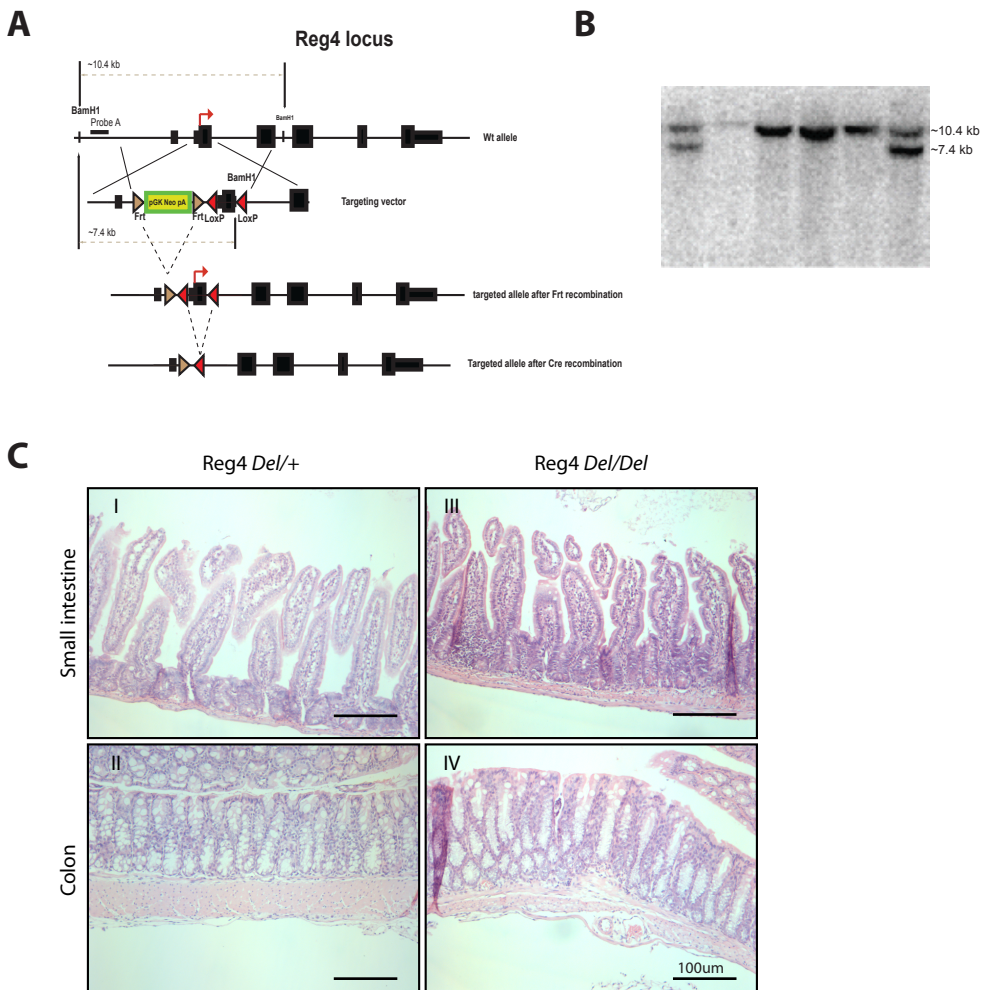


**Figure 4: Generation of the Reg4 conditional allele.**

A: Targetting strategy for the *Reg4* locus. B: Homologous recombination of the *Reg4* locus was confirmed with Southernblotting C: When crossed to a PGKcre deleter mouse line, no phenotype was observed in the small intestine and colon of the Reg4<sup>del/del</sup> mice. Scalebars represent 100µm.

## Discussion:

During homeostasis, the *Reg* genes are expressed in the intestine and pancreas. *Reg* genes are commonly upregulated in pathologies and during regeneration. Originally, Regs were thought to be involved in regenerative processes, but recent evidence revealed a role for Reg3g in innate immunity of the small intestine, its bactericidal properties dependent on a c-type lectin-binding domain<sup>10-12</sup>. To address the role of the *Reg* gene family, we will cross the *Reg4<sup>del/del</sup>*, PGKcre mice with the *Reg<sup>FAM</sup>* to create a full *Reg<sup>FAM</sup>*, *Reg4<sup>del/del</sup>* knockout. Moreover, we will cross the *Reg<sup>FAM</sup>* mice to mice harboring a villin Cre. In these mice the Cre recombinase is specifically expressed in the intestinal epithelium, deleting the *Reg* family specifically in the intestine. Subsequently we will analyze the bacterial composition in the intestine. Analysis of these animals will most likely lead to novel insights into the role of the *Reg* family in the intestine.

## Materials & Methods:

### Immunohistochemistry and In situ hybridizations:

Murine tissues were fixed using 4% Paraformaldehyde at 4°C, paraffin embedded and sectioned at 4-10 µm. In vitro transcription and In situ hybridization was performed as described previously<sup>15</sup>. For in vitro transcription orthologues of murine *Reg* mRNA transcripts were obtained from the IMAGE consortium.

### Crypt isolation:

Crypt isolation was performed as described previously<sup>16</sup>.

### RNA isolation cDNA synthesis & qPCR:

RNA was isolated using RNeasy mini kit (Qiagen) according to manufacturers protocol. cDNA synthesis was performed with 50-1000 ng RNA using GoScript (Promega) according to manufacturers protocol. qPCR was performed using Sybr green (Bio-Rad) according to manufacturers protocol with primers listed in supplementary table 1.

### Generation and treatment of *Reg<sup>FAM</sup>* and *Reg4<sup>loxP/loxP</sup>* mice

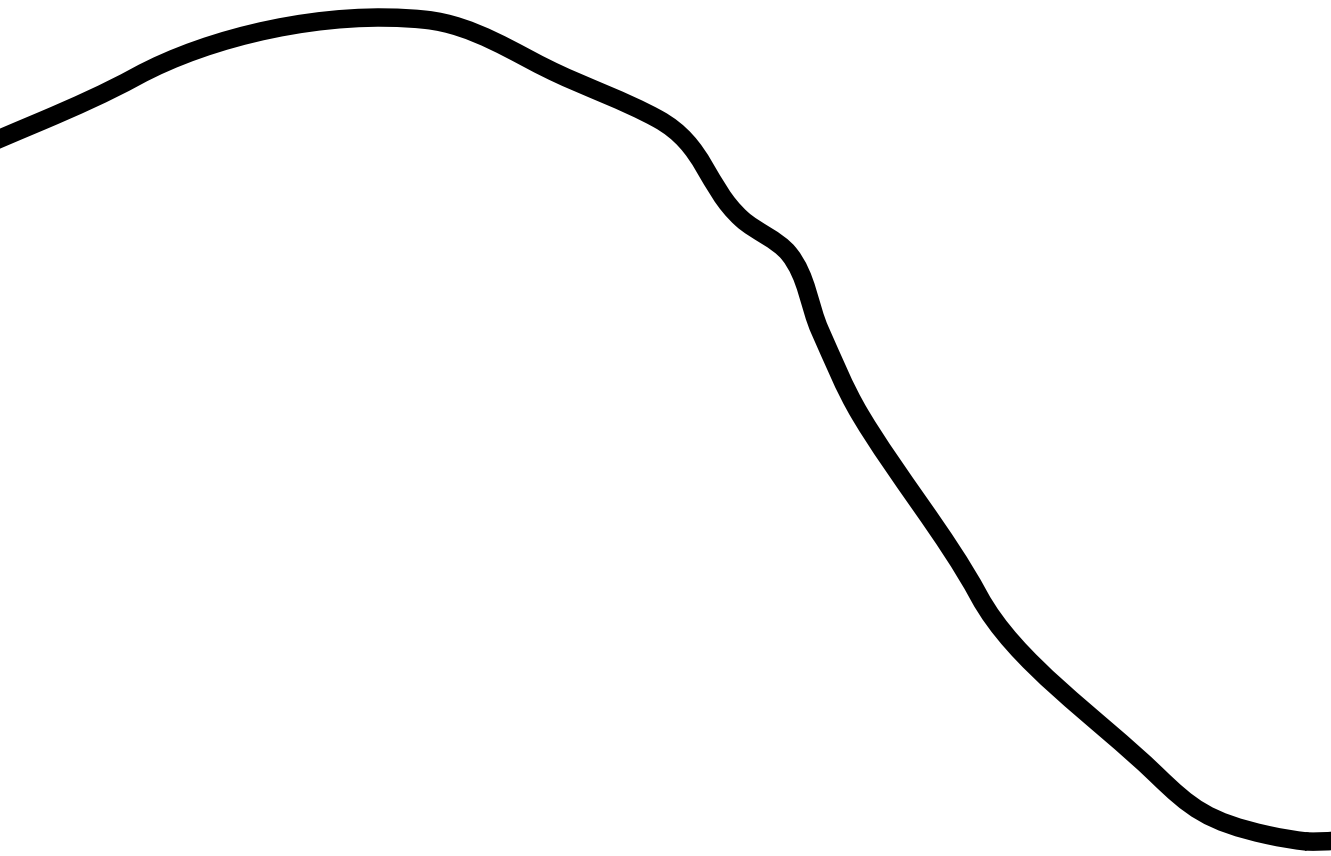
All mice work was done in accordance with rules and regulations of the Dutch animal welfare laws of the Netherlands. *Reg3b* and *Reg3g* constructs were cloned into the polylinker of pBLEUScript SK+ (Stratagene). *Reg4* construct was cloned into pL451 vector. 100 µg of targeting construct was linearized and electroporated (800V, 3 µF) in male 129/Ola-derived IB-10 embryonic stem cells. Recombined ES-cell clones expressing the neomycin resistance gene were selected with G418 (200 µg/ml) or Hygromycin B (150 µg/ml). Recombination was confirmed by Southern blotting.

In *Reg4* mice Frt flanked neomycin was excised in vivo by crossing with

the FLPeR delete strain. Reg4<sup>del/del</sup> mice were created by crossing with the general Cre-rebominase expressing PGKCre mouse line <sup>14</sup>.

## References:

- 1 Zhang, Y.-W., Ding, L.-S. & Lai, M.-D. Reg gene family and human diseases. *World journal of gastroenterology: WJG* 9, 2635-2641 (2003).
- 2 Miyashita, H. *et al.* Human REG family genes are tandemly ordered in a 95-kilobase region of chromosome 2p12. *FEBS letters* 377, 429-433, doi:10.1016/0014-5793(95)01381-4 (1995).
- 3 Narushima, Y. *et al.* Structure, chromosomal localization and expression of mouse genes encoding type III Reg, RegIII alpha, RegIII beta, RegIII gamma. *Gene* 185, 159-168 (1997).
- 4 Van der Flier, L. *et al.* The Intestinal Wnt/TCF Signature. *Gastroenterology* 132, 628-632, doi:10.1053/j.gastro.2006.08.039 (2007).
- 5 van Beelen Granlund, A. *et al.* REG gene expression in inflamed and healthy colon mucosa explored by in situ hybridisation. *Cell and tissue research* 352, 639-646, doi:10.1007/s00441-013-1592-z (2013).
- 6 Lieu, H.-T. *et al.* Reg2 inactivation increases sensitivity to Fas hepatotoxicity and delays liver regeneration post-hepatectomy in mice. *Hepatology (Baltimore, Md.)* 44, 1452-1464, doi:10.1002/hep.21434 (2006).
- 7 Terazono, K. *et al.* A novel gene activated in regenerating islets. *The Journal of biological chemistry* 263, 2111-2114 (1988).
- 8 Unno, M. *et al.* Production and characterization of Reg knockout mice: reduced proliferation of pancreatic beta-cells in Reg knockout mice. *Diabetes* 51 Suppl 3, 83 (2002).
- 9 Ose, T. *et al.* Reg I-knockout mice reveal its role in regulation of cell growth that is required in generation and maintenance of the villous structure of small intestine. *Oncogene* 26, 349-359, doi:10.1038/sj.onc.1209799 (2007).
- 10 Vaishnav, S. *et al.* The antibacterial lectin RegIIIgamma promotes the spatial segregation of microbiota and host in the intestine. *Science (New York, N.Y.)* 334, 255-258, doi:10.1126/science.1209791 (2011).
- 11 Cash, H., Whitham, C., Behrendt, C. & Hooper, L. Symbiotic bacteria direct expression of an intestinal bactericidal lectin. *Science (New York, N.Y.)* 313, 1126-1130, doi:10.1126/science.1127119 (2006).
- 12 Mukherjee, S. *et al.* Regulation of C-type lectin antimicrobial activity by a flexible N-terminal prosegment. *The Journal of biological chemistry* 284, 4881-4888, doi:10.1074/jbc.M808077200 (2009).
- 13 Farley, F., Soriano, P., Steffen, L. & Dymecki, S. Widespread recombinase expression using FLPeR (flipper) mice. *Genesis (New York, N.Y. : 2000)* 28, 106-110, doi:10.1002/1522-968X(200011/12)28:3/4<106::AID-GENE30>3.0.CO;2-T (2000).
- 14 Lallemand, Y., Luria, V., Haffner-Krausz, R. & Lonai, P. Maternally expressed PGK-Cre transgene as a tool for early and uniform activation of the Cre site-specific recombinase. *Transgenic research* 7, 105-112, doi:10.1023/A:1008868325009 (1998).
- 15 Gregorieff, A. *et al.* Expression pattern of Wnt signaling components in the adult intestine. *Gastroenterology* 129, 626-638, doi:10.1016/j.gastro.2005.06.007 (2005).
- 16 van der Flier, L. *et al.* Transcription factor achaete scute-like 2 controls intestinal stem cell fate. *Cell* 136, 903-912, doi:10.1016/j.cell.2009.01.031 (2009).



# Chapter 4: Secretion of antimicrobial Paneth cell products is directly controlled by immune cell-derived Interferon- $\gamma$

Henner F. Farin<sup>1\*</sup>, Wouter R. Karthaus<sup>1\*</sup>, Pekka Kujala<sup>2</sup>, Maryam Rakhshandehroo<sup>3</sup>, Robert Vries<sup>1</sup>, Eric Kalkhoven<sup>3,4</sup>, Edward E. S. Nieuwenhuis<sup>5</sup> and Hans Clevers<sup>1,6</sup>



# Secretion of antimicrobial Paneth cell products is directly controlled by immune cell-derived Interferon- $\gamma$

**Henner F. Farin<sup>1\*</sup>, Wouter R. Karthaus<sup>1\*</sup>, Pekka Kujala<sup>2</sup>, Maryam Rakhshandehroo<sup>3</sup>, Robert Vries<sup>1</sup>, Eric Kalkhoven<sup>3,4</sup>, Edward E. S. Nieuwenhuis<sup>5</sup> and Hans Clevers<sup>1,6</sup>**

<sup>1</sup>Hubrecht Institute for Developmental Biology and Stem Cell Research & University Medical Centre Utrecht, Uppsalalaan 8, 3584CT Utrecht, Netherlands.

<sup>2</sup>Antoni van Leeuwenhoek Hospital/Netherlands Cancer Institute, Plesmanlaan 121, 1066 CX Amsterdam, Netherlands.

<sup>3</sup>Section of Metabolic Diseases, Molecular Cancer Research, University Medical Center Utrecht, Utrecht, the Netherlands.

<sup>4</sup>Netherlands Metabolomics Center, Leiden, The Netherlands.

<sup>5</sup>Department of Pediatric Gastroenterology, Wilhelmina Children's Hospital, University Medical Center Utrecht, Utrecht, Netherlands.

<sup>6</sup>Correspondence to Hans Clevers, Hubrecht Institute for Developmental Biology and Stem Cell Research & University Medical Centre Utrecht, Uppsalalaan 8, 3584CT Utrecht, Netherlands; h.clevers@hubrecht.eu; Tel: 31 (0) 30 212 1800 ;Fax: 31 (0) 30 251 6464.

\* Contributed equally

## ABSTRACT

In the intestine, Paneth cells are terminally differentiated, highly specialized secretory epithelial cells located at the base of the crypts of Lieberkühn. Besides their antimicrobial function, Paneth cells serve as a component of the intestinal stem cell niche. By secretion of granules containing bactericidal proteins like defensins/cryptidins and lysozyme, Paneth cells regulate the microbiome of the gut. The mechanisms that control Paneth cell degranulation are not well characterized. Here we show using the small intestinal organoid culture system that Paneth cell degranulation does not directly occur upon stimulation with bacterial fragments or inactivated bacteria. In contrast, we find that the pro-inflammatory cytokine Interferon  $\gamma$  (IFN- $\gamma$ ) induces complete epithelial degranulation. Using live cell imaging, we show that this secretion event occurs rapidly and in an 'all-or-nothing'

fashion. IFN- $\gamma$  containing supernatants from *in vitro* stimulated iNKT cells mediate degranulation in an IFN- $\gamma$ -dependent manner. Furthermore, we show *in vivo* (using the anti-CD3 antibody injection model) that endogenous IFN- $\gamma$  mediates Paneth and also Goblet cell degranulation. Our identification of IFN- $\gamma$  as a potent secretagogue of Paneth cells describes a novel effector mechanism by which immune responses may regulate the gut microbiome.

## INTRODUCTION

Homeostasis of the intestine depends on a complex interplay between the gut microbiota, the intestinal epithelium and immune cells (Duerkop et al., 2009). The intestinal epithelium serves as a physical barrier to separate luminal microbes from the bodies' interior milieu. Innate and adaptive immune responses limit bacterial invasion after barrier dysfunction. Besides its passive role as physical barrier the epithelium also actively secretes antimicrobial proteins into the gut lumen (Mukherjee et al., 2008). In the small intestine Paneth cells (PCs) – highly specialized, terminally differentiated cells located at the bottom of the crypts of Lieberkühn – play a key role by releasing granules containing antimicrobial proteins like lysozyme and  $\alpha$ -defensins (also called cryptdins) (Clevers and Bevins, 2012). PCs act as niche cells for intestinal stem cells by providing Wnt, Notch and EGF signals (Sato et al., 2011) and their maturation depends on Wnt signaling (Van Es et al., 2005; Wehkamp et al. 2007).

The presence of functional PCs is essential for resistance against several enteric bacterial pathogens such as *Salmonella* and *Shigella* (Wilson et al., 1999; Fernandez et al., 2008) and to maintain a normal composition of the gut microbiota (Salzman et al., 2010). Infection with *Toxoplasmosis gondii*, which causes IFN- $\gamma$  dependent loss of PCs results in bacterial dysbiosis that was identified as a disease-mediating factor (Raetz et al., 2013). A number of gene mutations associated with human Crohn's disease affect PC function (Barrett et al., 2008; Wehkamp and Stange, 2010). Of note, allelic variants of *NOD2* that encodes an intracellular receptor of the bacterial cell wall component muramyl dipeptide are associated with decreased expression of defensins in humans and mice (Wehkamp et al., 2004; Kobayashi et al., 2005). Another risk gene, *ATGL1611*, encodes a protein involved in autophagy. Mice with hypomorphic *Atgl1611* mutations show PC defects, which is dependent on simultaneous infection with norovirus (Cadwell et al. 2008; Cadwell et al., 2010). PCs are also sensitive to endoplasmatic reticulum stress, as identified by mutations in the transcription factor gene XBP1 (Kaser et al., 2008).

Given the central role for PCs in gut mucosal immunity, it is crucial to understand the mechanisms that control secretion of antimicrobial proteins. While granule release into the lumen may occur continuously at a low rate, diverse stimuli are known to trigger collective discharge of PCs (Ayabe et al., 2000). In particular, neurotransmitters that activate muscarinic acetylcholine receptors are potent inducers of PC degranulation (Sato et al., 1992). In germ-free mice, recolonization of the intestine by bacteria results in rapid degranulation that is completely blocked by muscarinic antagonists (Sato, 1988). These observations indicate that acetylcholine releasing enteric neurons act as a stimulus. On the other hand PCs respond to bacterial presence in a Myd88/Toll like receptor (TLR) dependent fashion (Brandl et al., 2007; Vaishnava et al., 2008). Both oral administration of TLR ligands *in vivo* (Rumio et al 2011), as well as stimulation of isolated murine crypts with bacterial ligands (Ayabe et al., 2000) have been described. In addition, acute intestinal damage e.g. after ischemia/reperfusion, (Lee et al., 2013) as well as activation of iNKT cells induces PC degranulation (Nieuwenhuis et al., 2009), suggesting a role for unknown immune cell derived factors.

Clearly, PC degranulation underlies complex control but identification of direct stimuli has been challenged by intrinsic crosstalk between the different tissue compartments *in vivo*. Here we have set out to characterize PC degranulation directly using the purely epithelial 'organoid' model (Sato et al., 2009). In 3D matrigel, organoids can be generated from single Lgr5-positive intestinal stem cells. The organoids recapitulate normal crypt-villus architecture and undergo homeostatic self-renewal. These 'mini guts' are closed structures, consisting of a single lining of epithelial cells, polarized with their apical brush border facing the lumen and budding protrusions that reflect the basolateral side of crypts. PCs can be readily identified in the crypt equivalents using light microscopy or by marker expression. PCs, present in each budding crypt have been demonstrated to play a critical role as stem cell niche by secretion of factors like Wnt3 (Sato et al., 2011a; Farin et al., 2012). Here we use this unique cellular model system to address which primary signals can induce PC degranulation. We report a differential sensitivity of PCs for bacterial ligands, cytokines and muscarinic stimulation and identify IFN- $\gamma$  as a critical immune mediator for the secretion of antimicrobial factors into the gut lumen.



## RESULTS

### **Isolated Paneth cells are refractory to bacterial stimulation.**

To test if PC degranulation is induced in direct response to bacterial stimulation, we studied the effect of bacterial antigens that were added to the culture medium of small intestinal organoids. Twelve hours after addition of muramyl dipeptide (MDP), lipopolysaccharide (LPS), flagellin, peptidoglycan (PGN), or heat inactivated *E. coli* PC granules were visualized using UEA-1 (*Ulex europaeus* agglutinin 1) lectin staining (Fig. 1A). We observed no change in organoid morphology and normal PC granules under all conditions tested. As a positive control cholinergic stimulation with Carbamylcholine (Cch) caused the complete loss of epithelial granules demonstrating physiologic competence of cultured PCs similar to their counterparts *in vivo* (Sato et al., 1992). The striking absence of any PC secretory response to bacterial stimuli was quantified by Western blot analysis of lysozyme content in organoids that were mechanically sheared and extensively washed to separate the pool of intracellular lysozyme from the pool that had been secreted into the crypt lumen (Fig. 1BC).

Addition of the various agents through the culture medium results in basolateral exposure to bacterial antigens, similar to disruption of the epithelial barrier *in vivo*. We next explored the effects of exposure on both the apical and basal sites. For this, we generated organoid fragments by mechanical shearing. These were resuspended in culture medium containing the panel of bacterial agents. Lysozyme content was quantified after 2 hours at 37°C – an experimental setting analogous to the stimulation of freshly isolated crypts used previously (Ayabe et al., 2000). No significant decrease of the epithelial lysozyme content was measured for any of the bacterial stimuli, while controls using Cch again resulted a complete discharge of PCs (Fig. 1BC). We conclude that bacterial stimulation from both basolateral and apical epithelial sides represents no direct trigger for PC degranulation in our system.

By RT-PCR analysis we found that the expression of microbial pattern receptors (*Tlr2,3,7,8,9*, *MD-2* and *Cd14*) is maintained in organoids compared to freshly isolated crypts (Fig. 1D), arguing against non-responsiveness due to transcriptional down-regulation. Western Blot analysis of TNF- $\alpha$  stimulated organoids showed strong induction of I $\kappa$ B $\alpha$  phosphorylation (Fig. 1E). Inducibility of NF $\kappa$ B-pathway activity suggests that upstream events in the TLR signaling mediate refractoriness to bacterial stimuli.

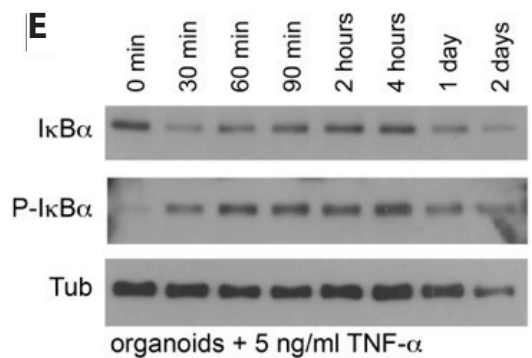
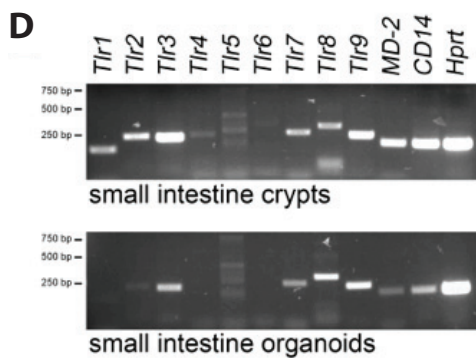
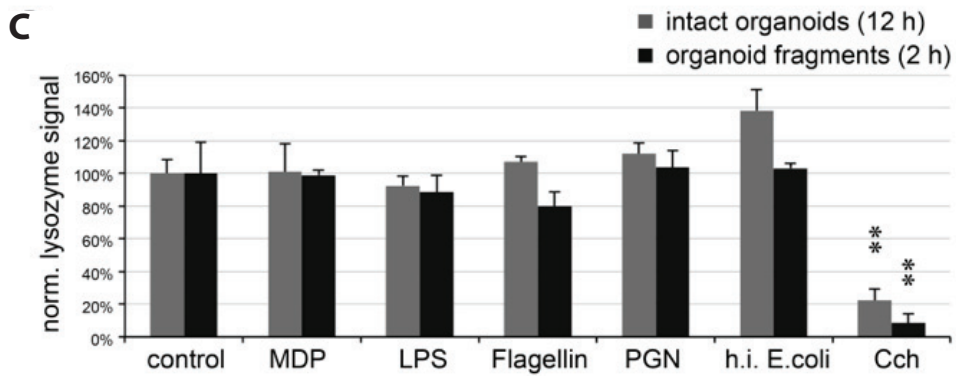
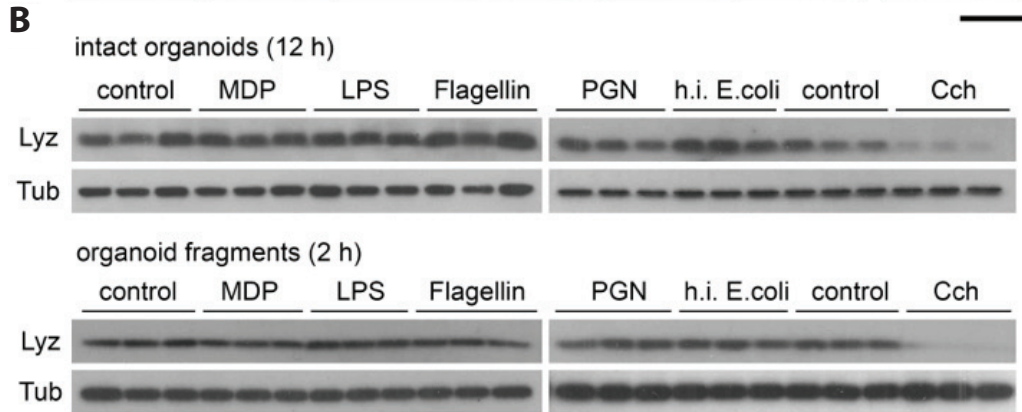
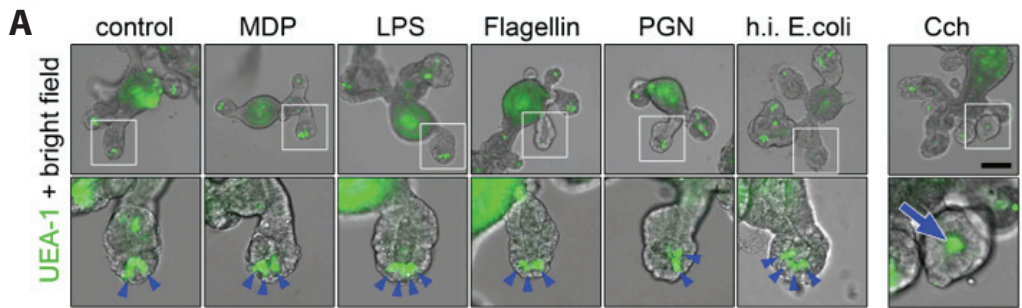


## Figure 1: Paneth cell degranulation in intestinal epithelial cultures after muscarinergic but not after bacterial stimulation.

A UEA-1 lectin staining of small intestinal organoids 12 hours after addition of diverse bacterial agents to the culture medium. Maintenance of PC granules (blue arrowheads) in the presence of 100 µg/ml muramyl dipeptide (MDP), 1 µg/ml Lipopolysaccharide (LPS), 0.1 µg/ml Flagellin, 10 µg/ml Peptidoglycan (PGN), or heat inactivated *E. coli* bacteria (h.i. *E. coli*). Carbamylcholine (Cch, 25 µM) caused release of PC granules into the crypt lumen (blue arrow). Whole organoids and magnified crypts are shown. Scale bars 100 µm. B Western Blot analysis of epithelial lysozyme content. Basolateral stimulation of intact organoids in matrigel for 12 hours (top), or fragmented organoids in suspension for 2 hours (apical and basal stimulation, bottom). Cells were washed to separate luminal lysozyme. Tubulin was probed for normalization. Experiments were performed in three independent wells. C Quantification of epithelial lysozyme content from Western Blot data shown in B. Densitometric analysis of lysozyme signals normalized to Tubulin expression. Error bars show standard deviation. Significant changes compared to controls are found after Cch treatment only (\*\* :  $P < 0.01$ ; t-test). D Expression of microbial pattern receptors; RT-PCR analysis using cDNA from isolated crypts and cultured organoids. Hprt was analyzed for normalization. E NFκB signaling in organoids after TNF-α stimulation (5 ng/ml). Time course experiment: Western Blot shows decrease of total IκBα levels and induction of Phospho-IκBα. Tubulin was probed for normalization.

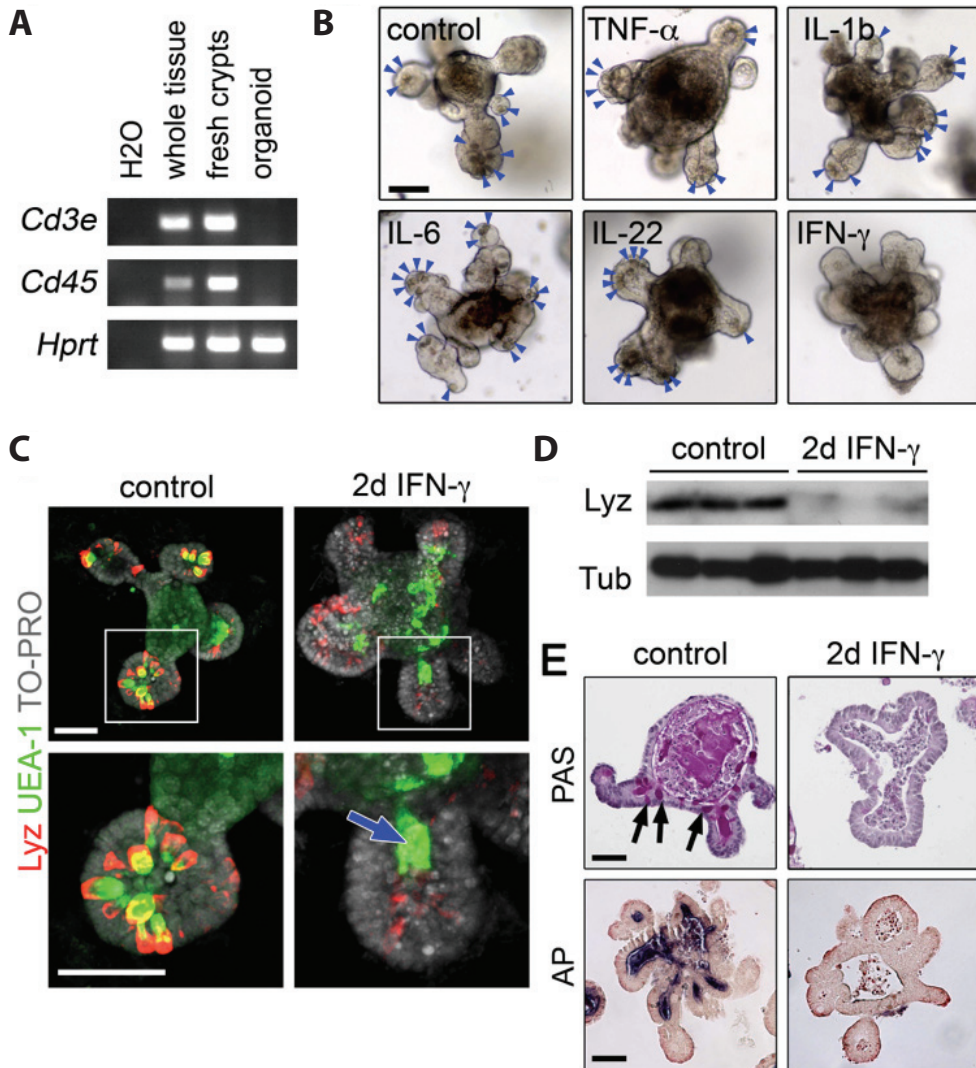


**Figure 2: IFN- $\gamma$  induced Paneth cell degranulation.**

A Presence of leukocytes as shown by RT-PCR analysis of Cd3e (T-cells) and Cd45 (leukocytes) in freshly isolated crypts but not in organoids from small intestine. Hprt expression was used for normalization. B Morphological effects of cytokines on PCs. Small intestinal organoids 2 days after addition of mouse recombinant TNF- $\alpha$ , IL-1b, IL-6 or IL-22 (all at 20 ng/ml) or IFN- $\gamma$  (5 ng/ml) to the culture medium. PCs were observed in all cultures (blue arrowheads) except in IFN- $\gamma$  treated organoids. C IFN- $\gamma$  treatment (2 days; 5 ng/ml) causes loss of lysozyme immunostaining in PCs (red) and accumulation of UEA-1 positive mucus (green) in the crypt lumen (blue arrow). 3D projected confocal images, nuclei (grey) stained with TO-PRO3. D Western Blot quantification of epithelial lysozyme content 2 days after stimulation using 1 ng/ml IFN- $\gamma$  (performed in triplicates as in Fig. 1B). E Histological analysis after IFN- $\gamma$  treatment (2 days; 5 ng/ml). PAS staining shows loss of mucus-filled Goblet cells (black arrow) and AP staining shows reduced differentiation of enterocyte brush border. All scale bars 50  $\mu$ m.

### **A direct role for IFN- $\gamma$ in loss of Paneth cells granules.**

We hypothesized that PC degranulation observed in freshly isolated intestinal crypts (Ayabe et al., 2000) might depend on bacterial sensing by co-isolated leukocytes. Using RT-PCR analysis we indeed found that *Cd3e* and *Cd45* expressing immune cells were present in primary crypt preparations but not in established organoid cultures (Fig. 2A). We subsequently aimed to identify immune cell mediators that might indirectly cause PC degranulation following bacterial stimulation by testing the activity of a number of (pro-inflammatory) cytokines. We found that 2 day treatment with 1 ng/ml IFN- $\gamma$  caused complete loss of PC granules as observed by morphology, lysozyme immunostaining and measurement of epithelial lysozyme content (Fig. 2B-D). In contrast, PCs were morphologically unaffected in the presence of recombinant TNF- $\alpha$ , IL-1b, IL-6 or IL-22 (all at 20 ng/ml; 2 days; Fig. 2A). Histologically, IFN- $\gamma$  treated organoids were characterized by a loss of mucus-containing goblet cells (Periodic acid-Schiff [PAS] staining) and mature enterocytes (as observed by alkaline phosphatase [AP] staining) (Fig. 2E), demonstrating a direct effect of this cytokine also on the other differentiated cell lineages.

### **Maintenance of Paneth cells after IFN- $\gamma$ induced degranulation.**

Recent experiments have shown that prolonged IFN- $\gamma$  exposure in vivo during *T. gondii* infection results in a complex intestinal pathology that is characterized but also caused by the loss of PCs (Raetz et al., 2013). The directness of this phenotype, however, was not addressed. We therefore tested the consequences of IFN- $\gamma$  exposure during several organoid passages and found a successive and dose-dependent reduction in organoid number (Fig. 3A). By FACS analysis of cleaved-Caspase3 stained cells revealed a strong apoptotic response 24 hours after addition of IFN- $\gamma$  (Fig. 3B). Together these data show that IFN- $\gamma$  directly affects epithelial homeostasis by induction of programmed cell death. Next we performed immunostainings using CD24 and Dll1 as membrane markers to trace PCs and their secretory precursors (Sato et al., 2011a; van Es et al., 2012). Despite the absence of granules we found clear immunoreactivity for both markers 2 days after IFN- $\gamma$  treatment (Fig. 3C compare Fig. 2). In addition, the preserved mRNA expression of *Defa6* at the budding-tips of treated organoids (Fig. 3D) showed that during the initial response to IFN- $\gamma$ , PCs are preserved from apoptosis and thus massively degranulate. Expression of the intestinal stem cell marker *Olfm4* (Van der Flier et al. 2009) showed that discharged PCs could still provide the obligatory stem cell niche signals (Fig. 3D). 4 days after withdrawal of IFN- $\gamma$  from the culture medium the organoid morphology had normalized and granules were restored suggesting a recharging of PCs granules (Fig. 3E).

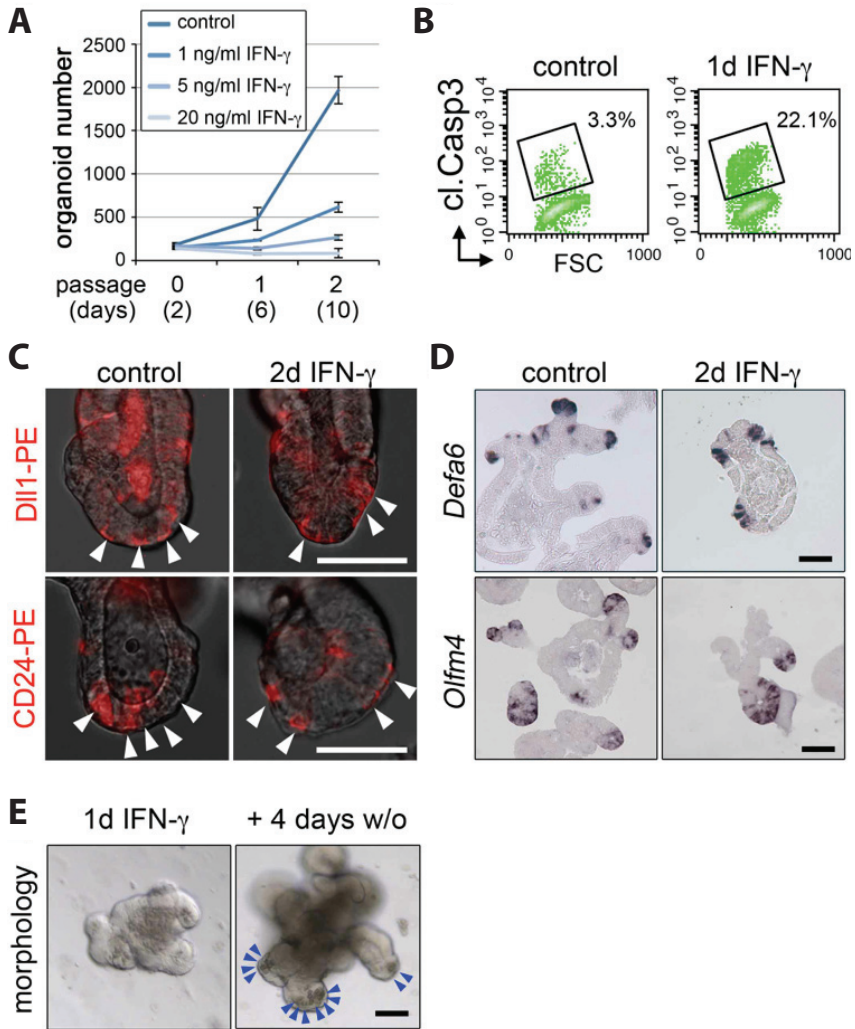


**Figure 3: Reduced organoid growth but maintenance of Paneth cells after IFN- $\gamma$ .**

A Growth curve shows reduced expansion in the presence of IFN- $\gamma$ . Mean organoid number of  $n = 3$  independent wells  $\pm$  standard deviation. IFN- $\gamma$  at all concentrations tested caused a significantly reduced number compared to controls (passage 1:  $P < 0.05$  and passage 2:  $P < 0.001$ , respectively, as determined by t-test). B Quantification of apoptosis by FACS analysis. Cleaved Caspase3 immunostaining (plotted vs. forward scatter, FSC) shows increased number of apoptotic cells 1 day after IFN- $\gamma$  treatment (5 ng/ml). C Immunostaining of the membrane markers Dll1 and CD24 shows maintenance of PCs 2 days after stimulation with 5 ng/ml IFN- $\gamma$ . PE conjugated antibodies were used. D In situ hybridization analysis shows maintained expression of the PC marker Defa6 and the stem cell marker Olfm4 after IFN- $\gamma$  treatment (5 ng/ml for 2 days). E PC granules reform after 1 day treatment with 5 ng/ml IFN- $\gamma$  and subsequent culture for 4 days in normal medium. Morphology images, blue arrowheads show PC granules. All scale bars 50  $\mu\text{m}$ .

### **IFN- $\gamma$ triggers rapid and collective exocytosis of Paneth cells.**

To study the kinetics of the degranulation process in more detail we used time-lapse imaging. PC granules were labeled with ZP-1, a fluorescent and membrane permeable  $Zn^{2+}$  chelator (Giblin et al., 2005). Organoid morphology and marker distribution was followed after IFN- $\gamma$  addition using confocal microscopy (Fig. 4A and Supplemental Movies 1-3). We found that degranulation was not synchronous within a given crypt, but that individual PCs one by one extruded their fluorescent label. We observed the collective extrusion of all cellular granules rather than a continuous exocytosis of individual vesicles. On a cellular level this process was completed within several minutes and occurred in an 'all-or-nothing' fashion. Between different organoids, the onset and completion of degranulation was variable, but clearly dependent on the IFN- $\gamma$  concentration (6-12 hours at 5 ng/ml and 4-8 hours with 20 ng/ml IFN- $\gamma$ ).

Transmission electron microscopy showed a collective extrusion of PC granules (Fig. 4B, 6 hour time point, 5 ng/ml IFN- $\gamma$ ). Here, generation of large apical vacuoles was observed, reminiscent of the ultrastructural changes after muscarinergic stimulation *in vivo* (Satoh et al., 1992). After secretion into the crypt lumen the electron-dense granules dissolved and the ZP-1 fluorescent signal rapidly dispersed (Fig. 4B, Supplemental Movies 2,3). Twelve hours after treatment (20 ng/ml IFN- $\gamma$ ), the crypts showed maintenance of discharged PCs that were identified by the presence of small residual electron dense granules and their localization at the crypt bottom adjacent to stem cells. We found no indication of PC mitochondrial damage that has been observed by electron microscopy after IFN- $\gamma$  exposure during *T. gondii* infection (Raetz et al., 2013), arguing that longer exposure to IFN- $\gamma$  and/or additional factors are required to induce elimination of PCs. Together, our observations demonstrate that antimicrobial PC products can be rapidly mobilized by an immune alert signal.

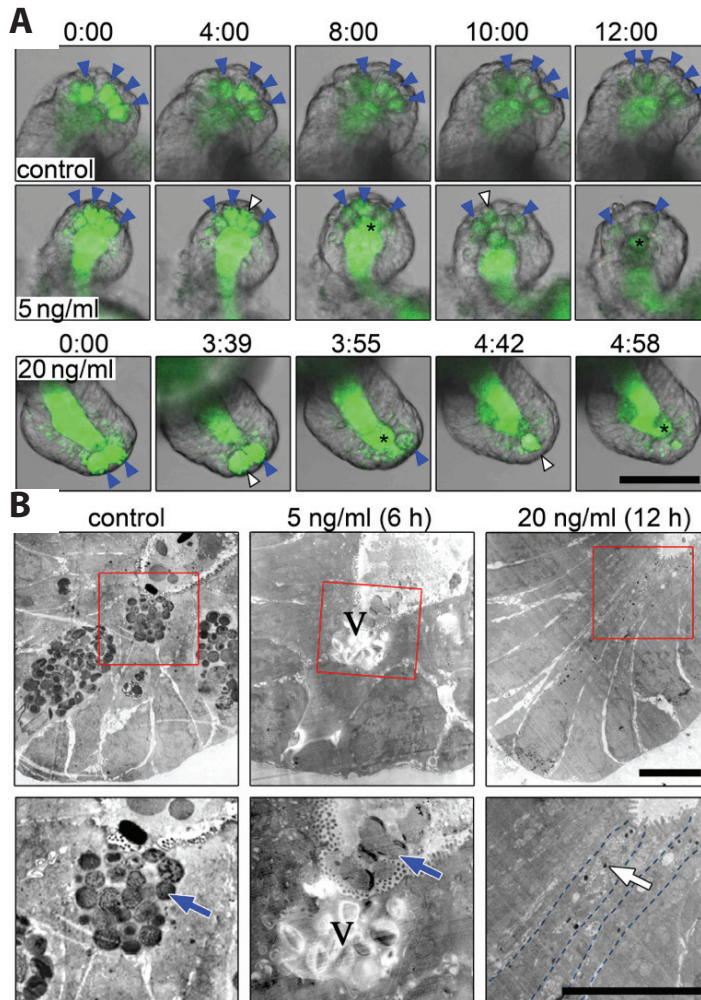


### Figure 4: 'All-or-nothing' degranulation after IFN- $\gamma$ treatment.

A Time-lapse analysis of PC degranulation (still images of Supplemental movies 1-3). Granules were labeled with the fluorescent  $Zn^{2+}$  chelator ZP-1 and followed by life microscopy. Time after addition of IFN- $\gamma$  is indicated on top (hours:minutes). Control cultures (top row) maintain granulated PCs (blue arrowheads). 5 ng/ml IFN- $\gamma$  causes extrusion of granules to the crypt lumen (asterisks; middle row). Black arrowheads mark individual PCs that release their entire granules during the next imaging interval. Note that the fluorescent signal decreases due to bleaching. High dose IFN- $\gamma$  (20 ng/ml; bottom row) leads to more rapid granule loss. Scale bar 50  $\mu$ m. B Ultrastructural analysis of PC degranulation. Transmission electron microscopic images of control cultures with intact electron-dense secretory granules (blue arrow; left panels). 6 hours after addition of 5 ng/ml IFN- $\gamma$  PC are observed that extrude their entire granules (blue arrow; middle panels). Formation of large apical vacuoles is observed (V). After 12 hours (20 ng/ml IFN- $\gamma$ ; right panels) PCs contain few granules of reduced size (white arrow). PC membranes were labeled with hatched lines. Magnified regions (red boxes) are shown below. Scale bars 5  $\mu$ m.



### **IFN- $\gamma$ -mediated PC degranulation in response to stimulated iNKT cells.**

Next we studied if endogenous cytokine levels that are released from stimulated leukocytes are sufficient to induce PC degranulation. We used the mouse invariant natural killer T (iNKT) hybridoma line DN32.D3 that secretes IFN- $\gamma$  and other immune mediators upon CD1D-dependent antigen presentation of the lipid antigen  $\alpha$ -galactosylceramide ( $\alpha$ -GC) (Nieuwenhuis et al., 2009). Conditioned cell culture supernatants (SNs) of control iNKT cells and after  $\alpha$ -GC stimulation in the presence or absence of CD1D expressing Hela cells were produced and transferred to organoids (see scheme in Fig. 5A). Stimulation of iNKT cells caused a pronounced release of IFN- $\gamma$  as observed by ELISA (Fig. 5B). Two days after addition of SNs, PC degranulation was analyzed using UEA-1 lectin staining and Western blot quantification of residual epithelial lysozyme. We found strong degranulation that was dependent on both the bacterial stimulus and antigen presentation (Fig. 5C-E). Pretreatment with a neutralizing anti-IFN- $\gamma$  antibody efficiently blocked activity in SNs from activated iNKT cells (Fig. 5F) and also neutralized the effect of recombinant IFN- $\gamma$ . These results show that IFN- $\gamma$  (at physiologic levels) represents the main soluble mediator of PC degranulation from iNKT cells.

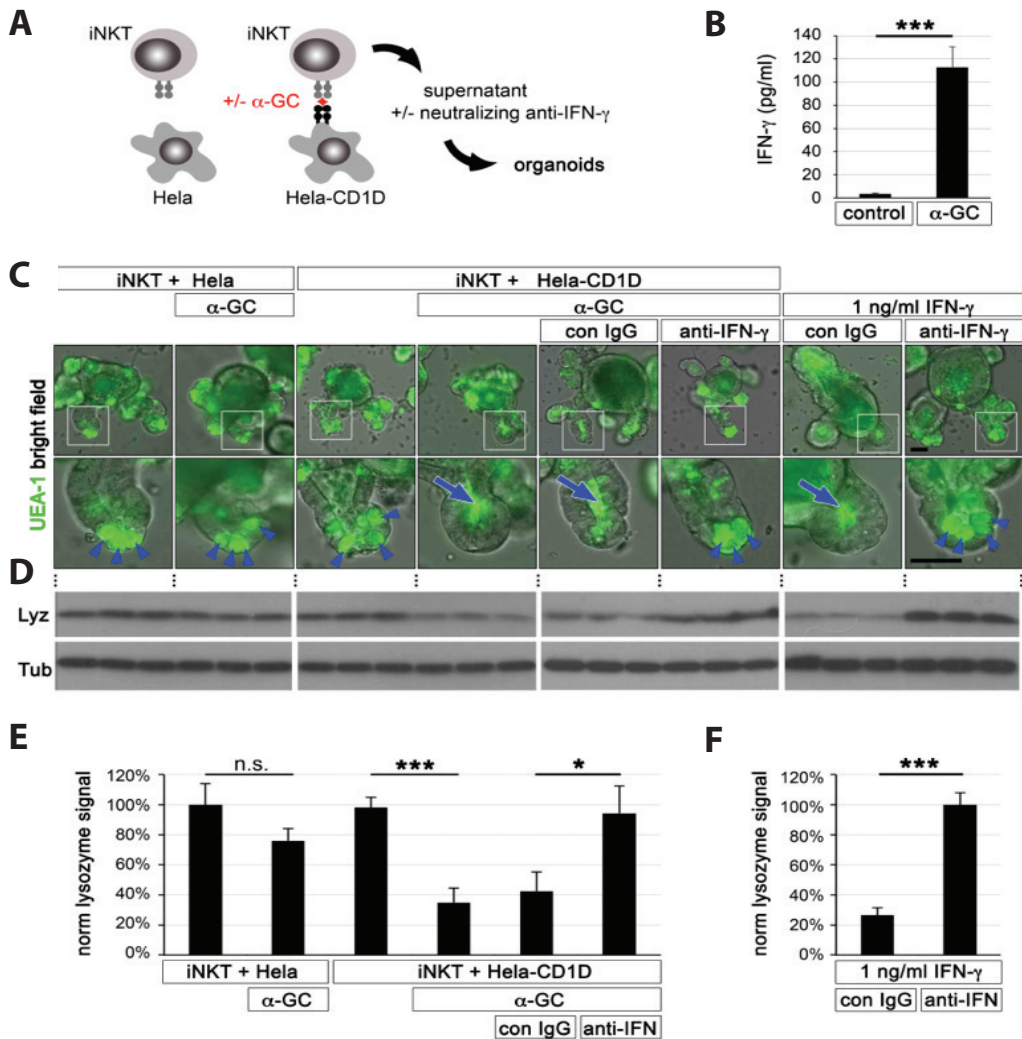


**Figure 5: Lipid antigen stimulation of iNKT cells triggers Paneth cell degranulation in an IFN- $\gamma$  dependent manner.**

A Experimental strategy. Cell culture supernatants (SNs) were collected from activated iNKT cells and transferred to the culture medium of small intestinal organoids. iNKT cell activation in the presence of the lipid antigen  $\alpha$ -galactosylceramide ( $\alpha$ -GC) and HeLa-CD1D antigen presentation. SNs were pre-incubated with neutralizing anti-IFN- $\gamma$  antibody or control IgG. B ELISA quantification of IFN- $\gamma$  secretion in SNs from control and  $\alpha$ -GC stimulated iNKT cells (both in presence of HeLa-CD1D cells). Average concentration of quadruplicate measurements is shown ( $\pm$  SD; \*\*\* :  $P < 10^{-4}$ ; t-test). C UEA-1 lectin staining of small intestinal organoids 2 days after addition iNKT SNs. PC granules (blue arrowheads) are discharged to the crypt lumen (blue arrows) after iNKT stimulation. Anti-IFN- $\gamma$  treatment blocks the activity of SNs and recombinant IFN- $\gamma$ . Scale bars 100  $\mu$ m. D Western Blot analysis of epithelial lysozyme content; conditions as in B. Organoids were fragmented and washed to separate luminal lysozyme. Tubulin was probed for normalization. Experiments performed in three independent culture wells. E F Quantification of epithelial lysozyme content of experiments shown in D. Densitometric analysis of Western Blot signals that were normalized to tubulin expression levels. Error bars show standard deviation of triplicate cultures. Significant changes were labeled (\* :  $P < 0.05$ ; \*\*\* :  $P < 0.001$ ; t-test).

## **IFN- $\gamma$ acts as a potent intestinal secretagogue following T cell activation in vivo.**

Acute T cell stimulation using anti-CD3 injection in vivo causes a severe but transient intestinal pathology that is characterized by epithelial apoptosis and massive villus blunting (Merger et al., 2001; Miura et al., 2005). However, it is unclear which of these effects can be attributed to IFN- $\gamma$  and whether PC granules are released upon immune activation in vivo. We addressed these questions genetically by intraperitoneal injection of anti-CD3 antibody in C57BL/6 wild-type and IFN- $\gamma$  mutant mice. Intestines were collected for lysozyme immunohistochemistry 24 hours later. In wild-type mice, anti-CD3 injection caused a marked reduction of the number of lysozyme-positive PCs that were counted per crypt section (Fig. 6A), confirming our in vitro observation that PC granules are rapidly mobilized after immune stimulation. This effect was highly significant and strongest in the proximal intestine (duodenum), where the number of stained PCs was reduced by half (Fig. 6B;  $n = 7$ ;  $P < 10^{-6}$ ). In homozygous IFN- $\gamma$  mutant mice, however, lysozyme-positive PCs were maintained in all regions of the intestine, demonstrating that IFN- $\gamma$  is specifically required for granule loss. Induction of apoptosis was quantified by counting the number of cleaved Caspase3-positive crypts cells and was unaffected in IFN- $\gamma$  mutant intestines, arguing that anti-CD3 treatment causes a strong cytotoxic T cell response in both genotypes (Fig. 6CD). The severe villus damage that was most apparent in distal regions of the intestine (ileum) was ameliorated in IFN- $\gamma$  mutant mice (Fig. 6E). Moreover, PAS staining showed an IFN- $\gamma$  dependent release of Goblet cell mucus of the colonic epithelium (Fig. 6E). In colon organoids extrusion of Goblet cell mucus was recapitulated after IFN- $\gamma$  treatment (Fig. 6F), demonstrating a more general role of this cytokine as a direct intestinal secretagogue for both Paneth and Goblet cells.

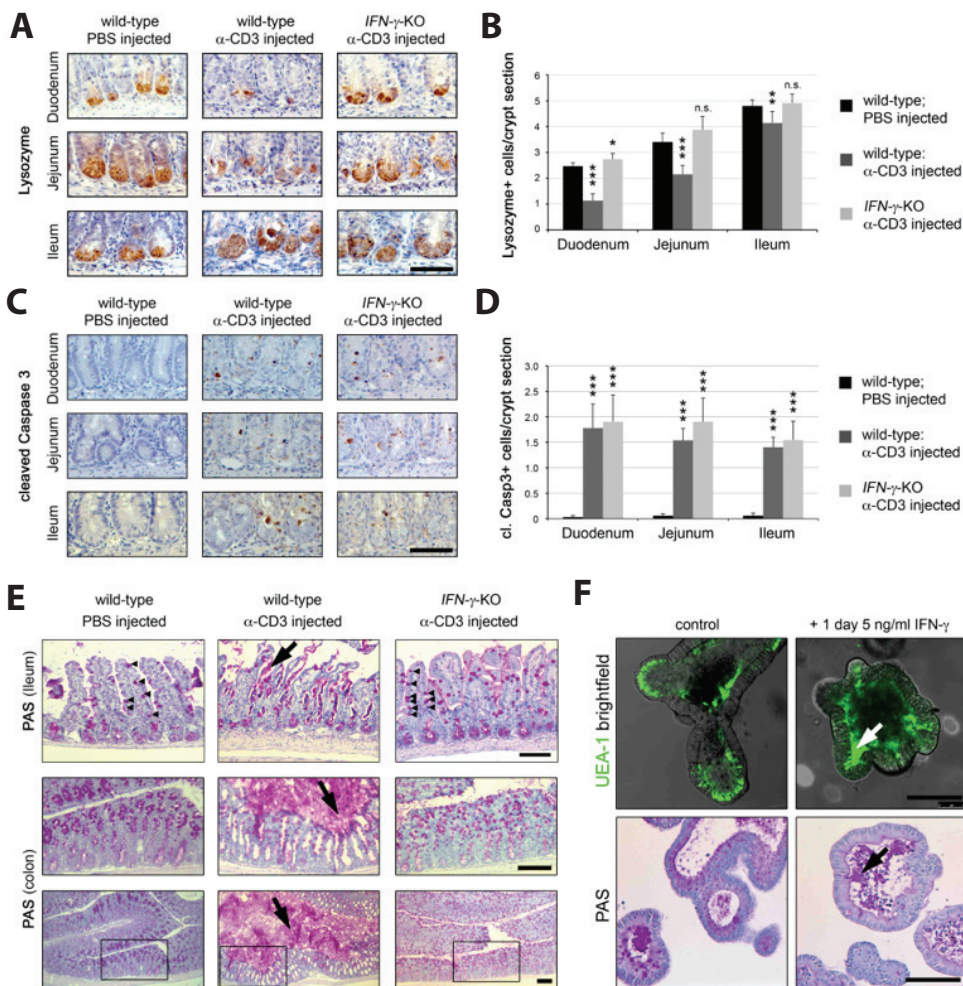


**Figure 6: IFN- $\gamma$  acts as potent Paneth and Goblet cell secretagogue after T cell activation in vivo.**

A Lysozyme immunostaining of PC granules in control mice (C57BL/6; PBS injected; left) or 24 hours after T-cell activation by intraperitoneal injection of anti-CD3 (50  $\mu$ g/mouse; middle). Marked reduction of lysozyme in proximal/middle regions (duodenum/ileum) and weaker in distal regions (ileum) of the small intestine. In IFN- $\gamma$  mutant mice PC granules are unaffected (right). B Quantification of lysozyme positive cells (as in A). PCs counted per crypt section in  $n = 7$  animals per condition (45 crypts/animal/region). Mean PC number  $\pm$  SD is shown. \*:  $P < 0.05$ ; \*\*:  $P < 0.01$ ; \*\*\*:  $P < 10^{-4}$ ; t-test compared to control-injected mice. C Cleaved Caspase3 immunostaining of apoptotic cells on intestinal sections 24 hours after anti-CD3 stimulation. Pronounced inflammatory response in wild-type and IFN- $\gamma$  mutant mice with similar induction of apoptosis in crypts. D Quantification of cleaved Caspase3 positive cells (as in C). Counted in  $n = 7$  animals per condition (45 crypts/animal/region). Mean cell number  $\pm$  SD is shown. \*\*\*:  $P < 10^{-6}$ ; t-test compared to control-injected mice. E PAS staining shows widespread extrusion of Goblet cell mucus (black arrows) in wild-types but not IFN- $\gamma$  mutants. In the ileum (top row) Goblet cells on one villus were labeled with black arrowheads. Note the IFN- $\gamma$  dependent villus damage. In the colon magnified regions (middle) and overview images (bottom row) are shown. F Secretion of Goblet cell mucus in colon organoids upon IFN- $\gamma$  treatment (arrows; 24 hours after addition of 5 ng/ml IFN- $\gamma$ ). Top: UEA-1-Alexa488 lectin staining and bottom: PAS staining. Scale bars 100  $\mu$ m in A, C, F and 200  $\mu$ m in E.

## DISCUSSION

Gut mucosal immunity is controlled by complex interactions amongst epithelium, microbiota and the immune system, which complicates the dissection of signaling mechanisms. Here we show using pure epithelial cultures, that release of antimicrobial PC products is directly controlled by immune signals. IFN- $\gamma$  was identified as the main mediator of PC degranulation after CD1D dependent stimulation of iNKT cells (Nieuwenhuis et al., 2009) and after anti-CD3 stimulation of T cells *in vivo*. We propose that the pro-inflammatory cytokine may represent a 'danger signal' that allows PCs to react on microbial challenges. The exact cellular source of IFN- $\gamma$  – most likely – depends on the physiological situation. Activation of intra-epithelial lymphocytes could represent one paracrine source of IFN- $\gamma$  (Guy-Grand et al., 1998; Cheroutre et al., 2011).

Organoid cultures have allowed us to visualize the rapid and complete discharging of PCs. The same was also achieved by muscarinergic stimulation, but cultured PCs were insensitive to a broad spectrum of microbe-associated molecular patterns, in contrast to previous data obtained using freshly isolated crypts (Ayabe et al., 2000). While evidence suggests that microbial patterns can directly trigger PC function *in vivo* (Rumio et al., 2011; Brandl et al., 2007; Vaishnava et al. 2008), lack of epithelial *Tlr4* and *Tlr5* expression indicates an indirect effect after stimulation of primary crypts with the cognate ligands LPS and flagellin (Ayabe et al., 2000). Also the fact that degranulation after bacterial inoculation of germ-free mice is inhibited by atropine favors an indirect mechanism, such as involvement of acetylcholine secreting enteric neurons (Sato, 1988). Interestingly, bacterial colonization was required for PC loss after *T. gondii* infection (Raetz et al., 2013). Here however, bacterial sensing (and Myd88 expression) by T cells was required and not in the epithelium, demonstrating that continuous immune stimuli act on PCs in this model. Given the broad distribution of bacterial antigens within the gut lumen non-responsiveness to microbial patterns could be beneficial to avoid continuous stimulation by commensals.

Our study shows that organoid cultures represent a useful model to address PC function: 1) The use of 'pure' epithelium prevents indirect effects of co-isolated (intraepithelial) leukocytes that are unavoidable in primary material. 2) Organoids, even ex matrigel, are less fragile than fresh crypts; the latter start to degenerate instantly after isolation and allow short stimulations only (max. 1 hour). 3) Related to this, organoids offer a more sensitive system as full

PC discharging can be achieved, while maximal secretion using fresh tissue never exceeds more than 20-30% under the conditions used (Ayabe et al., 2000).

We found that IFN- $\gamma$  acts as a potent intestinal secretagogue both on Paneth and Goblet cells. Goblet cell mucus serves as matrix to retain and concentrate antimicrobial PC products (Meyer-Hoffert et al., 2008). The concerted secretion of these two cell types could therefore synergize to form an efficient buffer zone against bacteria. Given that T cell activation can cause strong damage to the intestine such as apoptosis and disruption of the intestinal barrier (Merger et al., 2002; Miura et al., 2005) this massive release of antimicrobial factors might help to limit bacterial entry. However, inappropriate IFN- $\gamma$  stimuli such as present chronic norovirus infections in *Atg16L1* mice or during toxoplasmosis can cause granule defects or PC loss (Cadwell et al., 2010; Raetz et al., 2013), arguing that a proper balance of inflammatory signals is crucial. Future studies should address if PC dysfunction and associated changes of the gut flora are causally involved in other IFN- $\gamma$  driven IBD models (Kontoyiannis et al., 2002; Saha et al., 2010). IFN- $\gamma$  dependent pathologies such as graft vs. host disease, and celiac disease have been associated with reduced PC granules previously (Nilsen et al., 1998; Di Sabatino et al., 2008; Erigucchi et al., 2012). Given that organoid cultures can be established from human biopsies (Sato et al., 2011b), the phenotypic characterization of PC function *in vitro* could provide an important diagnostic tool to dissect disease mechanisms in these patients. The pharmacologic modulation of IFN- $\gamma$  signaling to control PC function and survival could allow a new strategy to improve host defense.

## METHODS

### Organoid culture

Small intestinal and were established from wild-type C57BL/6 mice, cultured as described previously (Sato et al. 2009; Farin et al., 2012) and passaged weekly at a 1:5 split ratio. Organoids were stimulated for the indicated times by addition of recombinant murine IFN- $\gamma$  (1 to 20 ng/ml; R&D Systems), mTNF- $\alpha$  (Peprotech), mL-1b (Sigma-Aldrich), mL-6 (eBioscience), mL-22 (R&D Systems; all at 20 ng/ml) or Cch (25  $\mu$ M, Sigma-Aldrich). Bacterial stimuli were muramyl dipeptide (100  $\mu$ g/ml; Invivogen), lipopolysaccharide (1  $\mu$ g/ml: Sigma-Aldrich from *E. coli* 026:B7), flagellin (0.1  $\mu$ g/ml; Invivogen from *S. typhimurium*) and peptidoglycan (10  $\mu$ g/ml; Invivogen from *S. aureus*). Log phase *E. coli* bacteria (strain K-12) were heat inactivated for 10 min at 98°C; per organoid cell 100 bacteria were added. Mouse colon organoids were cultured as described previously for human colon cultures (Sato et al., 2011b). Colon organoids were differentiated towards Goblet cells by addition of  $\gamma$ -secretase inhibitor DAPT (10  $\mu$ M; Sigma) for 5 days prior to IFN- $\gamma$  treatment. For stimulation of fragmented epithelia, organoids were collected in cold medium, mechanically sheared using glass Pasteur pipettes. Separation of crypts was confirmed by light microscopy and 100 crypts each were stimulated for 2 hours at 37°C, 5% CO<sub>2</sub>.

### RT-PCR analysis

DNAse treated RNA was used for RT-PCR analysis as described (Farin et al., 2012). For a list of primers used see Supplemental Table 1.

### Lysozyme quantification and Western blotting

Organoids were collected in cold medium, sheared by pipetting to generate epithelial fragments that were subsequently washed twice in ice-cold medium to separate cells from debris and lysozyme secreted into the crypt lumen. Samples were lysed using RIPA buffer (50 mM Tris-HCl pH 8.0; 150 mM NaCl; 0.1% SDS; 0.5% Na-Deoxycholate; 1% NP-40) containing Complete™ protease and phosphatase inhibitors (Roche). Protein content was quantified using standard Bradford assay. 10  $\mu$ g of protein was run on a 14% SDS page and subsequently transferred to a PVDF membrane and probed with rabbit-anti-lysozyme (Dako; 1:10000 in TBS-T 5% milk) and for normalization mouse-anti- $\alpha$ -tubulin (Sigma-Aldrich; 1:3000). Following washes membranes were incubated with secondary HRP conjugated antibodies (goat anti-rabbit HRP 1:20000 and rabbit anti-mouse 1:6000 both G&E healthcare) and exposed to X-ray films using ECL reagents (G&E Healthcare) and signals were quantified

using ImageJ software. Other antibodies used were mouse-anti  $\text{I}\kappa\text{B}\alpha$  (clone L35A5) and mouse-anti-Phospho- $\text{I}\kappa\text{B}\alpha$  (Ser32/36; clone 5A5; both from Cell Signaling Technology).

### **Organoid stainings, life microscopy and transmission electron microscopy**

Whole-mount organoid immunofluorescence and immunohistochemistry, histological stainings and *in situ* hybridization on formalin fixed paraffin sections organoids were performed as described (Farin et al., 2012). Antibodies used were rabbit-anti-lysozyme (Dako; 1:500) and rabbit-anti-cleaved Caspase-3 (Cell Signaling). For lectin staining organoids were fixed in matrigel (2% PFA; o/n at 4°C). After permeabilization using 0.2 % Triton X 100 organoids were stained by addition of FITC-coupled *Ulex europaeus* lectin (UAE-1-FITC; Sigma Aldrich; 5  $\mu\text{g}/\text{ml}$ , 1 hour at RT), washed and documented on an EVOS *fl* inverse fluorescence microscope (Advanced Microscopy Group). For membrane stainings organoids were collected in cold medium and incubated (unfixed) with PE conjugated monoclonal antibodies anti-CD24 (clone M1/69) or anti-Dll1-PE (clone HMD1-5; both from eBioscience; final concentration of 1  $\mu\text{g}/\text{ml}$ ) for 1 hour on ice, following washes and documentation on an EVOS *fl* microscope.

For life cell imaging organoids were seeded on glass-bottom plates in drops of 50 % matrigel/ 50% medium to facilitate dye penetration. After 3 days of culture PC granules were labeled by addition 10  $\mu\text{M}$  ZP-1 (Santa Cruz Biotech.) to the culture medium 16 hours, before the cultures were washed twice with  $\text{CO}_2$  equilibrated warm medium and transferred to the culture chamber (37°C; 5 %  $\text{CO}_2$ ; 20%  $\text{O}_2$ ) of a Leica SP5 confocal microscope. Images acquired 15 min intervals using low laser power to avoid bleaching.

Transmission electron microscopy was done as described previously (Sato et al. 2009).

### **Flow cytometry**

Organoids were collected in in TrypLE™ solution (Life Technologies) and single cell suspensions were obtained after 2 cycles of mechanic break-up (using narrow-tipped pulled glass pasteur pipettes) and incubation at 37 °C (5 min). Cells were washed twice in PBS 1% BSA, and resuspended at RT in 500  $\mu\text{l}$  PBS including 1 % BSA and 2000 U/ml DNaseI (Roche). Cells were fixed by addition of an equal volume of 4 % Paraformaldehyde (in PBS) for 15 min at RT, before washing, permeabilization using 0.1% Triton X100 and antibody incubation (all in PBS 1 % BSA) using rabbit-anti-cleaved Caspase-3 (as above; 1:20 dilution; 1 hour at RT). After washes cells were incubated with



Alexa-488 coupled secondary antibody (from Molecular probes; 1:50 dilution; 30 minutes at RT) before washes, filtering (40 µm mesh) and measurement on a FACSCalibur (BD). Single cells were gated using FSC and SSC parameters.

### **iNKT conditioned medium**

Hela cells with or without stable overexpression of hCD1D were grown in DMEM supplemented with 10% heat inactivated bovine calf serum, 1 X Glutamax, 1 X penicillin/streptomycin (all from life technologies) and incubated with 100 ng/ml α-Galactosylceramide (α-GC) for 24 hours. Subsequently, iNKT DN32.D3 hybridoma cells (Bendelac et al., 1995) were incubated with Hela and Hela-CD1D cells for another 24 hours in serum free advanced DMEM/F12 medium supplemented with 1 X L-Glutamine, 1 X penicillin/streptomycin (life technologies), and rhIL-2 (10 U/ml; Proleukin; Novartis). Supernatants were centrifuged for cell depletion and included into the regular organoid medium as 40 % (v/v). IFN-γ levels were measured with a commercially available Elisa kit from BD Biosciences. A standard curve was recorded using recombinant mouse IFN-γ protein. In some experiments SNs were treated with functional grade anti-mouse IFN-γ monoclonal (clone XMG1.2) or rat IgG1 K isotype control (clone eBRG1; both from eBioscience; final concentrations 0.5 µg/ml) 30 minutes prior to addition to the organoids.

### **Mouse experiments and anti-CD3 injections**

All procedures were performed in compliance with local animal welfare laws, guidelines and policies. *IFN-γ* knockout (Dalton et al., 1993) and sex/age matched wild-type C57BL/6 mice were obtained from the Jackson Laboratory. 8-week-old wild-type and knock-out mice were injected with functional grade anti-mouse CD3e antibody (50 µg per animal; clone 145-2C11; eBioscience), or carrier alone (PBS). Mice were sacrificed 24 hours post injection and the intestine was processed for histology as described (van Es et al., 2005). For quantification of lysozyme and anti-cleaved Caspase-3 positive cells (antibodies as above) in each segment of the intestine 3 times 15 adjacent crypts were examined (45 crypts/animal/segment).

### **Acknowledgements**

We want to thank Maaïke van den Born, Harry Begthel, Jeroen Korving, Stieneke van den Brink and Karien Hamer for technical assistance and Bon-kyoung Koo for critical discussions.

## Author information

The authors disclose the following: H.C. is an inventor of several patents involving the organoid culture system. The remaining authors disclose no conflicts. HFF was supported by an EMBO long-term fellowship.

### References:

- Ayabe, T., D.P. Satchell, C.L. Wilson, W.C. Parks, M.E. Selsted, and A.J. Ouellette. 2000. Secretion of microbicidal alpha-defensins by intestinal Paneth cells in response to bacteria. *Nat. Immunol.* 1:113–118. doi:10.1038/77783.
- Barrett, J.C., S. Hansoul, D.L. Nicolae, J.H. Cho, R.H. Duerr, J.D. Rioux, S.R. Brant, M.S. Silverberg, K.D. Taylor, M.M. Barmada, A. Bitton, T. Dassopoulos, L.W. Datta, T. Green, A.M. Griffiths, E.O. Kistner, M.T. Murtha, M.D. Regueiro, J.I. Rotter, L.P. Schumm, A.H. Steinhardt, S.R. Targan, R.J. Xavier, C. Libioulle, C. Sandor, M. Lathrop, J. Belaiche, O. Dewit, I. Gut, S. Heath, D. Laukens, M. Mni, P. Rutgeerts, A. Van Gossom, D. Zelenika, D. Franchimont, J.-P. Hugot, M. de Vos, S. Vermeire, E. Louis, L.R. Cardon, C.A. Anderson, H. Drummond, E. Nimmo, T. Ahmad, N.J. Prescott, C.M. Onnie, S.A. Fisher, J. Marchini, J. Ghori, S. Bumpstead, R. Gwilliam, M. Tremelling, P. Deloukas, J. Mansfield, D. Jewell, J. Satsangi, C.G. Mathew, M. Parkes, M. Georges, and M.J. Daly. 2008. Genome-wide association defines more than 30 distinct susceptibility loci for Crohn's disease. *Nat. Genet.* 40:955–962. doi:10.1038/ng.175.
- Bendelac, O. Lantz, M.E. Quimby, J.W. Yewdell, J.R. Bennink, and R.R. Brutkiewicz. 1995. CD1 recognition by mouse NK1 T lymphocytes. *Science.* 268:863–865.
- Brandl, K., G. Plitas, B. Schnabl, R.P. DeMatteo, and E.G. Pamer. 2007. MyD88-mediated signals induce the bactericidal lectin RegIII gamma and protect mice against intestinal *Listeria monocytogenes* infection. *J. Exp. Med.* 204:1891–1900. doi:10.1084/jem.20070563.
- Cadwell, K., J.Y. Liu, S.L. Brown, H. Miyoshi, J. Loh, J.K. Lennerz, C. Kishi, W. Kc, J.A. Carrero, and S. Hunt. 2008. A key role for autophagy and the autophagy gene *Atg16L1* in mouse and human intestinal Paneth cells. *Nature.* 456:259–263.
- Cadwell, K., K.K. Patel, N.S. Maloney, T.-C. Liu, A.C. Ng, C.E. Storer, R.D. Head, R. Xavier, T.S. Stappenbeck, and H.W. Virgin. 2010. Virus-Plus-Susceptibility Gene Interaction Determines Crohn's Disease Gene *Atg16L1* Phenotypes in Intestine. *Cell.* 141:1135–1145.
- Cheroutre, H., F. Lambolez, and D. Mucida. 2011. The light and dark sides of intestinal intraepithelial lymphocytes. *Nat. Rev. Immunol.* 11:445–456. doi:10.1038/nri3007.
- Clevers, H.C., and C.L. Bevins. 2013. Paneth cells: maestros of the small intestinal crypts. *Annu. Rev. Physiol.* 75:289–311. doi:10.1146/annurev-physiol-030212-183744.
- Dalton, D.K., S. Pitts-Meek, S. Keshav, I.S. Figari, A. Bradley, and T.A. Stewart. 1993. Multiple defects of immune cell function in mice with disrupted interferon-gamma genes. *Science.* 259:1739–1742.
- Duerkop, B.A., S. Vaishnav, and L.V. Hooper. 2009. Immune responses to the microbiota at the intestinal mucosal surface. *Immunity.* 31:368–376. doi:10.1016/j.immuni.2009.08.009.
- Eriguchi, Y., S. Takashima, H. Oka, S. Shimoji, K. Nakamura, H. Uryu, S. Shimoda, H. Iwasaki, N.

- Shimono, and T. Ayabe. 2012. Graft-versus-host disease disrupts intestinal microbial ecology by inhibiting Paneth cell production of  $\alpha$ -defensins. *Blood*. 120:223–231.
- Van Es, J.H., P. Jay, A. Gregorieff, M.E. van Gijn, S. Jonkheer, P. Hatzis, A. Thiele, M. van den Born, H. Begthel, T. Brabletz, M.M. Taketo, and H. Clevers. 2005. Wnt signalling induces maturation of Paneth cells in intestinal crypts. *Nat. Cell Biol.* 7:381–386. doi:10.1038/ncb1240.
- Van Es, J.H., T. Sato, M. van de Wetering, A. Lyubimova, A.N.Y. Nee, A. Gregorieff, N. Sasaki, L. Zeinstra, M. van den Born, J. Korving, A.C.M. Martens, N. Barker, A. van Oudenaarden, and H. Clevers. 2012. Dll1+ secretory progenitor cells revert to stem cells upon crypt damage. *Nat. Cell Biol.* 14:1099–1104. doi:10.1038/ncb2581.
- Farin, H.F., J.H. Van Es, and H. Clevers. 2012. Redundant sources of Wnt regulate intestinal stem cells and promote formation of paneth cells. *Gastroenterology*. 143:1518-1529. doi: 10.1053/j.gastro.2012.08.031.
- Fernandez, M.-I., B. Regnault, C. Mulet, M. Tanguy, P. Jay, P.J. Sansonetti, and T. Pédrón. 2008. Maturation of paneth cells induces the refractory state of newborn mice to Shigella infection. *J. Immunol.* 180:4924–4930.
- Van der Flier, L.G., M.E. van Gijn, P. Hatzis, P. Kujala, A. Haegebarth, D.E. Stange, H. Begthel, M. van den Born, V. Guryev, I. Oving, J.H. van Es, N. Barker, P.J. Peters, M. van de Wetering, and H. Clevers. 2009. Transcription factor achaete scute-like 2 controls intestinal stem cell fate. *Cell*. 136:903–912. doi:10.1016/j.cell.2009.01.031.
- Giblin, L.J., C.J. Chang, A.F. Bentley, C. Frederickson, S.J. Lippard, and C.J. Frederickson. 2006. Zinc-secreting Paneth cells studied by ZP fluorescence. *Journal of Histochemistry & Cytochemistry*. 54:311–316.
- Guy-Grand, D., J.P. DiSanto, P. Henchoz, M. Malassis-Séris, and P. Vassalli. 1998. Small bowel enteropathy: role of intraepithelial lymphocytes and of cytokines (IL-12, IFN-gamma, TNF) in the induction of epithelial cell death and renewal. *Eur. J. Immunol.* 28:730–744. doi:10.1002/(SICI)1521-4141(199802)28:02<730::AID-IMMU730>62;3.CO;2-U.
- Kaser, A., A.-H. Lee, A. Franke, J.N. Glickman, S. Zeissig, H. Tilg, E.E.S. Nieuwenhuis, D.E. Higgins, S. Schreiber, L.H. Glimcher, and R.S. Blumberg. 2008. XBP1 links ER stress to intestinal inflammation and confers genetic risk for human inflammatory bowel disease. *Cell*. 134:743–756. doi:10.1016/j.cell.2008.07.021.
- Kobayashi, K.S., M. Chamaillard, Y. Ogura, O. Henegariu, N. Inohara, G. Nuñez, and R.A. Flavell. 2005. Nod2-dependent regulation of innate and adaptive immunity in the intestinal tract. *Science*. 307:731–734. doi:10.1126/science.1104911.
- Kontoyiannis, D., G. Boulougouris, M. Manoloukos, M. Armaka, M. Apostolaki, T. Pizarro, A. Kotlyarov, I. Forster, R. Flavell, and M. Gaestel. 2002. Genetic dissection of the cellular pathways and signaling mechanisms in modeled tumor necrosis factor–induced Crohn’s-like inflammatory bowel disease. *The Journal of experimental medicine*. 196:1563–1574.
- Lee, H.T., M. Kim, J.Y. Kim, K.M. Brown, A. Ham, V.D. D’Agati, and Y. Mori-Akiyama. 2013. Critical role of interleukin-17A in murine intestinal ischemia-reperfusion injury. *Am. J. Physiol. Gastrointest. Liver Physiol.* 304:G12–25. doi:10.1152/ajpgi.00201.2012.
- Merger, M., J.L. Viney, R. Borojevic, D. Steele-Norwood, P. Zhou, D.A. Clark, R. Riddell, R. Maric, E.R. Podack, and K. Croitoru. 2002. Defining the roles of perforin, Fas/FasL, and tumour necrosis

factor alpha in T cell induced mucosal damage in the mouse intestine. *Gut*. 51:155–163.

Meyer-Hoffert, U., M.W. Hornef, B. Henriques-Normark, L.-G. Axelsson, T. Midtvedt, K. Pütsep, and M. Andersson. 2008. Secreted enteric antimicrobial activity localises to the mucus surface layer. *Gut*. 57:764–771.

Miura, N., M. Yamamoto, M. Fukutake, N. Ohtake, S. Iizuka, A. Ishige, H. Sasaki, K. Fukuda, T. Yamamoto, and S. Hayakawa. 2005. Anti-CD3 induces bi-phasic apoptosis in murine intestinal epithelial cells: possible involvement of the Fas/Fas ligand system in different T cell compartments. *International immunology*. 17:513–522.

Mukherjee, S., S. Vaishnava, and L.V. Hooper. 2008. Multi-layered regulation of intestinal antimicrobial defense. *Cell. Mol. Life Sci*. 65:3019–3027. doi:10.1007/s00018-008-8182-3.

Nieuwenhuis, E.E., T. Matsumoto, D. Lindenbergh, R. Willemsen, A. Kaser, Y. Simons-Oosterhuis, S. Brugman, K. Yamaguchi, H. Ishikawa, and Y. Aiba. 2009. Cd1d-dependent regulation of bacterial colonization in the intestine of mice. *The Journal of clinical investigation*. 119:1241.

Nilsen, E.M., F.L. Jahnsen, K.E. Lundin, F.E. Johansen, O. Fausa, L.M. Sollid, J. Jahnsen, H. Scott, and P. Brandtzaeg. 1998. Gluten induces an intestinal cytokine response strongly dominated by interferon gamma in patients with celiac disease. *Gastroenterology*. 115:551–563.

Raetz, M., S. Hwang, C.L. Wilhelm, D. Kirkland, A. Benson, C.R. Sturge, J. Mirpuri, S. Vaishnava, B. Hou, and A.L. DeFranco. 2012. Parasite-induced TH1 cells and intestinal dysbiosis cooperate in IFN- $\gamma$ -dependent elimination of Paneth cells. *Nature immunology*. 14:136–142.

Rumio, C., M. Sommariva, L. Sfondrini, M. Palazzo, D. Morelli, L. Viganò, L. De Cecco, E. Tagliabue, and A. Balsari. 2012. Induction of Paneth cell degranulation by orally administered Toll-like receptor ligands. *J. Cell. Physiol*. 227:1107–1113. doi:10.1002/jcp.22830.

Di Sabatino, A., E. Miceli, W. Dhaliwal, P. Biancheri, R. Salerno, L. Cantoro, A. Vanoli, M. De Vincenzi, C.D.V. Blanco, T.T. MacDonald, and G.R. Corazza. 2008. Distribution, proliferation, and function of Paneth cells in uncomplicated and complicated adult celiac disease. *Am. J. Clin. Pathol*. 130:34–42. doi:10.1309/5ADNAR4VN11TTKQ6.

Saha, S., X. Jing, S.Y. Park, S. Wang, X. Li, D. Gupta, and R. Dziarski. 2010. Peptidoglycan recognition proteins protect mice from experimental colitis by promoting normal gut flora and preventing induction of interferon- $\gamma$ . *Cell host & microbe*. 8:147–162.

Salzman, N.H., K. Hung, D. Haribhai, H. Chu, J. Karlsson-Sjöberg, E. Amir, P. Teggatz, M. Barman, M. Hayward, D. Eastwood, M. Stoel, Y. Zhou, E. Sodergren, G.M. Weinstock, C.L. Bevins, C.B. Williams, and N.A. Bos. 2010. Enteric defensins are essential regulators of intestinal microbial ecology. *Nat. Immunol*. 11:76–83. doi:10.1038/ni.1825.

Sato, T., J.H. van Es, H.J. Snippert, D.E. Stange, R.G. Vries, M. van den Born, N. Barker, N.F. Shroyer, M. van de Wetering, and H. Clevers. 2011a. Paneth cells constitute the niche for Lgr5 stem cells in intestinal crypts. *Nature*. 469:415–418. doi:10.1038/nature09637.

Sato, T., D.E. Stange, M. Ferrante, R.G.J. Vries, J.H. Van Es, S. Van den Brink, W.J. Van Houdt, A. Pronk, J. Van Gorp, P.D. Siersema, and H. Clevers. 2011b. Long-term expansion of epithelial organoids from human colon, adenoma, adenocarcinoma, and Barrett's epithelium. *Gastroenterology*. 141:1762–1772. doi:10.1053/j.gastro.2011.07.050.

Sato, T., R.G. Vries, H.J. Snippert, M. van de Wetering, N. Barker, D.E. Stange, J.H. van Es, A. Abo, P. Kujala, P.J. Peters, and H. Clevers. 2009. Single Lgr5 stem cells build crypt-villus structures in

in vitro without a mesenchymal niche. *Nature*. 459:262–265. doi:10.1038/nature07935.

Satoh, Y. 1988. Atropine inhibits the degranulation of Paneth cells in ex-germ-free mice. *Cell Tissue Res*. 253:397–402.

Satoh, Y., K. Ishikawa, Y. Oomori, S. Takeda, and K. Ono. 1992. Bethanechol and a G-protein activator, NaF/AlCl<sub>3</sub>, induce secretory response in Paneth cells of mouse intestine. *Cell Tissue Res*. 269:213–220.

Vaishnava, S., C.L. Behrendt, A.S. Ismail, L. Eckmann, and L.V. Hooper. 2008. Paneth cells directly sense gut commensals and maintain homeostasis at the intestinal host-microbial interface. *Proc. Natl. Acad. Sci. U.S.A.* 105:20858–20863. doi:10.1073/pnas.0808723105.

Wehkamp, J., J. Harder, M. Weichenthal, M. Schwab, E. Schäffeler, M. Schlee, K.R. Herrlinger, A. Stallmach, F. Noack, P. Fritz, J.M. Schröder, C.L. Bevins, K. Fellermann, and E.F. Stange. 2004. NOD2 (CARD15) mutations in Crohn's disease are associated with diminished mucosal alpha-defensin expression. *Gut*. 53:1658–1664. doi:10.1136/gut.2003.032805.

Wehkamp, J., and E.F. Stange. 2010. Paneth's disease. *J Crohns Colitis*. 4:523–531. doi:10.1016/j.crohns.2010.05.010.

Wehkamp, J., G. Wang, I. Kübler, S. Nuding, A. Gregorieff, A. Schnabel, R.J. Kays, K. Fellermann, O. Burk, M. Schwab, H. Clevers, C.L. Bevins, and E.F. Stange. 2007. The Paneth cell alpha-defensin deficiency of ileal Crohn's disease is linked to Wnt/Tcf-4. *J. Immunol*. 179:3109–3118.

Wilson, C.L., A.J. Ouellette, D.P. Satchell, T. Ayabe, Y.S. López-Boado, J.L. Stratman, S.J. Hultgren, L.M. Matrisian, and W.C. Parks. 1999. Regulation of intestinal alpha-defensin activation by the metalloproteinase matrilysin in innate host defense. *Science*. 286:113–117.

## SUPPLEMENTAL DATA

### Supplemental Movies 1-3 Time-lapse analysis of Paneth cell degranulation after IFN- $\gamma$ exposure.

Images were acquired in 15 minute intervals. Confocal signals of single Z-planes are shown and overlaid to bright field signals.

**Supplemental Movie 1** Control small intestinal organoid were followed for 12 hours after labeling of PC granules with the fluorescent dye ZP-1. Note that the fluorescent signal decreases due to bleaching, but that PC granules are unaffected during the culture period.

**Supplemental Movie 2** Addition of 5 ng/ml IFN- $\gamma$  causes a progressive and complete PC degranulation within 12 hours. Note that individual PCs one by one extruding their entire granules into the crypt lumen. A rapid process that occurs in a 'all or nothing' fashion.

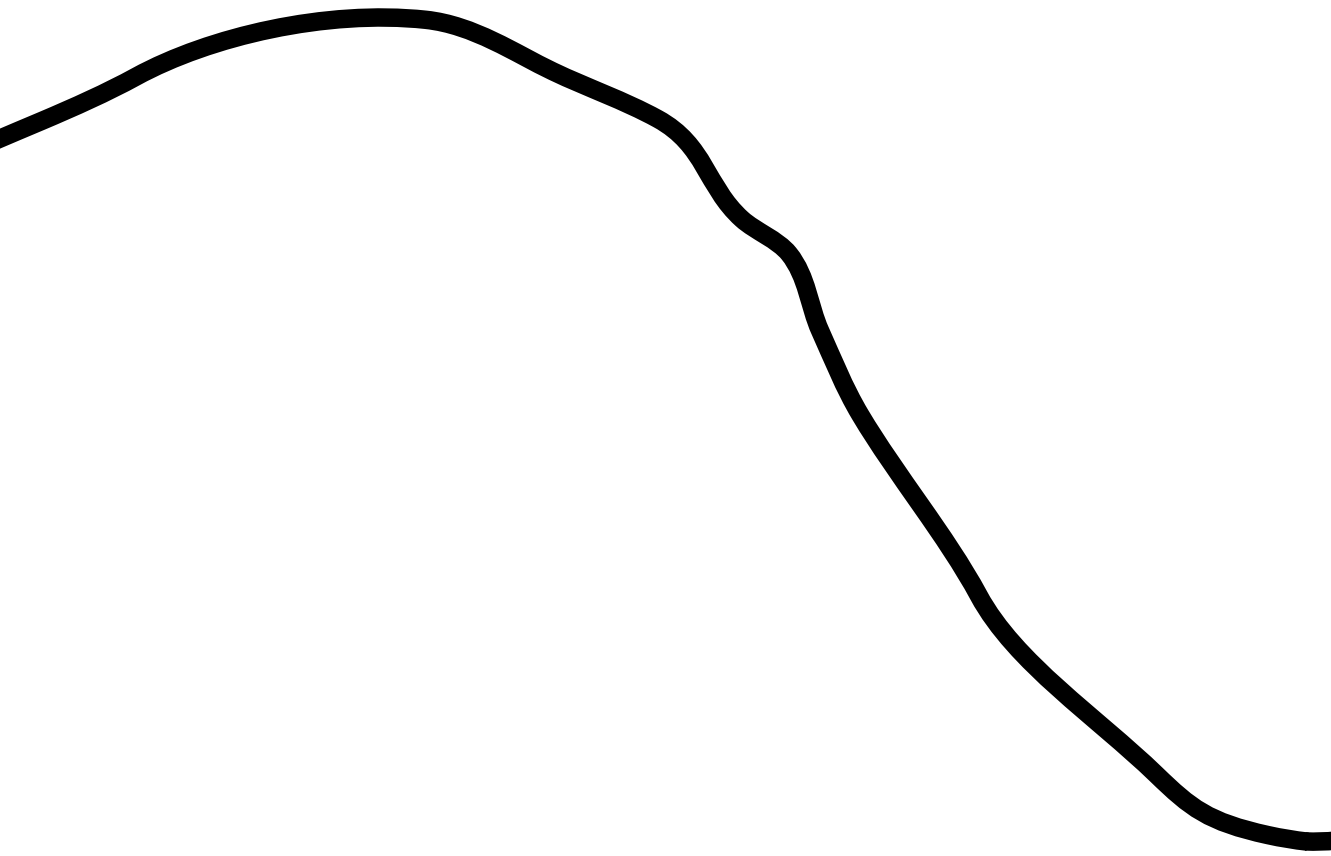
**Supplemental Movie 3** High dose IFN- $\gamma$  treatment 20 ng/ml causes a more rapid discharging of PCs (within 8 hours).

### Supplemental Table 1 Primer sequences used for RT-PCR analysis

gene name	target mRNA	primer sense	primer antisense	product size (bp)
<i>Tlr1</i>	NM_030682.2	TGGTTTAAATGAGTGTGTTGTGAA	ATGGCCATAGACATTCCTGA	143
<i>Tlr2</i>	NM_011905	GTGTCCGCAATCATAGTTTC	CTCTGAGATTTGACGCTTTG	232
<i>Tlr3</i>	NM_126166	CCCATAATCTGGGCTGAATC	TCTTCTGAGTTGGTTGTGAG	218
<i>Tlr4</i>	NM_021297	ATCCCTGCATAGAGGTAGTT	CAAGTTTGAGAGGTGGTGTA	242
<i>Tlr5</i>	NM_016928	ATTTCAACCAGAGATCTGCC	ATTGAGGATCCAGGGAATCTG	270
<i>Tlr6</i>	NM_011604	CAGTGCTGGAATAGAGCTTG	GTTCAATTAGAGAACGGGGTC	173
<i>Tlr7</i>	NM_133211	TGAAAATGGTGTGTTTCGATGTG	GGAATCTGGAGAGATGCTTG	259
<i>Tlr8</i>	NM_133212	TATAGAACATGGAACATGCCC	TTTGGCATTGTGGTTTCAGAT	305
<i>Tlr9</i>	NM_031178	CAACATGGTTCTCCGTCG	TGATACGGTTGGAGATCA	231
<i>MD-2</i>	NM_016923	GCTGCTTTCTCCATATTGA	AGTTTCCTCTTGAATGAAC	185
<i>CD14</i>	NM_009841	AGAATCTACCGACCATGGAGC	GTACAATTCCACATCTGCCG	182
<i>CD3e</i>	NM_007648.4	CACTCTGGGCTTGCTGATGG	TTGCGGATGGGCTCATAGTC	159
<i>CD45</i>	NM_001111316.2	ACACCCAGTGATGAACTGAGC	AGCAGCGTGGATAACACACC	161
<i>Hprt</i>	NM_013556.2	AAGCTTGCTGGTGAAGGA	TTGCGCTCATCTTAGGCTTT	186

All primer pairs either target an exon-exon junction or span a large intron to allow discrimination between cDNA and genomic DNA.







# Chapter 5: A novel epithelial culture system reveals ligand-independent Androgen Receptor signaling in the prostate

Wouter R. Karthaus<sup>1</sup>, Phil J. laquinta<sup>2\*</sup>, Ana Gracanin<sup>1</sup>, Jarno Drost<sup>1</sup>, John Whongvipat<sup>2</sup>, Vivian S.W. Li<sup>1</sup>, Norman Sachs<sup>1</sup>, Yu Chen<sup>2\*</sup>, Robert G.J. Vries, Charles L. Sawyers<sup>2,3,4\*</sup> and Hans C. Clevers<sup>1</sup>



# A novel epithelial culture system reveals ligand-independent Androgen Receptor signaling in the prostate

**Wouter R. Karthaus<sup>1</sup>, Phil J. Iaquinta<sup>2\*</sup>, Ana Gracanin<sup>1</sup>, Jarno Drost<sup>1</sup>, John Whongvipat<sup>2</sup>, Vivian S.W. Li<sup>1</sup>, Norman Sachs<sup>1</sup>, Yu Chen<sup>2\*</sup>, Robert G.J. Vries, Charles L. Sawyers<sup>2,3,4\*</sup> and Hans C. Clevers<sup>1</sup>**

Hubrecht Institute, Royal Netherlands Academy of Arts and Sciences & University Medical Center Utrecht, 3584 CT, Utrecht<sup>1</sup>

Human Oncology and Pathogenesis Program<sup>2</sup>, Department of Medicine, Howard Hughes Medical Institute<sup>3</sup>, Memorial Sloan Kettering Cancer Center, New York, NY 10065, USA\*

Prostate cancer (PCa) is one of the most common cancers in the western world. A limiting factor for the study of PCa has been the lack of suitable in vitro models. Particularly, whereas prostate epithelium is dependent on AR signaling in vivo, to date no cell culture system exists that reliably recapitulates this dependency in vitro. Here we describe a novel long-term 3D culture system for mouse and human primary prostate epithelium. In the absence of androgens, the organoids are composed of two layers: CK5<sup>+</sup> basal and CK8<sup>+</sup> luminal cells. Androgen addition has dual effects; as it leads to a 3-fold increase in growth rate, while simultaneously inducing differentiation, size increase and polarization of the luminal cells. Tumor organoids that recapitulate the disease phenotype can be grown efficiently from several murine models of PCa and from primary human PCa cases and are suitable for functional studies using a range of standard experimental manipulations. With this serum-free system, we demonstrate a possible ligand-independent growth inhibitory effect of anti-androgen drugs, thereby providing the first evidence that the androgen receptor (AR) can function independent of ligand in PCa. This technology has potential to substantially impact future PCa drug development.

## Introduction

The prostate is a secretory gland that plays a pivotal role in the male reproductive system. Its development and adult function is dependent on androgens<sup>1</sup>. Prostate cancer (PCa) is one of the most common malignancies in the western world, with over 200,000 new cases annually in the US<sup>2</sup>. The Androgen Receptor (AR) represents an important target for treatment of PCa, either indirectly by surgical or chemical castration, or directly by

administration of AR inhibitors <sup>3</sup>. Unfortunately, treatment commonly results in the development of resistance against inhibition of AR activity, a state also known as castration resistance <sup>4</sup>. The pathogenesis of prostate cancer and the development of castration resistance are poorly understood, in part by the lack of suitable model systems to study the disease *ex vivo*.

Only a handful of PCa cell lines exist, as it has proven exceedingly hard to establish such cell lines from primary PCa tissue. Moreover, the available prostate cancer cell lines grow independently of AR signaling, making these lines poor models for the study of PCa pathogenesis and therapy resistance <sup>5,6</sup>.

The urogenital sinus mesenchyme (UGSM) recombination model represents a useful *in vivo* tool to study prostate cancer <sup>1,7,8</sup>. In this model, prostate epithelial cells are combined with mesenchyme derived from the urogenital sinus of murine embryos, transplanted under the kidney capsule and allowed to grow. Other approaches involve *in vitro* culture methods of primary prostate epithelium <sup>9-14</sup>. However, none of these systems generates tissues that resemble the *in vivo* composition of the prostate gland or contain androgens at physiological levels <sup>15</sup>. Most importantly, none of these methods allow longer-term propagation of the cells. We have previously described 3D culture conditions that allow long-term expansion of primary mouse and human epithelial organoids from small intestine <sup>16</sup>, colon <sup>17</sup> and stomach <sup>18</sup> and liver <sup>19</sup>. These cultures can be started from single Lgr5+ stem cells and are based on the addition of the Lgr5 ligand Rspodin1 <sup>20</sup>, a potent Wnt pathway agonist <sup>20,21,22</sup>. Organoids remain genetically and phenotypically stable over many months in culture, as exemplified by pathology-free transplantation of multiple mice with the organoid offspring of single Lgr5+ cells from colon <sup>23</sup> or liver <sup>19</sup>. Here we describe the development and use of an Rspodin1-based 3D culture method that allows long-term propagation of normal and malignant murine and human prostate epithelium.

## Results

### Establishment of murine prostate organoid cultures

Small fragments of murine prostate epithelium were embedded in matrigel and cultured in the 'generic' stem cell expansion medium containing the growth factors EGF, Noggin, and R-spondin1 (ENR;<sup>16</sup>). Because the murine prostate is composed of histologically distinct lobes <sup>24</sup>, we separately cultured the anterior prostate (AP), dorsolateral prostate (DLP) and ventral prostate (VP) epithelium (Figure 1A). Under standard conditions, only

the dorsolateral prostate was capable of growth (Supplementary figure 1A). We then tested additional culture components. In the presence of the TGF- $\beta$  receptor inhibitor a83-01 at 200 nM, epithelial fragments of all lobes yielded expanding organoids at plating efficiencies of close to 100% (Supplementary figure 1A). Prostate epithelium from all lobes formed cystic structures composed of two layers under these ENR+A83 conditions (Figure 1F). Prostate organoids could be cultured indefinitely at a split ratio of 1:3 (1.5 years at time of writing), while retaining a stable karyotype. We detected no changes in organoid morphology during this culture period.

The basal (outer) layer expressed typical basal prostate markers such as Cytokeratin (CK) 5 and p63 (Figure 1C,-E-F). The luminal (inner layer) expressed the luminal marker Cytokeratin 8 (figure 1C, 1E – 1F), thus demonstrating that the *in vitro* expanded organoids retain an architecture that resembles the *in vivo* composition. Importantly, the majority of cells expressed the androgen receptor and the prostate-specific transcription factor *Nkx3.1*<sup>25</sup>(Figure 1C-1F).

As expression of the AR was maintained in culture, we studied the effects of androgens on the organoids by adding the prototypic AR ligand Dihydrotestosterone (DHT) to established organoid cultures. Of note, AR signaling is believed to act as a differentiation factor<sup>11,12</sup>. In the presence of 1nM DHT, the AR translocated to the nucleus, indicative of an intact signaling pathway (Figure 1F). Within 72 hours upon DHT addition, the CK8+ve luminal cells became strongly polarized and increased in size (Figure 1F), while the organoids filled up with secreted material (Supplementary figure 1C). The CK5+ve basal cells remained morphologically unaffected. Gene expression studies in the absence and presence of DHT (0.1nM to 100 nM) by RT-PCR, revealed strong upregulation of the AR target genes *Fkbp5* and *Pscn* (figure 1D, Supplementary figure 1C). Moreover, decreased amounts of EGF in the medium (50, 5, 0.5 & 0 ng/ml) further increased the expression of AR target genes (Supplementary Figure 1C), confirming the previously demonstrated reciprocal interaction between the PI3 kinase pathway and AR shown by others<sup>26</sup>. No proliferation was seen upon withdrawal of EGF.

We found that R-spondin increases overall number of organoids formed during establishment. Noggin withdrawal had similar results (Figure 1E).

Surprisingly, we observed that addition of DHT did not only induce differentiation of the luminal epithelium of the organoids, but it also robustly enhanced the growth rate of the organoids, allowing weekly split

ratios of 1:5 rather than 1:3. When the prostate organoids were subjected to multiple cycles of DHT addition and withdrawal, switching between the two epithelial phenotypes occurred faithfully at each cycle, as a model for castration/regeneration effects *in vitro* (Supplementary Figure 1D).

To further document the stability of prostate organoids, we performed the UGSM recombination experiments with passage 8-organoids derived from the AP, DLP and VP. Approximately 50,000 epithelial cells were combined with mesenchymal cells and placed under the kidney capsule as described previously<sup>8</sup>. Organoid/UGSM transplants were harvested 2 months after transplantation. Histological analysis showed that organoids derived from different lobes formed glandular structures (Supplementary figure 1F), thus supporting the phenotypic stability of the organoids.

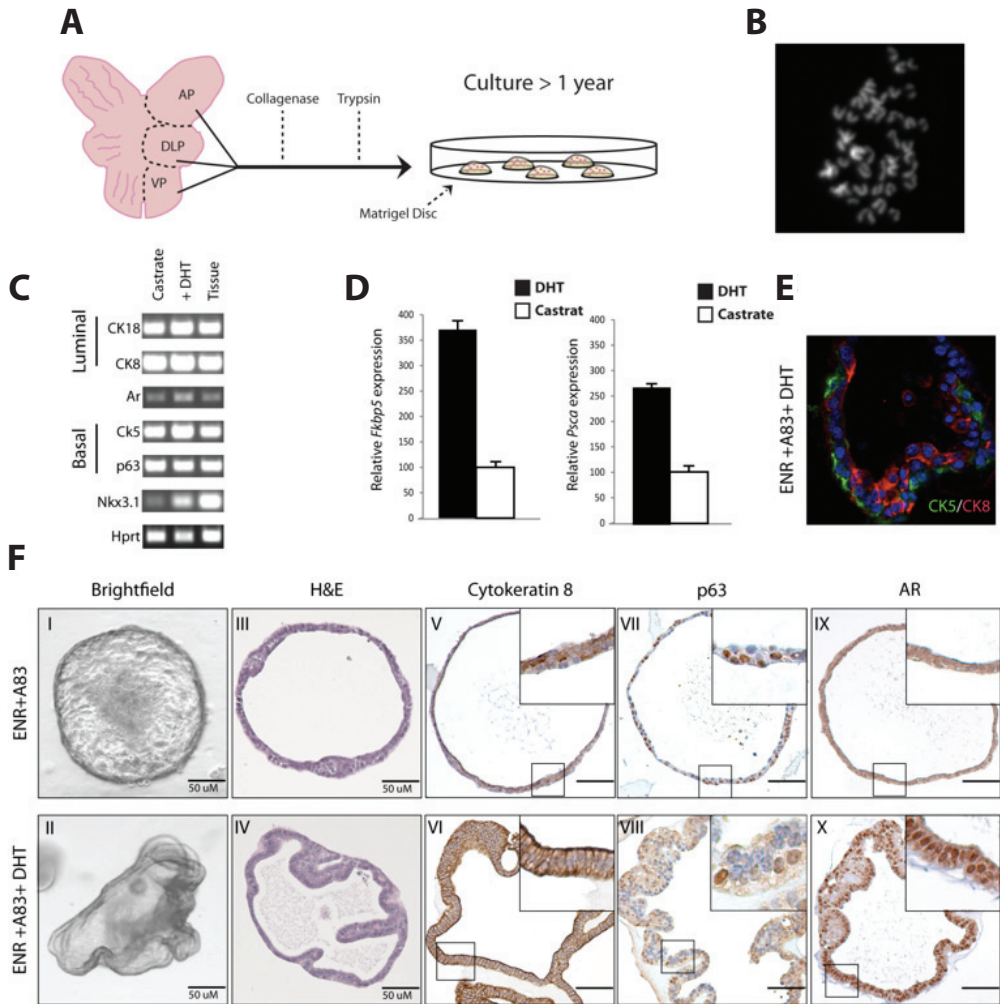


**Figure 1: Establishment of murine prostate cultures.**

A: Schematic overview of organoids establishment. Lobes were isolated separately, enzymatically digested to single cells and plated in matrigel B: Karyotyping of passage organoids 52 weeks (1 year) showing 40 chromosomes C: RT-PCR analysis of prostate organoids show that both luminal and basal markers are expressed D: Quantitative RT-PCR of AR targets *Psca* and *Fkbp5* in the presence of DHT (1nM) and in castrate conditions. In the presence of DHT *Fkbp5* and *Psca* are strongly upregulated. Results are presented as mean  $\pm$  standard deviation E: Immunofluorescent staining of Cytokeratin 5 and Cytokeratin 8 in a DHT treated organoid showing distinct luminal and basal cell populations F: Immunohistochemical analysis of murine organoids in the presence of DHT (1nM) and in castrate conditions. Brightfield image (I-II) H&E staining (III-IV), showing distinct folding in Prostate organoids treated with 1 nM DHT. Cytokeratin 8 (V-VI) showing luminal localization and strong polarization in DHT treated organoids. p63 (VII-VIII) with a basal staining pattern. Androgen receptor (IX-X) with strong nuclear staining in DHT treated samples indicating an activated AR signaling pathway. Scale bars represent 50  $\mu$ m.

## Murine Prostate organoids as a tool for cancer research

As a first step towards the establishment of prostate organoid technology as a tool for studying PCa, we established organoids from the different lobes of: 1) wild type mice (WT); 2) mice carrying the PBCre transgene and that were homozygous for a floxed *Pten* allele ( $Pten^{loxP/loxP}$ )<sup>27</sup>, a tumor suppressor gene often deleted or mutated in prostate cancer<sup>28-31</sup>; 3) mice expressing CRE recombinase under the prostate-specific composite promoter ARR<sub>2</sub>BP (PBCre)<sup>32</sup> crossed with mice conditionally overexpressing ERG from the ROSA locus<sup>33</sup>,  $Rosa^{loxP/stop/loxP\ ERG}$ . This mouse will be described in detail elsewhere) and is designed to result in prostate-specific overexpression of ERG, as a model for the *TMPRSS2:ERG* gene fusion commonly found in prostate cancer<sup>34</sup> 4) mice carrying the PBCre transgene, the  $Rosa^{loxP/stop/loxP\ ERG}$  allele, while being homozygous for the floxed *Pten* allele (Figure 2A).

87 Cultures carrying the prostate-specific *Pten* deletion initially formed organoids containing a lumen, but within a week the organoids were composed of multiple layers of stratified epithelium, eventually forming an essentially solid 3D structure (Figure 2B, Supplementary figure 2). Histologically, the PBCre  $Pten^{loxP/loxP}$  organoid resembled *in vivo* phenotypes observed previously<sup>26,35</sup>. ERG overexpression in the PBCre ERG cultures did not result in any obvious histological signs of hyperplasia (Figure 2B). The combination of *Pten* deletion and ERG overexpression resulted in the same hyperplastic phenotype seen for *Pten* deletion alone (Figure 2B, Supplementary figure 2), resembling the results observed by others<sup>36,37</sup>. Interestingly, the organoids overexpressing ERG in a *Pten*-mutant background showed signs of invasive behavior, with “fingers” protruding into the matrigel (Figure 2B). All organoids expressed the basal marker Ck5 and the luminal marker Ck8 (Supplementary figure 2) and responded strongly to DHT withdrawal (Supplementary figure 2B).

As a final validation, we performed UGSM recombination experiments with passage 8-organoids derived from the DLP from WT, PBCre and PBCre *Pten* mice. Approximately 50.000 organoid cells (passage 8) were combined with mesenchymal cells and placed under the kidney capsule. Organoid/UGSM transplants were harvested 2 months after transplantation. Histological analysis showed that organoids derived from different genotypes faithfully recapitulated the known histopathology (Supplementary figure 2A).

Independently, we blocked *Pten* expression by shRNA-mediated knock-down in *Pten*-WT organoids. We retrovirally introduced *Pten*- and control shRNA viruses into WT and PBCre ERG organoids. 24 hours post infection;

we applied Puromycin selection for 2 days to ensure that only infected organoids remained. We detected an 80-90% decrease in *Pten* expression levels 7 days post infection (Figure 2D; Supplementary figure 2C). This was accompanied by increased phosphorylation of AKT and Ribosomal protein s6 (Figure 2E, supplementary figure 2D), presumably resulting from increased activation of the PI3 kinase pathway following a decrease in expression of the *Pten* phosphatase. Indeed, the shPTEN-infected organoids resembled the 'hyperplastic' PBCre PTEN<sup>loxP/loxP</sup> organoids. No sign of such hyperplasia was observed in shSCR infected organoids (Figure 2F). In accordance with previous observations by Carver *et al.*<sup>26</sup>, we found that the hyper-activation of the PI3 Kinase pathway decreased the transcriptional output of the AR targets *Psca* and *Fkbp5* (Figure 2D, Supplementary Figure 2B).

Finally, we performed UGSM recombination with 50.000 cells derived from experiments with shPTEN- and shSCR-infected PBCre ERG organoids. Indeed, the glandular tissue derived from shPTEN-infected organoids was strongly hyperplastic, whereas the structures derived from shSCR-infected organoids showed no signs of hyperplasia (Figure 2C). In all, these results demonstrated that *in vitro* organoid phenotypes mimicked the *in vivo* phenotypes, and that retroviral expression/knockdown of genes can be used to identify and study genes involved in prostate cancer with this technology.

### Human healthy and cancerous prostate organoids

From our previous experience on translating organoid culture conditions from mouse to human gastrointestinal epithelium<sup>17</sup>, we anticipated that human prostate organoids would demonstrate additional growth factor requirements. To the ENR+A83+DHT media, we added Fibroblast growth factor (FGF) -10, -2, and prostaglandin E2 (PGE2). These factors were previously described to support proliferation of prostate and/or colon epithelium<sup>10,11,38,39</sup>. In addition, we added two factors that we had previously identified as being essential for human small intestinal cultures, i.e. nicotinamide, and the p38 inhibitor SB202190.

Using these conditions, we were able to expand human prostate epithelium for >12 months while remaining phenotypically unchanged and retaining a stable karyotype (Figure 3a). Initially, human prostate organoids formed solid spherical structures of stratified epithelium, that developed pronounced lumens after 2-3 weeks (Figure 3F). Such prostate organoids were composed of single-layered epithelium, but also contained areas with a double-layered epithelium. The majority of cells were positive for the luminal epithelial markers CK8 and AR (Figure 3E-F). Cells positive



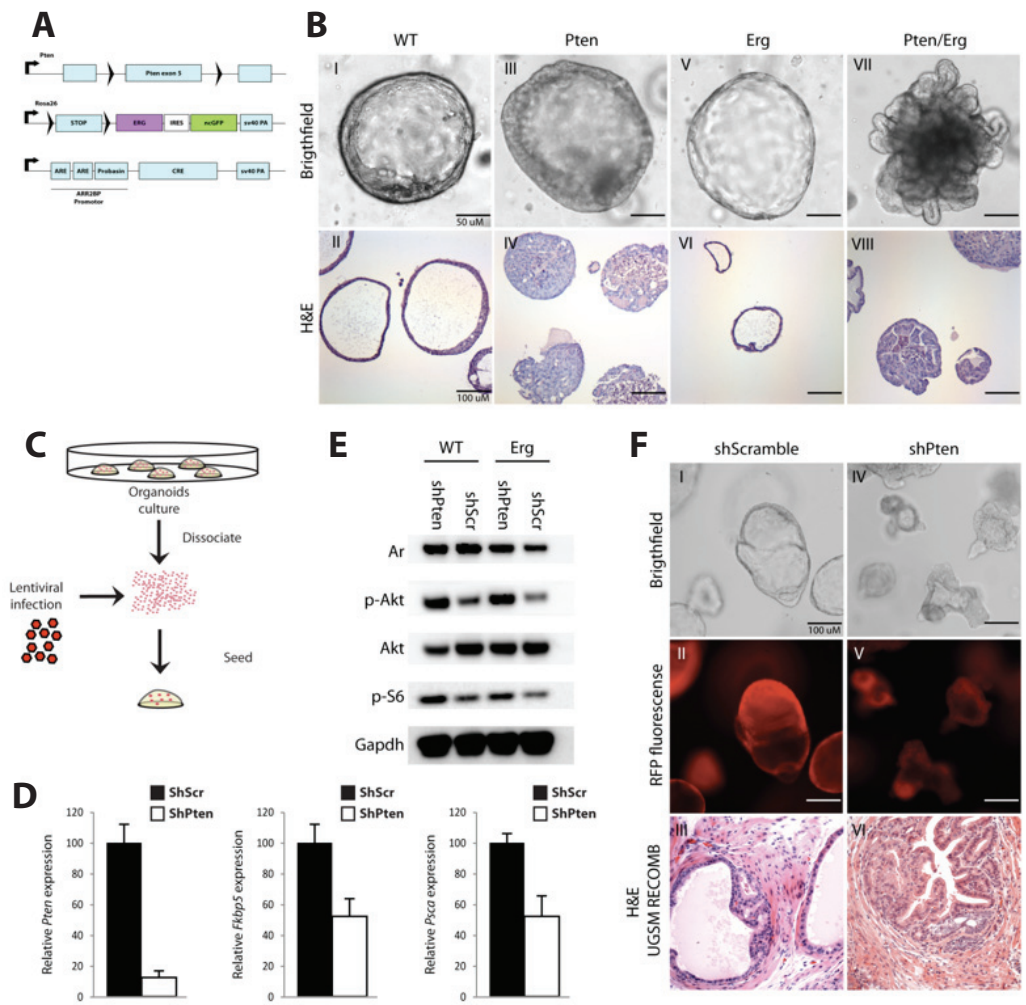


**Figure 2: Genetic models of PCa recapitulate in vivo phenotypes.**

A: Schematic overview of genetic mouse models used in experiments:  $Pten^{loxp/loxp}$ ,  $Rosa^{loxp-stop-loxp}$  ERG and the prostate specific deletion strain PBCre. B: Phenotypic analysis of organoids derived from genetic mouse models of prostate cancer brightfield and H&E images of Wildtype (WT) (I-II), PBCre  $Pten^{loxp/loxp}$  (III-IV) that form solid balls due to hyperplasticity. PBCre  $Rosa^{loxp-stop-loxp}$  ERG (V-VI) showing no signs of hyperplasticity and PBCre  $Pten^{loxp/loxp}$   $Rosa^{loxp-stop-loxp}$  ERG (VII-VIII) showing hyperplasticity and fingerlike protrusions in the matrigel. C: Schematic overview of experimental setup of viral infection. D: Quantitative RT-PCR analysis of *Pten*, and the AR targets *Fkbp5* and *Psca* expression in shPten and shScr infected organoids. *Pten* expression is strongly diminished (10%) in shPten infected organoids showing efficient knockdown. *Fkbp5* and *Psca* expression downregulated twofold in shPten infected organoids. Results are presented as mean  $\pm$  standard deviation. E: Western blot analysis of PI3-Kinase pathway components Akt and ribosomal protein S-6 in shPten and ShScr infected organoids. Phosphorylation of Akt and p-S6 are increased in shPten infected organoids. Gapdh was probed as a control. F: Brightfield image and fluorescence of shPten-RFP shScr-RFP infected PBCre ERG organoids (I-IV) H&E staining of shPten/shScr organoid-UGSM recombinations (III & VI) showing hyperplasticity in the shPten infected organoids and UGSM recombinations. RFP was coinfecting with the shVector showing high transduction efficiency (II & V). Scale bars represent 50 or 100  $\mu$ m.

for basal markers p63 and CK5 were always located in the outer layer of organoids (Figure 3E-3F). Ki67 staining revealed that organoids actively cycle in the presence and absence of androgens (Supplementary Figure 3B).

As for the mouse organoids, the human organoids expressed prostate-specific genes such as *Prostate specific antigen (PSA)* and the homeobox gene *NKX3.1* (figure 3C-D). Additionally, the human prostate organoids strongly responded to DHT (0.1 -100 nM) in terms of expression of AR targets. Indeed, the AR-target genes *PSA* and *NKX3.1* were markedly decreased upon withdrawal of DHT (Figure 3D). As for the mouse organoids, we found that titration of EGF (50, 5, 0.5 & 0 ng/ml) increased AR target gene expression. Similar to the mouse organoids EGF is the essential factor driving organoid proliferation. (Supplementary figure 3C).

Moreover we found that PGE2 (1-10nM) and FGF2 (10 ng/ml) was essential for sustain organoid growth as well as A83-01 and Nicotinamide (Supplementary figure 3C). Removal of SB202190 lead to keratinization of the organoids indicative of stress (Supplementary figure 3C).

Although proliferation rate was not affected by the removal of FGF10, Noggin and R-spondin we found that removal these factors strongly decreased AR expression levels, suggesting a role of these pathways in the maintenance and differentiation of luminal cells. (Supplementary figure 3C). A very important tool for the study of prostate cancer would be the easy generation of organoids from individual prostate cancer patients, independent of tumor genotype. We have established pairs of normal and tumor tissue from prostates of 10 patients undergoing radical prostatectomy with an efficiency of >95%. We did not note major differences in organoid morphologies between normal and tumor organoids (Figure 4A). When we probed for expression of the *TMPRSS2:ERG* fusion transcript, we found four weeks post establishment samples were still expressing the *TMPRSS2:ERG* fusion gene whereas control benign tissue from the same patient did not express the fusion gene (Figure 4B). When we analyzed organoids for the presence of basal cells, the loss of basal cells is a hallmark of PCa, we found p63-negative organoids are present among the bulk of the culture (Figure 4C). However we could not exclude the growth of benign epithelium in these cultures. To determine whether fusion negative samples were also tumor, we karyotyped several tumor organoids. We found only one tumor culture with 40% aneuploid cells, suggesting a mixed population of healthy and tumor cells (Figure 4D). In all other samples we did not find signs of tumor cells, most likely normal cells co-

isolated from the biopsy outcompete tumor cells, as was described before<sup>10</sup>.

To test whether prostate organoids retain the capacity of forming glandular tissue *in vivo* we performed UGSM recombination experiments with passage 8-cultures from both benign and tumor tissue from the same patient. Approximately 50.000 cells derived from organoids were combined with mesenchyme and placed under the kidney capsule as described previously<sup>8</sup>. Organoid/UGSM recombinations were harvested after 8 weeks of growth. Histological analysis showed that prostate organoids derived from benign tissue formed normal glands. Organoids derived from tumor tissue from the same patient formed both hyperplastic glands and normal gland (Supplementary Figure 3), again indicating a mixture of benign and cancer organoids.

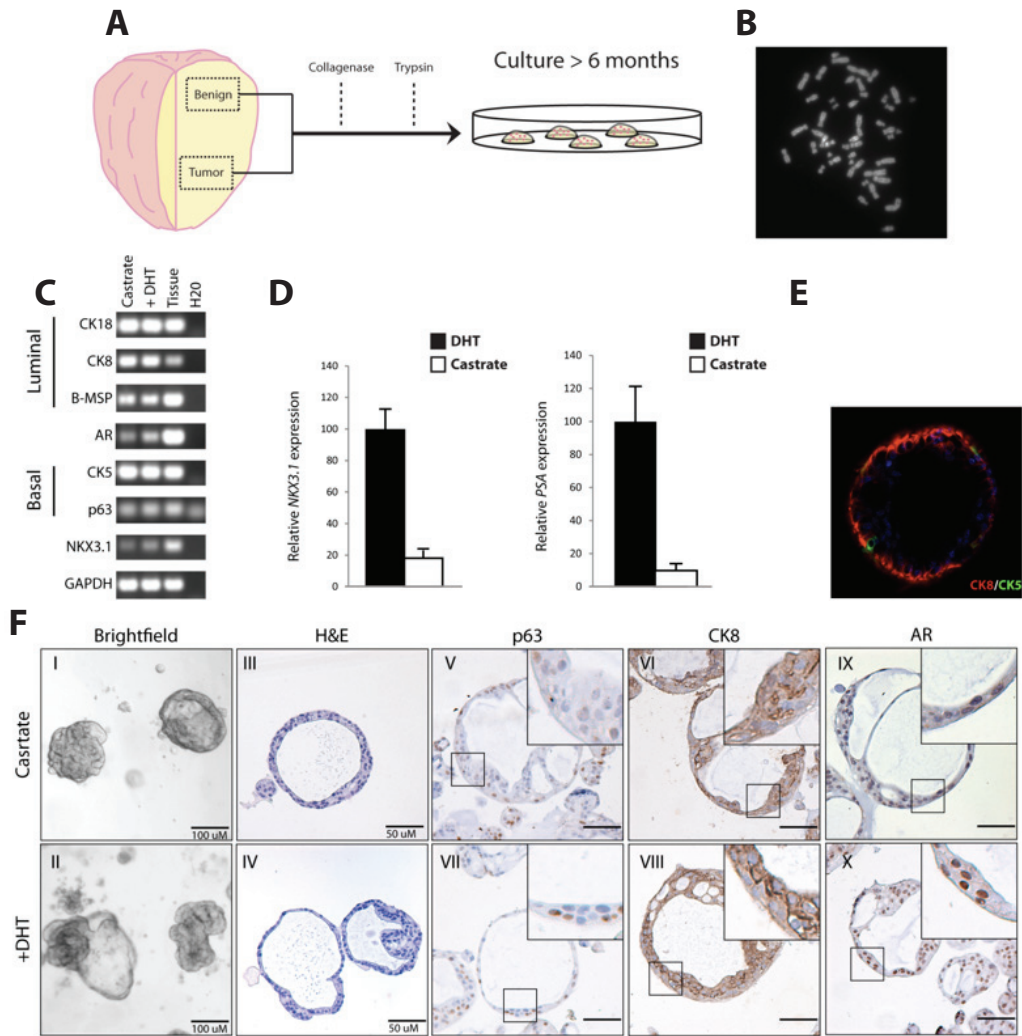


### Figure 3: Establishment of human prostate organoids.

A: Schematic overview of human prostate organoid establishment. Areas designated benign and tumor were isolated separately, enzymatically digested to single cells and plated in matrigel. B: Karyotyping of passage 20 organoids (6 months) showing 46 chromosomes. C: RT-PCR analysis of prostate organoids show that both luminal and basal markers are expressed. D: Quantitative RT-PCR of AR targets *NKX3.1* and *PSA* in the presence of DHT (1nM) and in castrate conditions. In the presence of DHT *NKX3.1* and *PSA* are strongly upregulated. Results are presented as mean  $\pm$  standard deviation. E: Immunofluorescent staining of Cytokeratin 5 and Cytokeratin 8 of a DHT treated organoid showing distinct luminal and basal cell populations. F: Immunohistochemical analysis of human prostate organoids in the presence of DHT (1nM) and in castrate conditions. Brightfield image (I-II) H&E staining (III-IV), showing no morphological differences in between treatments. p63 (V-VI) with a basal staining pattern. Cytokeratin 8 (VII-VIII) showing luminal localization. Androgen receptor (IX-X) with strong nuclear staining in DHT treated samples indicating an activated signaling pathway. Scale bars represent 50  $\mu$ m.

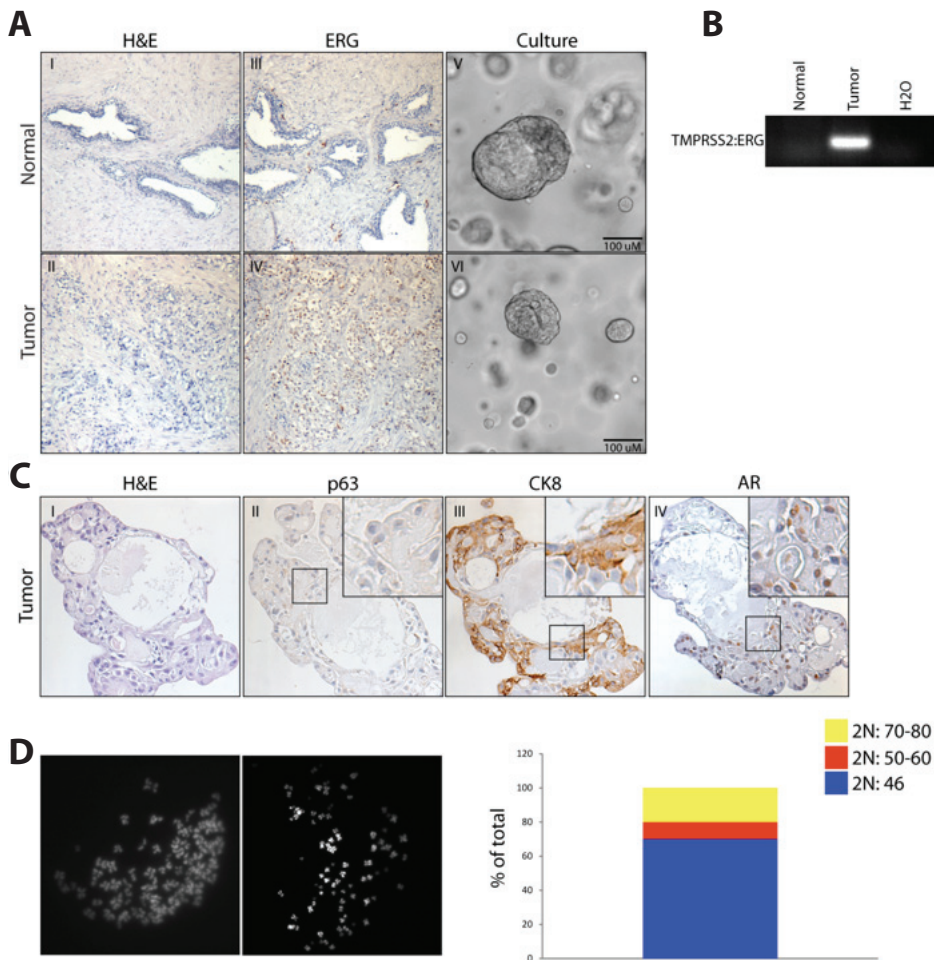


### Figure 4: Human tumor organoids.

A: (I-II) H&E staining of primary prostate cancer & benign control from one patient (III-IV) ERG staining of primary prostate cancer, showing clear nuclear signal in the prostate tumor (V-VI) brightfield image organoids derived from normal and tumor tissue show no differences in morphology B: RT-PCR analysis of *TMPRSS2:ERG* fusion transcript in normal and tumor derived organoids 4 weeks post establishment. Fusion transcript is exclusively detected in the tumor organoids. C: Immunohistochemical analysis of Tumor derived organoids. (I) H&E staining (II) p63 negative organoids are present among the bulk (III) CK8 staining (IV)AR staining, showing nuclear localization indicating an intact signaling pathway D: Karyotyping of a second prostate tumor. 30% of nuclei analyzed are aneuploid. Indicating a mixed population of tumor and healthy cells. Scale bars represent 100  $\mu$ M.

### **Murine Prostate organoids respond to clinically approved drugs**

Finally, we tested whether prostate organoids respond to clinically approved anti-androgen drugs *in vitro*. We analyzed the genetic mouse models of PCa to ensure that we have a homogeneous organoid population. First we optimized concentrations for the first generation anti-androgen Casodex/bicalutamide (IC<sub>50</sub> 160 nM) and the second-generation anti-androgens MDV3100/Enzalutamide (IC<sub>50</sub> 36 nM)<sup>40</sup> and ARN509 (IC<sub>50</sub> 16 nM)<sup>41</sup> by analysis of AR target gene expression in the presence of DHT. We found that PSA expression was comparable to castrate levels when organoids were treated with 1 μM – 10 μM Casodex, 100- nM - 1 μM MDV3100 and 100 nM -1 μM ARN-509 (Figure 5A). These effective concentrations were considerably lower than effective serum levels in patients or effective compound concentrations as determined in conventional fetal calf serum-containing cell culture methods<sup>40</sup>. Most likely, serum proteins sequester active compounds.

Murine prostate cancer organoids were cultured with AR inhibitors in the absence or presence of DHT. We seeded 2000 single cells to ensure equal starting conditions and measured organoid size using cellular imaging software (CellProfiler). After fourteen days, organoids that were grown in the combined presence of DHT and anti-androgens (100 nM ARN-509, 100 nM MDV3100 or 1 μM of Casodex) had developed to a size comparable or smaller to that obtained under castrate (i.e. no DHT) conditions (Figure 5, supplementary figure 5). Surprisingly, we found that AR inhibition under “castrate” conditions displayed further growth inhibition (Figure 5, supplementary figure 5) We hypothesized that the AR remains active in the absence of a ligand, as suggested elsewhere<sup>42,43 44</sup>). For this, we had to exclude that an alternative source of androgens was present in the serum-free culture. To only non-defined component in our culture system was Matrigel<sup>R</sup>. Prostate organoids may be capable of generating their own androgens<sup>45-48</sup>. To exclude this, we treated organoids with the 17 α-hydroxylase/C17,20 lyase inhibitor Abiraterone<sup>49</sup>. Treatment at 100 nM (IC<sub>50</sub> 1nm) did not influence the base-line expression of AR target genes (Supplementary Figure 5). We therefore concluded that androgens endogenously produced, were absent from our cultures under “castrate” conditions. To address if unspecified, off-target effects were causing the growth-inhibitory effects, we tested the inhibitors on mouse small intestine (SI) organoids, which are grown in comparable media<sup>16</sup>. We found that none of the inhibitors influenced the growth of the mouse SI organoids (Figure 5). These data agreed with the notion that the effects on prostate organoids were ‘on-target’, i.e. blocking the transcriptional effect of AR. The data implied that these (clinically approved) AR inhibitors suppress prostate tumor

growth through inhibition of the AR in an androgen-independent manner.

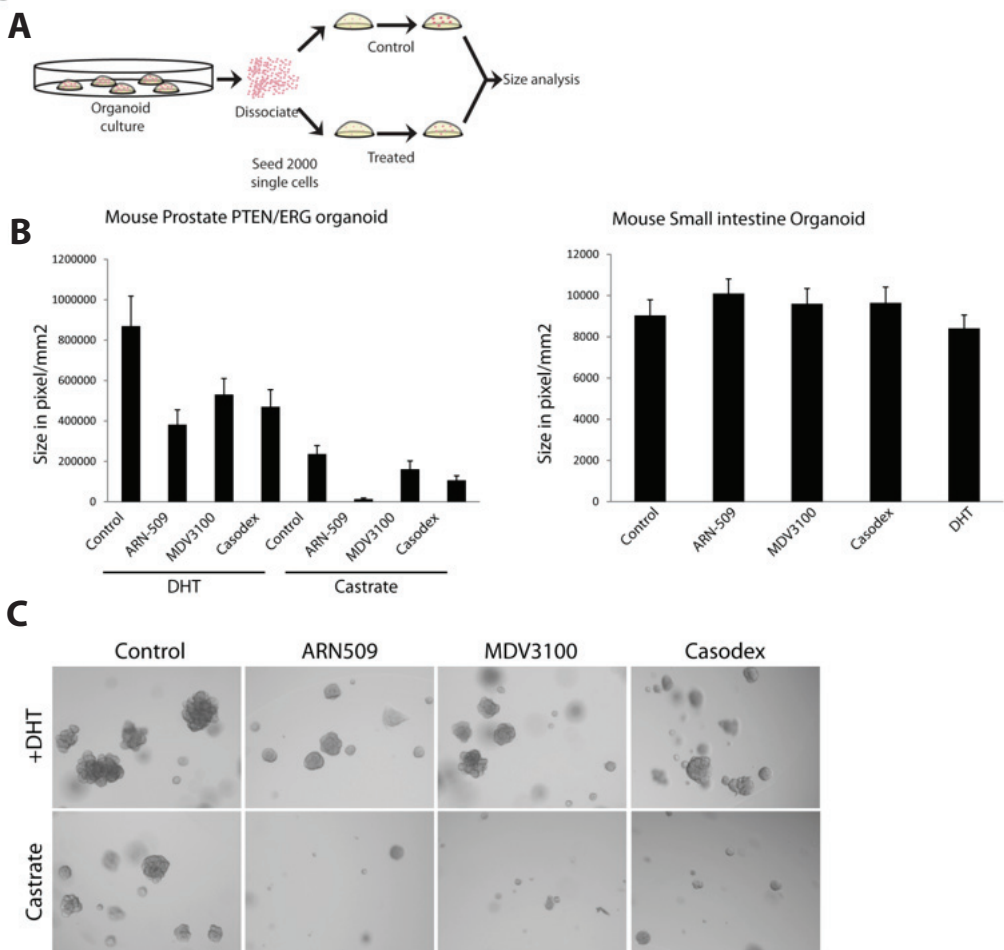


### Figure 5: Treatment of murine organoids with Clinically approved inhibitors.

A: Schematic overview of experimental setup. 2000 single cells were plated and subsequently treated with the AR inhibitors ARN-509, MDV3100 and Casodex for 2 weeks B: Quantification of organoid size 14 days after inhibitor treatment. Left: Murine PBCre Pten<sup>loxP/loxP</sup> Rosa<sup>loxP-stop-loxP</sup>ERG prostate tumor organoids treated with 100 nM ARN-509, 10 nM MDV3100, 1  $\mu$ M Casodex in the presence and absence of DHT (1 nM). Mean organoid size is reduced in the treated organoids. Under castrate conditions AR inhibitor treatment decreased mean organoid size further Right: As a control murine small intestinal organoids treated with 100 nM ARN-509, 100 nM MDV3100, 1  $\mu$ M Casodex in absence of DHT and with DHT (1 nM). No reduction on overall organoid size is observed. Results are presented as pixel/mm<sup>2</sup> mean  $\pm$  standard error of the mean C: Representative brightfield images of prostate organoids 14 days post treatment. Scale bars represent 50  $\mu$ M.

## Discussion

Based on our previous experience with organoid cultures, we have devised a culture system that allows long-term expansion of murine prostatic epithelium. Murine prostate organoids faithfully recapitulate *in vivo* phenotypes known from genetic models for prostate cancer. Moreover, the murine prostate organoids are easily manipulated with inhibitors and retroviruses, offering a new tool for the discovery and study of PCa. To our knowledge, we report the first culture system that allows long-term expansion of untransformed human prostate epithelium and, moreover, maintains androgen-responsiveness in culture. The culture conditions also allow in part propagation of human prostate cancer-derived organoids, however from most biopsies only benign organoids were derived. It is likely that benign cells outcompete the tumor cells as is observed by others<sup>10</sup>. Possibly this can be overcome by isolation of tumor cells from the bulk before seeding. Then possibly technology may fill the void that currently exists between the large-scale, genome-wide sequencing efforts of human cancers and the clinical data of individual patients.

Recently large scale genome-wide sequencing data has become available of primary PCa<sup>28,30</sup> and castration resistance prostate cancer (CRPC)<sup>50</sup>. Using the murine organoids one could study the influence of the genes on functional *in vitro* parameters such as growth, invasive behavior, drug-sensitivity or genome instability. Organoid culture may represent a straightforward, cheap and robust alternative to xenografting<sup>8</sup>. As a case in point, we have demonstrated that prostate organoids respond to the AR inhibitors Casodex, ARN509 and MDV3100 in terms of growth and gene expression signatures.

It appears of interest that the AR inhibitors suppress organoid growth even in the absence of androgens in the medium, indicative of a ligand-independent role of the AR. Several mechanisms for such a phenomenon have been suggested. Transcript variants of the AR are known, which lack the ligand-binding domain (LBD) coding exons 4-8, and are constitutively active<sup>(44,51,52)</sup>. Such variants require the co-expression of full-length AR and the activity can be blocked with anti-androgen treatments<sup>53</sup>. However, the absolute expression levels of these variants are low<sup>53</sup>. Alternatively, it has been proposed that the AR can be activated in the absence of an androgen ligand by stimulation of the Her2/neu receptor<sup>42</sup>. However, removal of EGF from the medium results in an increase of AR target expression in organoids, suggesting an alternative mechanism. The simplest explanation of our observations might rest in a baseline activity of the AR that does not require ligand.



In this culture system, DHT/AR signaling acts as a growth factor, but simultaneously induces luminal differentiation. In vivo the androgen receptor has also been shown to play dual roles in prostate. In mice epithelial specific deletion of the androgen receptor leads to dedifferentiation and increased number of proliferating cells<sup>54</sup>. However forced overexpression of the AR results in intraepithelial neoplasia in adult mice<sup>55,56</sup>. In prostate cancer lines the Janus-face of the AR is also observed<sup>57</sup>. In CRPC the transcriptional program regulated by the AR is significantly different compared to primary prostate cancer<sup>58</sup>. However the AR locus is commonly amplified or mutated in CRPC<sup>50,59</sup>. Possibly organoids could provide novel insights into these complex AR signaling events in both homeostasis and cancer.

A tantalizing hypothesis is that the AR plays these different roles in different cells types. Terminally differentiated luminal cells and a transit amplifying cells are positive for AR expression<sup>12</sup> However there is evidence that rare prostate stem/progenitor cells express AR and therefore are DHT responsive<sup>13,60</sup>. Under castrate conditions the ligand AR function in these progenitors would be active and blocking with anti-androgen treatment would target stem cells directly. However also a fraction of Trop2Hi, AR-negative fraction basal cells have shown act as stem cells<sup>9</sup>. In this scenario, stem cells would remain unaffected. However it is not excluded that AR expressing cells play a vital role in stem cell niche and therefore targeting AR would still be a bona fide treatment.

In all prostate organoids offer a novel model to study prostate development, homeostasis and cancer.

## Materials & Methods:

### Isolation & culture of prostate epithelial cells

Murine prostates were isolated from Wildtype C57Bl/6,  $Rosa^{loxP/stop/loxP} ERG$ ,  $Pten^{loxP/loxP}$  mice.  $Pten^{loxP/loxP} Rosa^{loxP/stop/loxP} ERG$ . All lines were crossbred to C57bl/6 background. Murine prostates were divided into three lobe pairs, the Anterior Prostate (AP), Dorsolateral Prostate (DLP) and Ventral Prostate<sup>61</sup>. Subsequently the each lobe was placed in 5-mg/ml collagenase type II (Gibco) in advanced DMEM/F12 and digested for 1 to 2 hours at 37°C. Glandular structures were washed with ADMEM/F12 and centrifuged at 100\*G. Subsequently structures were digested in 5ml TripleD (Gibco) with the addition Y-27632 10 μM (Sigma) for 15 min at 37°C. Trypsinized cells were washed and seeded in growth factor reduced matrigel (BD biosciences). Murine prostate epithelial cells

were cultures in ADMEM/F12 containing growth factors EGF 5-50 ng ml<sup>-1</sup> (Peprotech), R-spondin 1 conditioned medium or 500 ng ml<sup>-1</sup> recombinant R-spondin 1, Noggin conditioned medium or 100 ng ml<sup>-1</sup> recombinant Noggin (Peprotech) and the tgf-beta/alk inhibitor a83-01 (Tocris) to Dihydrotestosterone (Sigma) was added at 0.1-1 nM final concentration. Murine prostate organoids were passaged either via trituration with a glass Pasteur pipet or trypsinization with TrypLE for 5 min at 37 °C. Passage was performed every week with either a 1:3 (castrate conditions) or a 1:5 (+DHT conditions) ratio. Human prostate samples were obtained from patients undergoing radical prostatectomy according guidelines from the UMC Utrecht. Prostate pieces designated "normal" and "tumor" were minced and digested in 5 ml of 5 mg/ml collagenase type II (Gibco) in complete prostate medium (described below) and digested for 14-16 hours at 37°C gently shaking. . Subsequently structures were digested in 5ml TrypLE (Gibco) with addition of Y-27632 10 uM (Sigma) for 15 min at 37°C. Trypsinized cells were washed and seeded in growth factor reduced matrigel (BD biosciences). Human prostate organoids (benign & tumor) were cultures in ADMEM/F12 containing growth factors EGF 5-50 ng ml<sup>-1</sup> (Peprotech), R-spondin 1 conditioned medium (Reference ABO) or 500 ng ml<sup>-1</sup> recombinant R-spondin 1, Noggin conditioned medium or 100 ng ml<sup>-1</sup> recombinant Noggin (Peprotech), 10 ng ml<sup>-1</sup> FGF10 (Peprotech), 5 ng ml<sup>-1</sup> FGF2 (Peprotech), 10 nM Prostaglandin E<sub>2</sub> (Tocris), the tgf-beta/alk inhibitor a83-01 (Tocris), SB12021 (Sigma-Aldrich), and 100 mM Nicotinamide (Sigma-Aldrich) and Dihydrotestosterone (Sigma-Aldrich) was added at 0.1-1 nM final concentration. Human prostate organoids were passaged either via trituration with a glass Pasteur pipet or trypsinization with TrypLE for 5 min at 37 °C. Passage was performed weekly with a 1:2 ratio. Murine small intestinal organoids were cultured as described previously <sup>16</sup>.

### **Growth curves organoids**

Organoids cultured under standard conditions were trypsinized using TrypLE and passed through a strainer with a pore size of 40 µm to obtain a single cell solution. 2000 single cells were plated in 20 ul 3:7 ADMEM/F12: matrigel mix (48 well plate). Cells were treated with either 1 nm to 1 µM MDV3100 (Sawyers lab), 1 nM - 1 µM ARN-509 (Sawyers lab), 1 nM - 10 µM Casodex (Sigma) in the absence or presence of 1nM DHT. Organoid number was counted at 14 days post seeding and size was quantified by analyzing phase contrast pictures using cellular imaging software (CellProfiler). Experiment was done in triplicate and 3 pictures were taken per well at 40x for size analysis. Average organoid size is expressed as **pixel/mm<sup>2</sup>**.

## **UGSM essay**

UGSM recombination essay was performed as described previously<sup>8</sup>.

## **Karyotyping**

Karyotyping was performed as described previously<sup>16</sup>. In short, organoids were treated with Colcemid (Gibco) for 16 hours. Cells were trypsinized, washed and fixed using MeOH: acetic acid 1:1. Cells were washed 3x with MeOH: acetic acid 1:1. Cells were plated from height on glass slides and metaphase spreads were visualized using DAPI. Slides were mounted with vectashield and analyzed on a DM6000 Leica microscope.

## **Immunohistochemistry and Immunofluorescence**

Organoids were fixed using 4 Paraformaldehyde on 4 °C overnight. Fixed organoids were washed and transferred to paraffin according to standard techniques. Immunohistochemistry was performed as described previously. In short, antigen retrieval was performed by boiling samples for 10 minutes with either sodium citrate or EDTA buffers. Blocking was performed using 1% BSA in PBS0 for 30 minutes at room temperature. Following antibodies were used for staining on murine and human prostate organoids AR (1:1000, N-20, Santa Cruz) Ck5 (1:1000, AF-138, Covance), Ck8 (1:1000, C-51, Santa Cruz), PSA (1:1000, Dako), p63 (1:1000, 4A4, Millipore), ki67 (1:2000, Dako) ERG (1:500, EP111, Epitomics). Stainings were visualized using bright vision (Dako).

For immunofluorescent stainings organoids were fixed washed using ADMEM/F12 to remove matrigel. Subsequently organoids were fixed using 4% PFA in PBS for 1 hour on ice, followed by permeabilization/blocking with 1% BSA, 1% Triton X-100 in PBS0 for 30 min on Ice. Stainings were performed in 0.05% BSA 0.1% Triton X-100 in PBS0 overnight at 4°C. Organoids were stained using the following antibodies AR (1:200, N-20, Santa Cruz) Ck5 (1:500, AF-138, Covance), Ck8 (1:500, C-51, Santa Cruz). Subsequently organoids were washed with PBS0, 3x 10 minutes and subsequently stained with alexa-fluor (-488, -568, -647) conjugated antibodies in 0.05% BSA 0.1% triton X-100 in PBS0 for 1 hour in the dark at Room temperature. DNA was stained using DAPI or Topro3 during 2ndary antibody step.

## **RNA isolation, cDNA preparation, qPCR**

RNA was isolated from organoids using Qiagen RNeasy kits according to manufacturers protocol. 100-1000 ng RNA was reversetranscribed to cDNA using GoScript reverse transcriptase (Promega) according to manufacturers protocol. Quantative RT-PCR was performed using

IQ™ SYBR green mix (Bio-Rad) according to manufacturers protocol. QPCR was performed using primers from supplementary table 1.

### **Westernblot**

Samples were lysed using RIPA buffer (50 mM Tris-HCL pH 8.0, 150 mM NaCL, 0.1% SDS, 0,5% Na-Deoxycholate, 1% NP-40) containing Complete™ protease and phosphatase inhibitors (Roche). Protein content was quantified using standard Bradford assay. 10 uG of protein was loaded on gradient polyacrylamide gels (4-12%) and subsequently transferred to a PVDF membrane. Membranes were probed with antibodies directed against AR (1:000, N-20, Santa Cruz), Gapdh (1:2000 Abcam) Akt (1:1000 Cell signalling), phosphorylated-Akt (1:1000 cell signaling), Phosphorylated-S6 (1:1000, cell signaling). Following washes membranes were incubated with secondary HRP conjugated antibodies (goat anti-Rabbit HRP 1:2000, anti goat HRP 1:2000 and Rabbit anti-mouse 1:2000 all GE healthcare). ECL (G&E healthcare) Signal was detected using LAS 5000 (GE healthcare).

## References:

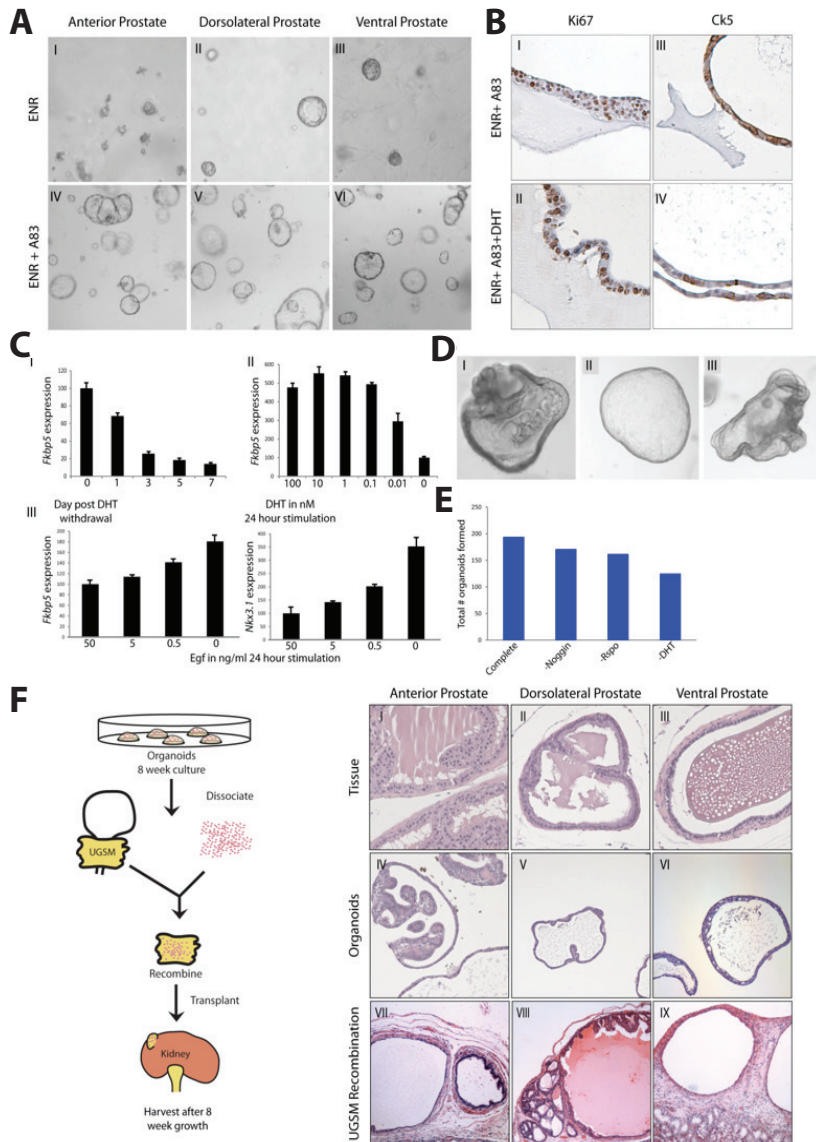
- 1 Cunha, G. The role of androgens in the epithelio-mesenchymal interactions involved in prostatic morphogenesis in embryonic mice. *The Anatomical record* **175**, 87-96, doi:10.1002/ar.1091750108 (1973).
- 2 Society, A. C. Cancer facts & figures 2010. *American Cancer Society Atlanta* (2010).
- 3 Denmeade, S. & Isaacs, J. A history of prostate cancer treatment. *Nature reviews. Cancer* **2**, 389-396, doi:10.1038/nrc801 (2002).
- 4 Singh, P., Yam, M., Russell, P. & Khatri, A. Molecular and traditional chemotherapy: a united front against prostate cancer. *Cancer letters* **293**, 1-14, doi:10.1016/j.canlet.2009.11.019 (2010).
- 5 Sobel, R. & Sadar, M. Cell lines used in prostate cancer research: a compendium of old and new lines--part 1. *The Journal of urology* **173**, 342-359, doi:10.1097/01.ju.0000141580.30910.57 (2005).
- 6 Sobel, R. & Sadar, M. Cell lines used in prostate cancer research: a compendium of old and new lines--part 2. *The Journal of urology* **173**, 360-372, doi:10.1097/01.ju.0000149989.01263.dc (2005).
- 7 Cunha, G. *et al.* Hormonal, cellular, and molecular regulation of normal and neoplastic prostatic development. *The Journal of steroid biochemistry and molecular biology* **92**, 221-236, doi:10.1016/j.jsbmb.2004.10.017 (2004).
- 8 Xin, L., Ide, H., Kim, Y., Dubey, P. & Witte, O. In vivo regeneration of murine prostate from dissociated cell populations of postnatal epithelia and urogenital sinus mesenchyme. *Proceedings of the National Academy of Sciences of the United States of America* **100 Suppl 1**, 11896-11903, doi:10.1073/pnas.1734139100 (2003).
- 9 Goldstein, A. *et al.* Trop2 identifies a subpopulation of murine and human prostate basal cells with stem cell characteristics. *Proceedings of the National Academy of Sciences of the United States of America* **105**, 20882-20887, doi:10.1073/pnas.0811411106 (2008).
- 10 Garraway, I. *et al.* Human prostate sphere-forming cells represent a subset of basal epithelial cells capable of glandular regeneration in vivo. *The Prostate* **70**, 491-501, doi:10.1002/pros.21083 (2010).
- 11 Xin, L., Lukacs, R., Lawson, D., Cheng, D. & Witte, O. Self-renewal and multilineage differentiation in vitro from murine prostate stem cells. *Stem cells (Dayton, Ohio)* **25**, 2760-2769, doi:10.1634/stemcells.2007-0355 (2007).
- 12 Litvinov, I. *et al.* Low-calcium serum-free defined medium selects for growth of normal prostatic epithelial stem cells. *Cancer research* **66**, 8598-8607, doi:10.1158/0008-5472.CAN-06-1228 (2006).
- 13 Vander Griend, D. *et al.* The role of CD133 in normal human prostate stem cells and malignant cancer-initiating cells. *Cancer research* **68**, 9703-9711, doi:10.1158/0008-5472.CAN-08-3084 (2008).
- 14 Niranjan, B. *et al.* Primary culture and propagation of human prostate epithelial cells. *Methods in molecular biology (Clifton, N.J.)* **945**, 365-382, doi:10.1007/978-1-62703-125-7\_22 (2013).
- 15 Sedelaar, J. & Isaacs, J. Tissue culture media supplemented with 10% fetal calf serum contains a castrate level of testosterone. *The Prostate* **69**, 1724-1729, doi:10.1002/pros.21028 (2009).
- 16 Sato, T. *et al.* Single Lgr5 stem cells build crypt-villus structures in vitro without a mesenchymal niche. *Nature* **459**, 262-265, doi:10.1038/nature07935 (2009).

- 17 Sato, T. *et al.* Long-term expansion of epithelial organoids from human colon, adenoma, adenocarcinoma, and Barrett's epithelium. *Gastroenterology* **141**, 1762-1772, doi:10.1053/j.gastro.2011.07.050 (2011).
- 18 Barker, N. *et al.* Lgr5(+ve) stem cells drive self-renewal in the stomach and build long-lived gastric units in vitro. *Cell stem cell* **6**, 25-36, doi:10.1016/j.stem.2009.11.013 (2010).
- 19 Huch, M. *et al.* In vitro expansion of single Lgr5+ liver stem cells induced by Wnt-driven regeneration. *Nature* **494**, 247-250, doi:10.1038/nature11826 (2013).
- 20 de Lau, W. *et al.* Lgr5 homologues associate with Wnt receptors and mediate R-spondin signalling. *Nature* **476**, 293-297, doi:10.1038/nature10337 (2011).
- 21 Kim, K.-A. *et al.* R-Spondin family members regulate the Wnt pathway by a common mechanism. *Molecular biology of the cell* **19**, 2588-2596, doi:10.1091/mbc.E08-02-0187 (2008).
- 22 Carmon, K., Gong, X., Lin, Q., Thomas, A. & Liu, Q. R-spondins function as ligands of the orphan receptors LGR4 and LGR5 to regulate Wnt/beta-catenin signaling. *Proceedings of the National Academy of Sciences of the United States of America* **108**, 11452-11457, doi:10.1073/pnas.1106083108 (2011).
- 23 Yui, S. *et al.* Functional engraftment of colon epithelium expanded in vitro from a single adult Lgr5 stem cell. *Nature medicine* **18**, 618-623, doi:10.1038/nm.2695 (2012).
- 24 Paul, C. M., Annemarie, A. D., Rajvir, D. & Gerald, R. C. Hormonal, cellular, and molecular control of prostatic development. *Developmental Biology* **253**, doi:10.1016/S0012-1606(02)00031-3 (2003).
- 25 Bhatia-Gaur, R. *et al.* Roles for Nkx3.1 in prostate development and cancer. *Genes & development* **13**, 966-977, doi:10.1101/gad.13.8.966 (1999).
- 26 Carver, B. *et al.* Reciprocal feedback regulation of PI3K and androgen receptor signaling in PTEN-deficient prostate cancer. *Cancer cell* **19**, 575-586, doi:10.1016/j.ccr.2011.04.008 (2011).
- 27 Di Cristofano, A., Pesce, B., Cordon-Cardo, C. & Pandolfi, P. Pten is essential for embryonic development and tumour suppression. *Nature genetics* **19**, 348-355, doi:10.1038/1235 (1998).
- 28 Barbieri, C. *et al.* Exome sequencing identifies recurrent SPOP, FOXA1 and MED12 mutations in prostate cancer. *Nature genetics* **44**, 685-689, doi:10.1038/ng.2279 (2012).
- 29 El Sheikh, S., Romanska, H., Abel, P., Domin, J. & Lalani, E.-N. Predictive value of PTEN and AR coexpression of sustained responsiveness to hormonal therapy in prostate cancer--a pilot study. *Neoplasia (New York, N.Y.)* **10**, 949-953 (2008).
- 30 Taylor, B. *et al.* Integrative genomic profiling of human prostate cancer. *Cancer cell* **18**, 11-22, doi:10.1016/j.ccr.2010.05.026 (2010).
- 31 Robbins, C. *et al.* Copy number and targeted mutational analysis reveals novel somatic events in metastatic prostate tumors. *Genome research* **21**, 47-55, doi:10.1101/gr.107961.110 (2011).
- 32 Zhang, J., Thomas, T., Kasper, S. & Matusik, R. A small composite probasin promoter confers high levels of prostate-specific gene expression through regulation by androgens and glucocorticoids in vitro and in vivo. *Endocrinology* **141**, 4698-4710, doi:10.1210/en.141.12.4698 (2000).
- 33 Chen, Y. *et al.* ETS factors reprogram the androgen receptor cistrome and prime prostate tumorigenesis in response to PTEN loss. *Nature medicine*, doi:10.1038/

- nm.3216 (2013).
- 34 Tomlins, S. *et al.* Recurrent fusion of TMPRSS2 and ETS transcription factor genes in prostate cancer. *Science (New York, N.Y.)* **310**, 644-648, doi:10.1126/science.1117679 (2005).
- 35 Wang, S. *et al.* Pten deletion leads to the expansion of a prostatic stem/progenitor cell subpopulation and tumor initiation. *Proceedings of the National Academy of Sciences of the United States of America* **103**, 1480-1485, doi:10.1073/pnas.0510652103 (2006).
- 36 King, J. *et al.* Cooperativity of TMPRSS2-ERG with PI3-kinase pathway activation in prostate oncogenesis. *Nature genetics* **41**, 524-526, doi:10.1038/ng.371 (2009).
- 37 Carver, B. *et al.* Aberrant ERG expression cooperates with loss of PTEN to promote cancer progression in the prostate. *Nature genetics* **41**, 619-624, doi:10.1038/ng.370 (2009).
- 38 Memarzadeh, S. *et al.* Enhanced paracrine FGF10 expression promotes formation of multifocal prostate adenocarcinoma and an increase in epithelial androgen receptor. *Cancer cell* **12**, 572-585, doi:10.1016/j.ccr.2007.11.002 (2007).
- 39 Jung, P. *et al.* Isolation and in vitro expansion of human colonic stem cells. *Nature medicine* **17**, 1225-1227, doi:10.1038/nm.2470 (2011).
- 40 Tran, C. *et al.* Development of a second-generation antiandrogen for treatment of advanced prostate cancer. *Science (New York, N.Y.)* **324**, 787-790, doi:10.1126/science.1168175 (2009).
- 41 Clegg, N. *et al.* ARN-509: a novel antiandrogen for prostate cancer treatment. *Cancer research* **72**, 1494-1503, doi:10.1158/0008-5472.CAN-11-3948 (2012).
- 42 Craft, N., Shostak, Y., Carey, M. & Sawyers, C. A mechanism for hormone-independent prostate cancer through modulation of androgen receptor signaling by the HER-2/ neu tyrosine kinase. *Nature medicine* **5**, 280-285, doi:10.1038/6495 (1999).
- 43 Lyons, L. & Burnstein, K. Vav3, a Rho GTPase guanine nucleotide exchange factor, increases during progression to androgen independence in prostate cancer cells and potentiates androgen receptor transcriptional activity. *Molecular endocrinology (Baltimore, Md.)* **20**, 1061-1072, doi:10.1210/me.2005-0346 (2006).
- 44 Sun, S. *et al.* Castration resistance in human prostate cancer is conferred by a frequently occurring androgen receptor splice variant. *The Journal of clinical investigation* **120**, 2715-2730, doi:10.1172/JCI41824 (2010).
- 45 Stanbrough, M. *et al.* Increased expression of genes converting adrenal androgens to testosterone in androgen-independent prostate cancer. *Cancer research* **66**, 2815-2825, doi:10.1158/0008-5472.CAN-05-4000 (2006).
- 46 Montgomery, R. *et al.* Maintenance of intratumoral androgens in metastatic prostate cancer: a mechanism for castration-resistant tumor growth. *Cancer research* **68**, 4447-4454, doi:10.1158/0008-5472.CAN-08-0249 (2008).
- 47 Locke, J. *et al.* Androgen levels increase by intratumoral de novo steroidogenesis during progression of castration-resistant prostate cancer. *Cancer research* **68**, 6407-6415, doi:10.1158/0008-5472.CAN-07-5997 (2008).
- 48 Hamid, A. *et al.* Aldo-keto Reductase Family 1 Member C3 (AKR1C3) Is a Biomarker and Therapeutic Target for Castration-Resistant Prostate Cancer. *Molecular medicine (Cambridge, Mass.)* **18**, 1449-1455, doi:10.2119/molmed.2012.00296 (2013).
- 49 Attard, G., Belldegrun, A. & de Bono, J. Selective blockade of androgenic steroid synthesis by novel lyase inhibitors as a therapeutic strategy for treating metastatic prostate cancer. *BJU international* **96**, 1241-1246, doi:10.1111/j.1464-410X.2005.05821.x (2005).

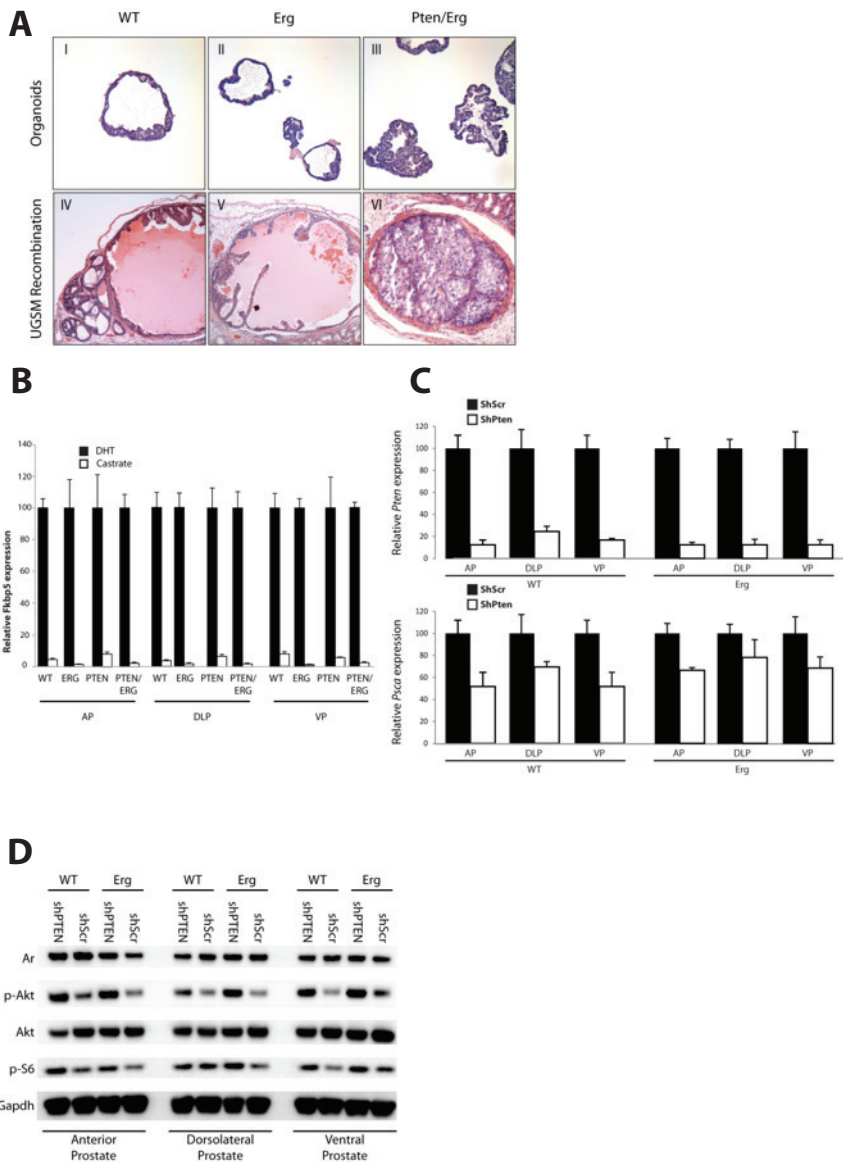
- 50 Grasso, C. *et al.* The mutational landscape of lethal castration-resistant prostate cancer. *Nature* **487**, 239-243, doi:10.1038/nature11125 (2012).
- 51 Hu, R. *et al.* Ligand-independent androgen receptor variants derived from splicing of cryptic exons signify hormone-refractory prostate cancer. *Cancer research* **69**, 16-22, doi:10.1158/0008-5472.CAN-08-2764 (2009).
- 52 Chan, S., Li, Y. & Dehm, S. Androgen receptor splice variants activate androgen receptor target genes and support aberrant prostate cancer cell growth independent of canonical androgen receptor nuclear localization signal. *The Journal of biological chemistry* **287**, 19736-19749, doi:10.1074/jbc.M112.352930 (2012).
- 53 Watson, P. *et al.* Constitutively active androgen receptor splice variants expressed in castration-resistant prostate cancer require full-length androgen receptor. *Proceedings of the National Academy of Sciences of the United States of America* **107**, 16759-16765, doi:10.1073/pnas.1012443107 (2010).
- 54 Simanainen, U. *et al.* Disruption of prostate epithelial androgen receptor impedes prostate lobe-specific growth and function. *Endocrinology* **148**, 2264-2272, doi:10.1210/en.2006-1223 (2007).
- 55 Stanbrough, M., Leav, I., Kwan, P., Buble, G. & Balk, S. Prostatic intraepithelial neoplasia in mice expressing an androgen receptor transgene in prostate epithelium. *Proceedings of the National Academy of Sciences of the United States of America* **98**, 10823-10828, doi:10.1073/pnas.191235898 (2001).
- 56 Zhu, C. *et al.* Conditional expression of the androgen receptor induces oncogenic transformation of the mouse prostate. *The Journal of biological chemistry* **286**, 33478-33488, doi:10.1074/jbc.M111.269894 (2011).
- 57 Litvinov, I. *et al.* PC3, but not DU145, human prostate cancer cells retain the coregulators required for tumor suppressor ability of androgen receptor. *The Prostate* **66**, 1329-1338, doi:10.1002/pros.20483 (2006).
- 58 Sharma, N. *et al.* The androgen receptor induces a distinct transcriptional program in castration-resistant prostate cancer in man. *Cancer cell* **23**, 35-47, doi:10.1016/j.ccr.2012.11.010 (2013).
- 59 Visakorpi, T. *et al.* In vivo amplification of the androgen receptor gene and progression of human prostate cancer. *Nature genetics* **9**, 401-406, doi:10.1038/ng0495-401 (1995).
- 60 Wang, X. *et al.* A luminal epithelial stem cell that is a cell of origin for prostate cancer. *Nature* **461**, 495-500, doi:10.1038/nature08361 (2009).
- 61 Marker, P., Donjacour, A., Dahiya, R. & Cunha, G. Hormonal, cellular, and molecular control of prostatic development. *Developmental biology* **253**, 165-174, doi:10.1016/S0012-1606(02)00031-3 (2003).





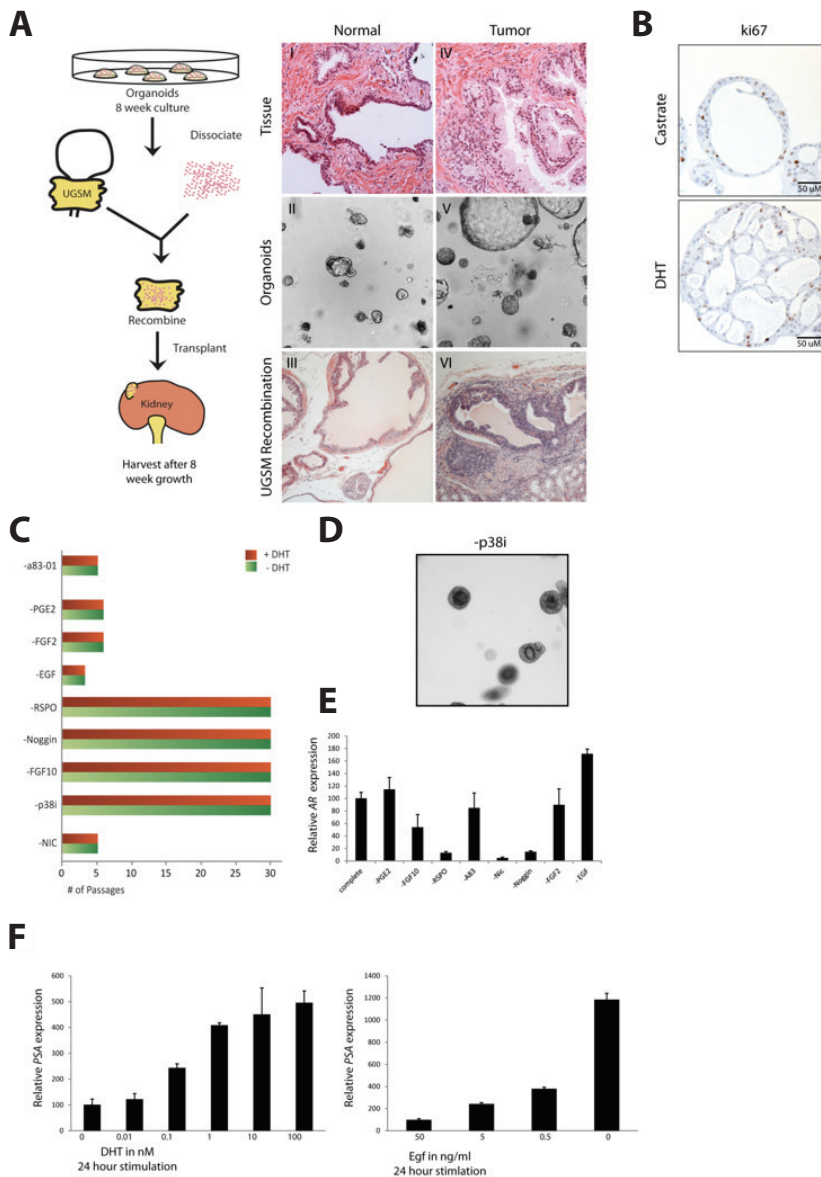
### Supplementary figure 1:

A: Brightfield pictures showing establishment of murine organoids from different lobes in the presence and absence of 200nM a83-001 B: Immunohistochemical analysis of murine organoids under DHT and Castrate conditions. I-II ki67 III-IV Cytokeartin 5 C: Quantative RT-PCR Analysis of AR target *Fkbp5* after DHT withdrawal from the medium (I), showing 24 hours of continued signalling. 24 hours after DHT stimulation titration (0 nM – 100 nM) (II), showing maximal stimulation from concentrations of 0.1 nM and up. 24 hours with increasing Egf concentrations (50 ng/ml – 0 ng/ml) (III) showing a strong increase in *Fkbp5* expression. Results are presented as mean  $\pm$  standard deviation D: Representative brightfield images of organoids undergoing cycles of DHT (1 nM) addition and withdrawal, showing distinct foldinds in DHT treated organoids E: Organoid forming efficiency of 2000 single cells is decreased absence of Noggin, R-spondin or DHT (1nM) F: left: Schematic overview of Organoid-UGSM recombination experimental setup right: H&E staining of murine prostate lobes, organoids derived of their respective lobes and UGSM recombinations. Showing no abnormalities are found. Scale bars represent 50  $\mu$ M.



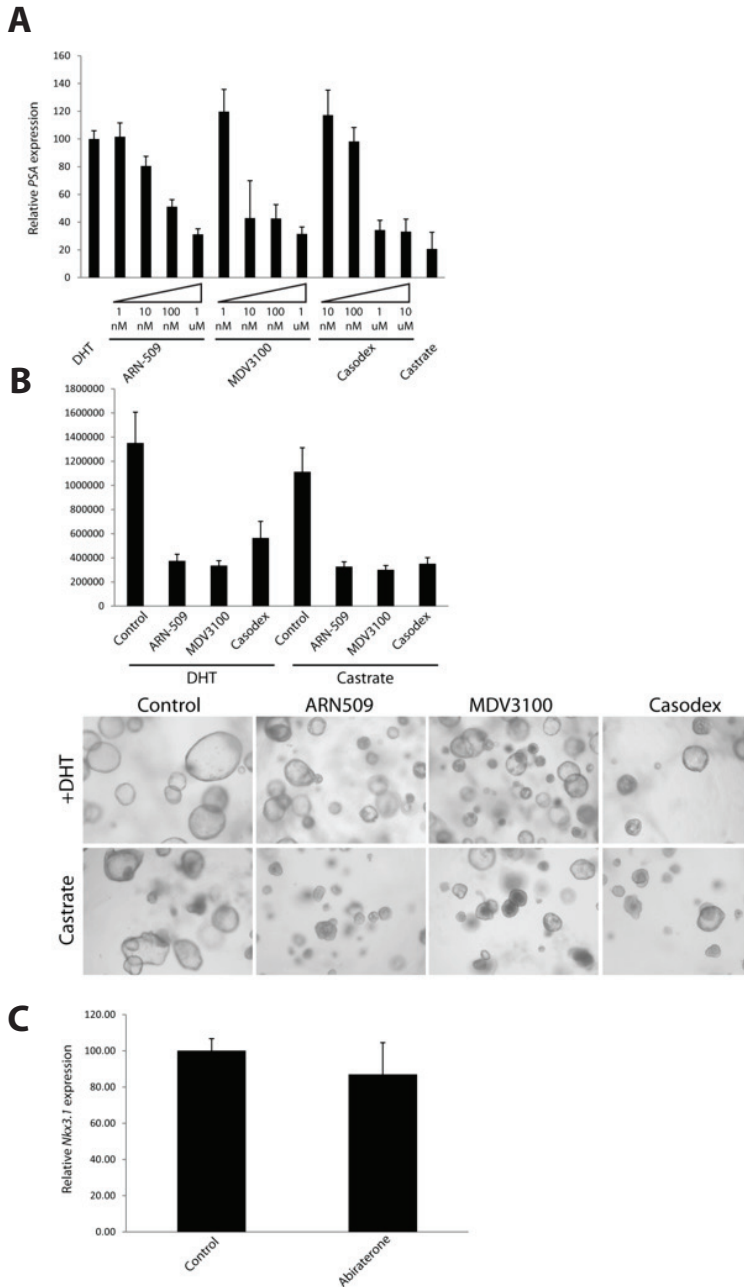
### Supplementary figure 2:

A: H&E staining of organoids derived from the dorsolateral lobe of wildtype, PBCre  $Rosa^{lox\text{-}stop\text{-}lox\text{-}P}^{Erg}$  and PBCre  $Pten^{lox\text{-}P/lox\text{-}P} Rosa^{lox\text{-}stop\text{-}lox\text{-}P}^{Erg}$  mice and organoids-UGSM recombination. In PBCre  $Pten^{lox\text{-}P/lox\text{-}P} Rosa^{lox\text{-}stop\text{-}lox\text{-}P}^{Erg}$  organoids and UGSM recombinations hyperplasticity is observed B: Quantitative RT-PCR analysis of *Psc* expression in organoids derived from all prostate lobes from all genotypes in the presence of DHT (1 nM) and in castrate conditions. All organoids derived from different lobes and genotypes are DHT responsive. Results are presented as mean  $\pm$  standard deviation C: Quantitative RT-PCR analysis of *Pten* and *Psc* expression in shPten and shScr infected organoids derived from all lobes from Wildtype and PBCre  $Rosa^{lox\text{-}stop\text{-}lox\text{-}P}^{Erg}$  mice. *Pten* and *Psc* expression is reduced in all shPten infected organoids. Results are presented as mean  $\pm$  standard deviation D: Western blot analysis of PI3-Kinase pathway components Akt and ribosomal protein S-6 in shPten and ShScr infected organoids derived from all lobes from Wildtype and PBCre mice. Phosphorylation of Akt and p-S6 are increased in shPten infected organoids. Gapdh was probed as a control. Scale bars represent 50  $\mu\text{m}$ .



### Supplementary figure 3:

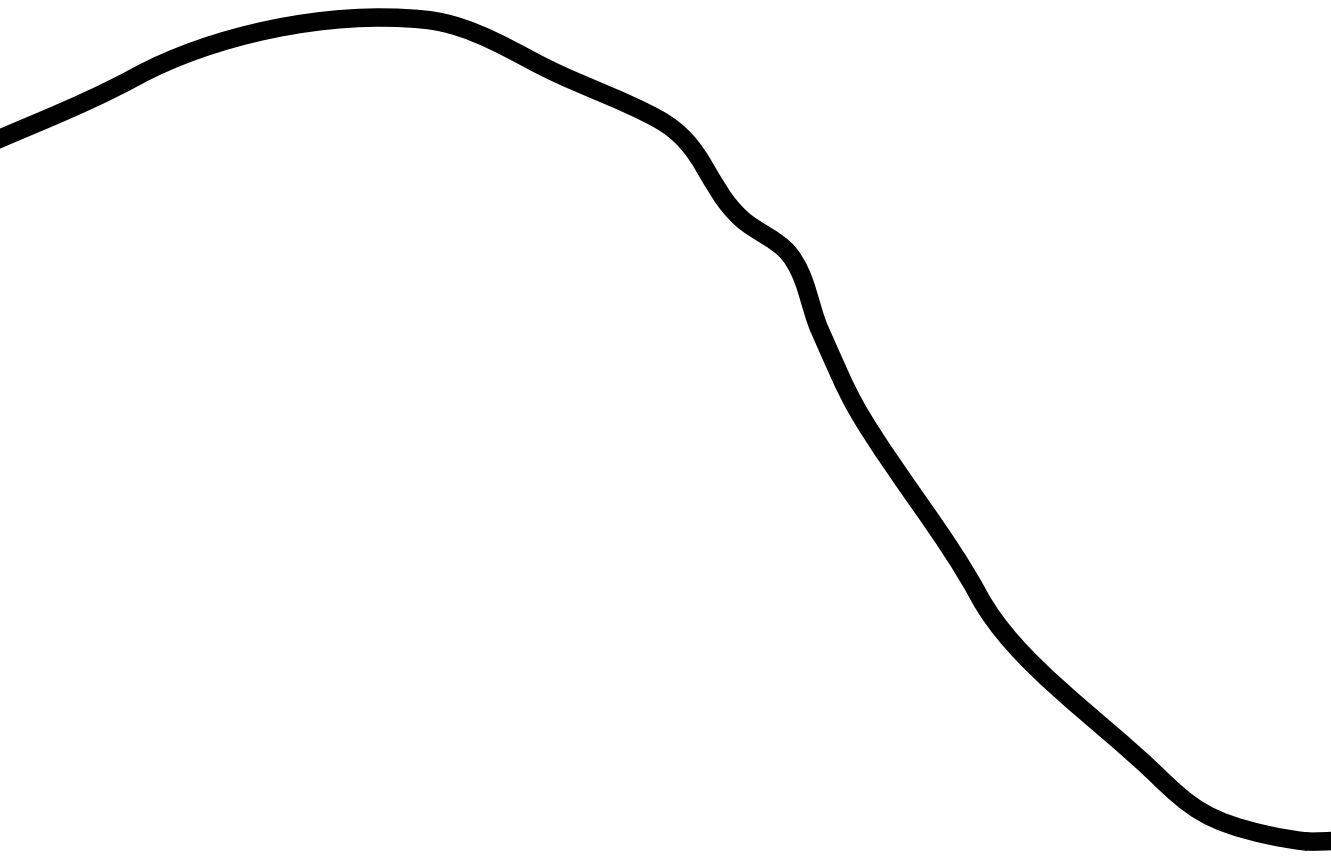
A: left: Schematic overview of Organoid-UGSM recombination experimental setup. 8 week old organoids were enzymatically digested to single cells. 50.000 single cells were recombined with UGSM and placed under the kidney capsule. Right: H&E staining of primary normal and tumor tissue (I & IV), bright field image of the organoids (II & V) and UGSM-recombinations (III & VI) B: Immunohistochemical analysis of ki67 in DHT and Castrate conditions. C: Passage number of the organoids in the absence of single components. Nicotinanid, EGF, A83 PGE2 and FGF2 are essential for organoid proliferation. D: Keratinization observed in the absence of p38 inhibitor SB202190. E: Absence of R-spondin, Noggin, FGF10 or Nicotinamide strongly reduces *AR* expression in the organoids. Results are presented as mean  $\pm$  standard deviation. F: Quantative RT-PCR Analysis of *AR* target *PSA* 24 hours after DHT stimulation, titration (0 nM – 100 nM) (I) 24 hours with titrated Egf (50 ng/ml – 0 ng/ml) (III). *PSA* is upregulated in the absence of EGF. Results are presented as mean  $\pm$  standard deviation.



### Supplementary Figure 5:

A: Quantitative RT-PCR Analysis of AR target *PSA* 24 hours after addition of AR inhibitors ARN-509 (1nM - 1 $\mu$ M), MDV3100 (1nM - 1 $\mu$ M) and Casodex (10nM - 10 $\mu$ M) in the presence of DHT (1nM), *PSA* levels are comparable to castrate at in the presence of 100 nM (ARN-509 & MDV3100) and 1  $\mu$ M Casodex B: Quantification of WT organoid size 14 days after inhibitor treatment ARN-509 (100nM), MDV3100 (100nM) and Casodex (1 $\mu$ M) in absence and in the presence of DHT(1 nM). Organoid size is reduced in treated organoids. Under castrate conditions AR inhibitor treatment decreased mean organoid size further. (N=3 wells) Results are presented as mean  $\pm$  standard error of the mean C: Quantitative RT-PCR Analysis of AR target *Nkx3.1* of organoids cultured in Matrigel 24 hours after addition of Abiraterone (100 nM).

<b>Species</b>	<b>Gene</b>	<b>Sequence (5'→3')</b>	<b>Template strand</b>
Mouse	AR	Forward primer Reverse primer Product length	GCCAGGAGTGGTGTGTGCCG AAGTTGCGGAAGCCAGGCAAGG 141
Mouse	Ck8	Forward primer Reverse primer Product length	AGTCCGCTCTCGAACCTCCGT GCTCCAGGAAGCGCACCTTGTC 412
Mouse	Ck18	Forward primer Reverse primer Product length	ACCTGAGGGCTCAGATCTTTGCGA AGGGTGCCTCAGCTCCGT 505
Mouse	Ck5	Forward primer Reverse primer Product length	GTGGGGGCAGCCGCTCTTTC TCCAGGAACCGCACCTTGTCG 520
Mouse	Ck14	Forward primer Reverse primer Product length	GCTGCCGCTTCCAGAGTTCCT GCTCTGCACTCTTGGTCTGGAACC 879
Mouse	p63	Forward primer Reverse primer Product length	AGCAGAAAAGAGGAGAGCAGC GGTTCGTGTACTGTGGCTCAC 250
Mouse	Probasin	Forward primer Reverse primer Product length	TGACGGGCCTTGCAAACAA TGCTTGACAGTTGTCCTGTCC 434
Mouse	Nkx3.1	Forward primer Reverse primer Product length	ACGCAGTCCAAGCGGCTCAC TGTGCATCAGACTCGGGTTCAGTC 224
Human	CK8	Forward primer Reverse primer Product length	ACCTGCAGGAAGGGATCTCCG AGGCCACCGCAAAGTTGCT 208
Human	CK18	Forward primer Reverse primer Product length	TGCCAGCTCTGGGTTGACCG TGTGGTGCTCTCCTCAATCTGCTG 157
Human	CK5	Forward primer Reverse primer Product length	CGAGGAATGCAGACTCAGTGAGAG GCTTCCACTGCTACCTCCGGC 166
Human	CK14	Forward primer Reverse primer Product length	TCCAGAGATGTGACCTCCTCCAGC ATTGCCAGGAGGGGTGAGGG 234
Human	p63 (tv4-5-6)	Forward primer Reverse primer Product length	CCTGGAGCCAGAAGAAAGGACAGC CAGGTTGCTGTACTGTGGCTCACT 109
Human	PSA	Forward primer Reverse primer Product length	TGGGGACCACCTGCTACGCC TCGGTGATCAGAATGACCCACGAG 208
Human	AR	Forward primer Reverse primer Product length	GGCGGGCCAGGAAAGCGACT TCCCTGGCAGTCTCCAAACGCAT 165
Human	NKX3.1	Forward primer Reverse primer Product length	CGTCCAAGCCGCTCACGTCC CCCAAGTGCCTTTCTGGCTCGG 235
Human	TMPRSS2:ERG	Forward primer Reverse primer	CAGGAGGCGGAGGCGGA GGCGTTGTAGCTGGGGGTGAG



# Chapter 6: Tnfrsf19 marks luminal progenitor cells in the prostate

Wouter R. Karthaus, Jarno Drost, Marc L. van de Wetering, Daniel E. Stange Johan H. van Es, Maaïke van den Born and Hans C. Clevers.



# Tnfrsf19 marks luminal progenitor cells in the prostate

**Wouter R. Karthaus, Jarno Drost, Marc L. van de Wetering, Daniel E. Stange Johan H. van Es, Maaïke van den Born and Hans C. Clevers.**  
Hubrecht Institute, Royal Netherlands Academy of Arts and Sciences & University Medical Center Utrecht, 3584 CT, Utrecht<sup>1</sup>

## **Abstract:**

The prostate is composed of multiple ducts that are lined with pseudo-stratified epithelium. The prostate epithelium is composed of luminal and basal cells, which can be distinguished by specific lineage markers. Lineage tracing experiments suggest that unipotent stem cells exist in both the luminal and basal lineage. Using the *Tnfrsf19<sup>Kl</sup>* mouse model we show that in the murine prostatic epithelium two distinct populations of luminal and basal cells express Tnfrsf19. Using lineage tracing we show that Tnfrsf19<sup>+ve</sup> luminal cells are unipotent progenitor cells and contribute to the luminal lineage during homeostasis and regeneration of the prostate *in vivo*. *In vitro*, Tnfrsf19<sup>+ve</sup> luminal cells display bipotentiality generating prostate organoid structures composed of both luminal and basal cells. Therefore, we conclude that Tnfrsf19 marks luminal progenitor cells in the prostate.

## **Introduction:**

The prostate is a male sex organ located at the base of the bladder surrounding the urethra, and produces approximately 30% of the seminal fluid.

The human prostate is composed of a single gland that is subdivided into three zones (central, transition and peripheral)<sup>1</sup>, whereas the murine prostate is subdivided into three histologically distinct lobes, the anterior Prostate (AP), Dorsolateral Prostate (DLP) and Ventral Prostate (VP)<sup>2</sup>. Prostatic ducts are lined by a pseudo-stratified epithelium in both species<sup>1,2</sup>. Three epithelial cell types are identified in the adult prostate: 1) basal cells, marked by Cytokeratin (Ck) 5, Ck14 and p63 2) Luminal cells, marked by Ck8, Ck18, Androgen receptor (Ar) and secretory proteins like Prostate specific antigen (PSA) 3) Neuroendocrine cells, marked by Chromogranin A and Synaptophysin<sup>3</sup>. In both the adult and developing prostate, intermediate cells expressing both basal and luminal markers have been identified<sup>4,5</sup>, but their identity and function remain unclear.



A hallmark of Prostate cancer (PCa) is the absence of the basal cell lineage. Interestingly, basal cells have often been implied as a cell of origin for cancer<sup>6-8</sup>, as deletion of the tumor suppressor Pten in basal cells results in a tumor with a luminal phenotype. However, deletion of Pten in luminal cells also leads to prostatic intraepithelial hyperplasia (PIN) with a similar phenotype<sup>9-11</sup>.

In several other somatic tissues, stem cells have been shown to represent the cells-of-origin of cancer<sup>12</sup>. In the adult prostate epithelium, a stem cell marker has not been reported. Pioneering lineage-tracing studies from basal Ck5+ve and luminal Ck8+ve cells have shown that in adult mice both lineages harbor unipotent stem cells<sup>10,13</sup>. However using the classic urogenital sinus mesenchyme (UGSM) recombination essay<sup>14</sup>, it has been shown that single Sca-1+, CD133+, CD44+, CD177+ cells, which are predominantly basal in mice and exclusively basal in human, can generate complete prostatic ducts<sup>15</sup>. Additional proof has come from a basal cell population that was identified by high Trop2 expression and was shown to have bipotential capacity<sup>16</sup>. Moreover, lineage tracings from Ck5+ve cells in 4-week-old mice show that basal cells are bipotential during postnatal development<sup>13</sup>. In a recent study by Wang and colleagues lineage tracing from Ck5+ve cells revealed that basal cells at a low degree are bipotential in the adult prostate<sup>11</sup>. In the same study, it is shown that 25% of basal cells are capable of forming spheres in an *in vitro* colony-forming assay, suggesting a large degree of plasticity among basal cells,

Lineage tracing from Ck8+ve and Ck18+ve cells suggest unipotency in the luminal lineage<sup>10,13</sup>. After castration (resulting in a strong reduction of serum androgen levels), approximately 90% of all luminal cells die within 3 weeks<sup>17</sup>. Within the luminal population, a subset of cells retains the expression of the homeobox gene *Nkx3.1*. These are known as castration resistant *Nkx3.1* positive cells or CARNs<sup>9</sup>. During regeneration of the prostate by exogenous androgens, CARNs contribute to both luminal and basal lineages, as evidence of the existence of bipotential cells in the luminal lineage. However, it remains unclear how CARNs are identified pre-castration and thus there is no possibility to isolate CARNs from prostates.

Previously, we have described a quiescent stem cell of the stomach corpus epithelium marked by the expression of the tumor necrosis factor receptor super family member 19 (Tnfrsf19) (Stange et al. Unpublished data). Tnfrsf19 is also expressed specifically in the Lgr5+ve stem cells of the intestine<sup>18</sup>. In this study, we describe both a basal and luminal cell population marked by Tnfrsf19 expression. Both are capable of forming prostate organoids in our

novel culture method (Karthaus et al. Chapter 5). Moreover, we show that luminal *Tnfrsf19*<sup>+ve</sup> luminal cells contribute to the tissue during homeostasis, survive castration and contribute to the regeneration of the prostate.

## Results:

### Expression of *Tnfrsf19* in the prostate:

We examined the expression of *Tnfrsf19* in the murine prostate using the *Tnfrsf19*<sup>KI</sup> mouse. In the *Tnfrsf19*<sup>KI</sup> mouse model, eGFP and CreERT2 are under the control of endogenous *Tnfrsf19* regulatory sequences (Stange et al. unpublished data). Therefore, eGFP expression recapitulates the endogenous *Tnfrsf19* expression. We found that the majority of basal cells are *Tnfrsf19* positive (*Tnfrsf19*<sup>+ve</sup>) (Figure 1B). In the luminal cells, *Tnfrsf19* expression was restricted to a population proximal to the urethra in all lobes (Figure 1C). In this area, label retaining luminal cells are known to remain during multiple cycles of castration regeneration, thus being castration resistant<sup>19</sup>. We verified the eGFP expression pattern using *in situ* hybridization (Figure 1D). Interestingly we found that *Tnfrsf19* expressing luminal cells remain present in the murine prostate 3 weeks after castration, suggesting that either *Tnfrsf19* expressing luminal cells survive castration or that *Tnfrsf19* expression is induced after castration.

### Lineage tracing from *Tnfrsf19*<sup>+ve</sup> cells

To analyze the contribution of *Tnfrsf19*<sup>+ve</sup> cells during homeostasis, *Tnfrsf19*<sup>KI</sup> mice were crossed to the *Rosa26YFP* Cre reporter mice<sup>20</sup> to allow lineage tracing. In *Rosa26YFP* mice an YFP coding sequence is preceded by roadblock sequence that is flanked by loxP sites. Upon tamoxifen injection, the CreERT2 recombinase is activated and removes the roadblock. This results in expression of YFP allowing visualization of genetically marked *Tnfrsf19*<sup>+ve</sup> cells and their progeny (Figure 2A). To activate the CreERT2 recombinase, *Tnfrsf19*<sup>KI</sup> mice were injected tamoxifen (Figure 2B). One day post injection, we found single labeled YFP cells in both the basal and luminal lineage exclusively in the proximal region in the AP, DLP and VP (Figure 2C). Given the long turnover time of the prostatic epithelium we followed lineage tracing for up to one year. One year post injection, we found multiple YFP positive clones of with sizes varying from 5 to 20 cells that stained positive for luminal markers CD24 and Ar and negative for basal markers Ck5 and CD49f. Thus the YFP<sup>+ve</sup> cells represent luminal cells. In the proximal region, we found several ribbons of YFP<sup>+ve</sup> cells among luminal *Tnfrsf19*<sup>+ve</sup> cells. Interestingly distal YFP<sup>+ve</sup> clones of *Tnfrsf19* negative luminal cells were found, suggesting that YFP labeled cell migrate from proximal to distal. No YFP<sup>+ve</sup> positive basal clones were found.

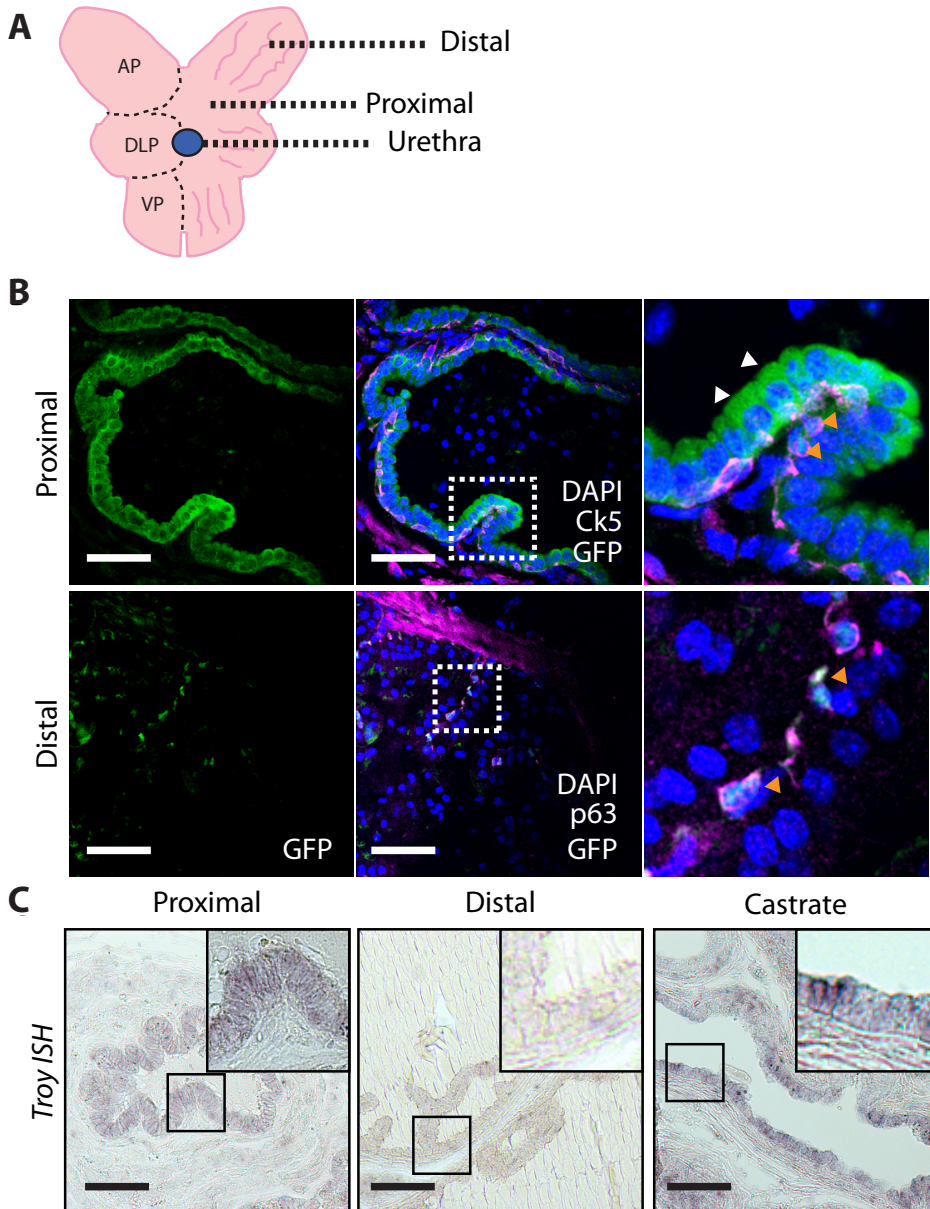


### Figure 1: *Tnfrsf19* expression pattern in the murine prostate.

A: Schematic overview of the murine prostate, showing different lobes Anterior Prostate (AP), Dorsolateral Prostate (DLP) and Ventral Prostate (VP) and proximal and distal regions of the prostate. B: Expression pattern of eGFP in the *Tnfrsf19<sup>KI</sup>* mouse model. In the proximal region both luminal (white arrow) and Ck5+ve basal cells (Magenta, orange arrow) express eGFP. In distal regions eGFP expression is confined to Ck5+ve basal cells. Anterior Prostate is shown. C: Verification of the eGFP expression pattern via ISH with *Tnfrsf19* specific probe. In the proximal region *Tnfrsf19* mRNA was detected in luminal and basal cells. Distal basal cells express *Tnfrsf19* at lower levels. In a castrated prostate *Tnfrsf19* expressing luminal cells are detected. Scale bars represent 50  $\mu$ M.

Given the proximal location of Tnfrsf19+ve luminal cells, we hypothesized that Tnfrsf19+ve luminal cells are castration-resistant and could contribute to the regeneration of the prostate. Upon castration, the prostate undergoes a process called involution. In this process 90% of luminal cells die whereas only a small fraction of basal cells are killed<sup>17</sup>. When testosterone serum levels are restored, the prostate regenerates to its original size. To test whether Tnfrsf19+ve cells survive castration, mice were injected with tamoxifen and subsequently castrated. Approximately 3 weeks post castration, the prostate became completely involuted and a testosterone-filled osmotic pump was placed subcutaneously to function as an exogenous androgen source, restoring serum levels to pre-castration levels<sup>21</sup>. Prostates were allowed to regenerate for 3 weeks before isolation (Figure 3A). After castration single luminal YFP-labelled Tnfrsf19+ve cells are found in the prostate (Figure 3C). Similar to the long-term tracing, YFP+ve clones stained positive for AR and CD24 and negative for the basal marker Ck5, thus representing luminal cells (Figure 3C-D). YFP+ve clones were predominantly found in the distal regions of the prostatic lobes (Figure 3). In conclusion, Tnfrsf19+ve luminal cells are castration-resistant and are capable of contributing to the luminal lineage during homeostasis and regeneration.

### **Tnfrsf19+ve cells display *in vitro* stemness potential**

Because several studies indicate that sub-populations of prostate epithelial cells are bipotent *ex vivo*<sup>9,11,16,22,23</sup> we postulated that Tnfrsf19+ve luminal cells might be bipotent *in vitro*, thus capable of generating all prostate lineages.

To assess the bipotentiality of Tnfrsf19+ve cells we performed an organoid formation assay using our novel prostate culture method (Karthaus et al., Chapter 5). Tnfrsf19+ve cells were isolated from all prostate lobes using FACS sorting based on eGFP expression. About 20% of all cells appeared to be Tnfrsf19+ve (Figure 4). To distinguish between luminal and basal epithelial lineage, cells were stained with a luminal specific (CD24) and basal specific (CD49f) antibody (Figure 4). Expression of luminal (*Nkx3.1* and *Probasin*) and basal (*Ck5*, *p63*) lineage markers was analyzed using qPCR, confirming that CD24+ve cells are of luminal origin and that CD49f+ve cells are of basal origin. Among the Tnfrsf19+ve cells, we found 3 subpopulations; 1) CD24+ve Cd49f-lo, 2) CD49f-hi CD24 negative (-ve) and 3) double negative. 200 Single cells per population were seeded under standard prostate organoid culture conditions (Egf, Noggin, R-spondin, a83-01, Dihydrotestosterone and Rho kinase inhibitor Y-27632). The total number of organoids was counted 14 days post seeding. We found that -on the whole- 3% of luminal cells were capable of forming an organoid structure, whereas 15% of CD49f-hi cells

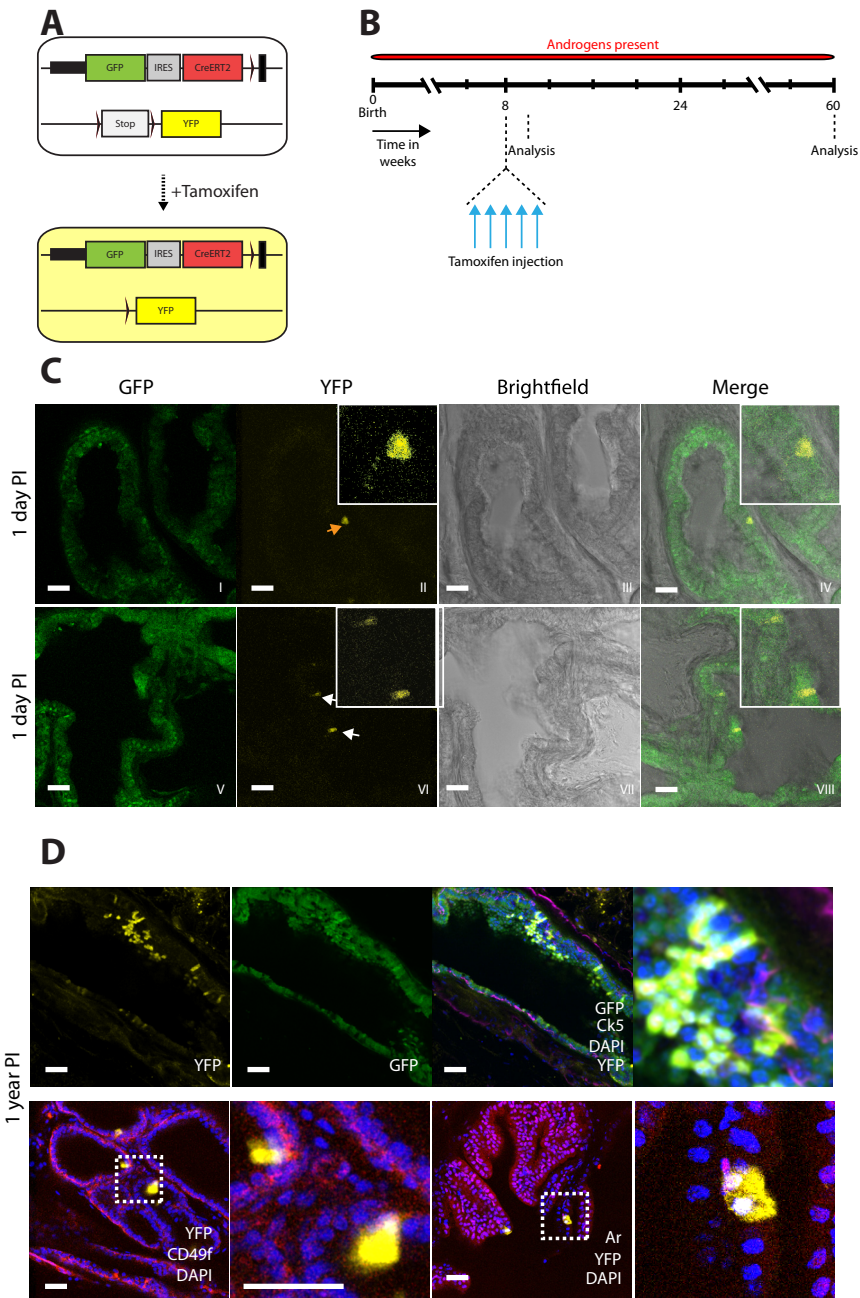


**Figure 2: Long term tracing from Tnfrsf19+ve cells.**

A: Schematic overview of Tnfrsf19<sup>ki</sup> and Rosa26YFP alleles used for lineage tracing experiments. Upon Tamoxifen injection CreERT2 removed the roadblock sequence from the R26 allele, allowing expression of YFP and lineage tracing. B: Induction scheme for long term lineage tracing C: 1 day post induction (PI) single Tnfrsf19+ve labeled basal (orange arrow) and luminal cells (white arrow) are observed in the prostate D: 1 year PI YFP labeled clones stain negative for basal markers (Ck5) and positive for luminal cell markers (CD24, Ar). Indicating long term lineage tracing occurred exclusively in the luminal cells. 3 mice were analyzed per timepoint. Scale bars represent 50  $\mu$ M.

were capable of forming an organoid (Figure 4). The organoid forming capacities of the GFP+ve populations was not significantly different among lobes (Supplementary figure 2). CD24 and CD49f negative GFP+ve cells and GFP negative cells did not form any organoids (Figure 2, Supplementary figure 2). Interestingly both Cd24+ and CD49f+ Tnfrsf19+ derived organoids were composed of basal and luminal cells. Our data shows that both luminal and basal Tnfrsf19+ve populations are bipotential *in vitro*.

## Discussion

Here we identify a luminal Tnfrsf19+ve cell population that contributes to the luminal lineage of the prostatic epithelium during homeostasis and regeneration. Moreover, we show that luminal Tnfrsf19+ve cells are unipotent *in vivo* and therefore conclude that Tnfrsf19 marks progenitor cells of the luminal lineage. The castration resistant Nkx3.1 positive cell population (CARNs) was previously shown to host a stem cell of luminal origin<sup>9</sup>. However, due to the broad expression pattern of Nkx3.1 in an intact prostate, the identification of CARNs is impossible. The fact that Tnfrsf19+ve luminal cells are castration resistant makes it plausible that they represent CARNs during homeostasis. In contrast to CARNs, we found no bipotentiality of Tnfrsf19+ve luminal cells *in vivo*. However *in vitro* Tnfrsf19+ve luminal cells were capable of forming all lineages. This is in agreement with several other studies. Mammary stem cells, for example, have also been shown to be unipotent within their respective lineages *in vivo*, that can be bipotent *ex vivo* and upon transplantation<sup>24</sup>

Tnfrsf19+ve basal cells are more potent in organoid formation than are luminal cells. This high degree of sphere forming capacity of basal cells has been previously observed by others<sup>11</sup>, suggesting high plasticity of basal cells. Remarkably, we did not observe any tracings from basal Tnfrsf19+ve cells. This is most likely due to low recombination efficiencies in basal cells. What regulates this switch from unipotency to bipotency remains unclear. Whether luminal Tnfrsf19+ve cells represent the cells-of-origin for prostate cancer remains to be determined. Several studies have shown that both basal and luminal cells are capable of initiating cancer<sup>6,10,11</sup>. Moreover, in other tissues, stem/progenitor cells have been shown to be the cell of origin in tumor formation<sup>12</sup>, This makes it plausible that also Tnfrsf19+ve cells could function as a cell of origin in prostate cancer. In conclusion, Tnfrsf19 marks a subset of luminal cells with stem/progenitor cell properties in the prostate. Further research of this cell population could yield vital insights into homeostasis, regeneration and cancer initiation of the prostate.

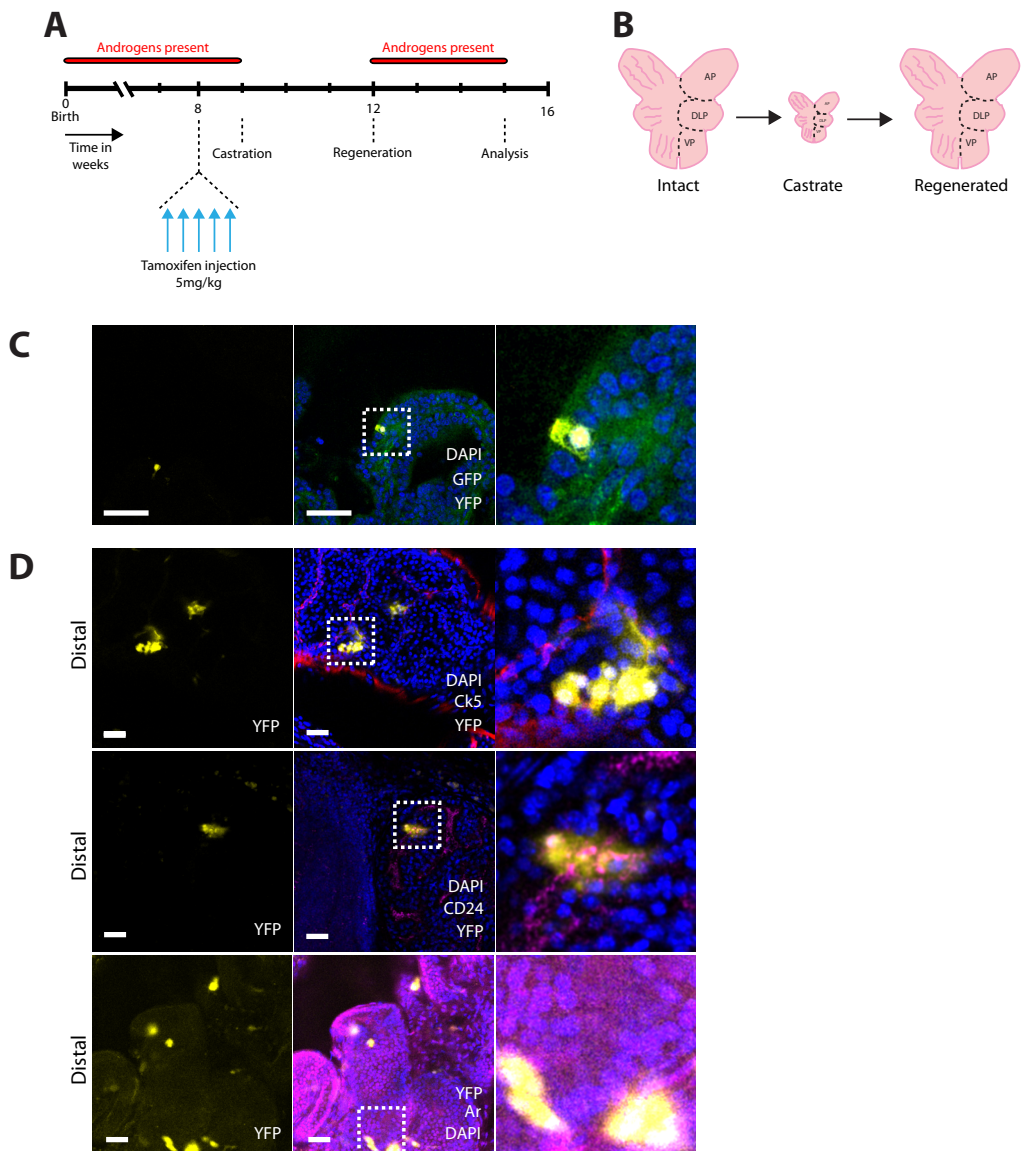


**Figure 3: Luminal cell tracing from *Tnfrsf19*+ve cells during regeneration of the prostate.**

A: Schematic overview of induction and castration/regeneration scheme. Mice are induced with tamoxifen en subsequently castrated. 3 weeks post castration exogenous testosterone was given to mice. 7 weeks PI inductions prostates were collected. B: Schematic overview of prostate size during a castration/regeneration cycle C: In a castrated prostate single luminal *Tnfrsf19*+ve YFP labeled cells are detected. D: After regeneration YFP labeled clones stain negative for basal markers (Ck5) and positive for luminal cell markers (CD24, Ar). YFP+ve clones were found in distal regions of the prostate. Indicating lineage tracing occurred exclusively in the luminal cells. 3 mice were analyzed per timepoint. Scale bars represent 50  $\mu$ M.

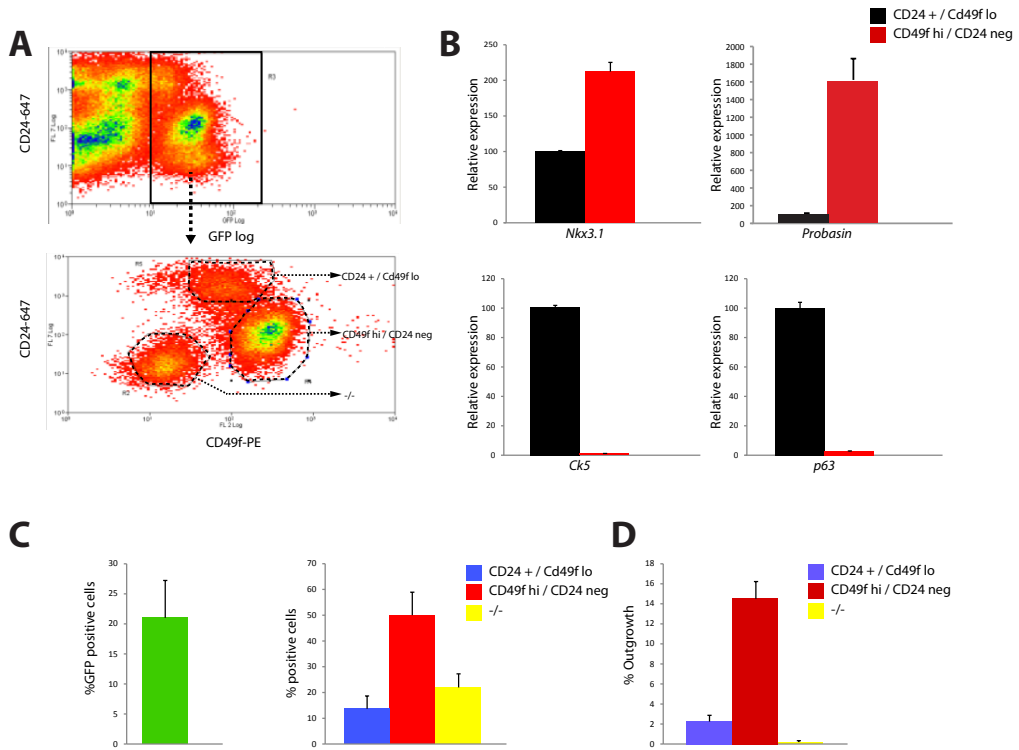


## Figure 4: Luminal and basal Tnfrsf19+ve cells both have organoid forming capacity.

A: Representative FACS profiles of eGFP cells from the murine prostate. Tnfrsf19+ve Luminal and basal cells were separated on the basis of CD24 (luminal) and CD49f (Basal) expression B: Analysis of luminal and basal expression markers via qPCR shows strong expression of luminal markers *Nkx3.1* and *Probasin* in the CD24+ve eGFP population and strong expression of basal markers *Ck5* and *p63* CD49f+ve eGFP verifying cellular identity of sorted populations. Results are present as mean  $\pm$  standard deviation C: Total percentage of eGFP+ve cells in the prostate and percentage of subpopulations of eGFP cells. Results are present as mean  $\pm$  standard deviation. D: Organoid forming capacity from single cells from eGFP+ve subpopulations. 2 weeks post seeding of 100 single cells total number of organoids was counted. CD49f+ve population displays high organoid forming capacity (15%). CD24+ve population has organoid forming capacity but at reduced levels (3%). CD24, CD49f negative Tnfrsf19+ve cells do not form organoids. (N=3) Results are presented as mean  $\pm$  standard deviation



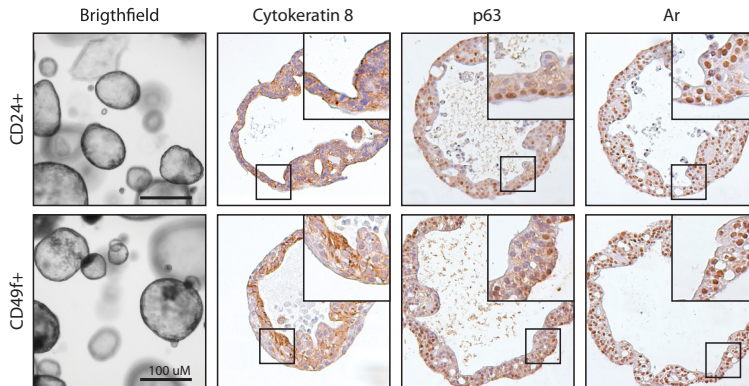


### Figure 5: Luminal and basal *Tnfrsf19*+ve cells are bipotential in vitro.

Immunohistochemical analysis of organoids formed by CD24+ve luminal and Cd49f+ve basal, *Tnfrsf19*+ve cells shows that both CK8+ve luminal and p63+ve basal lineages are formed in organoid culture conditions. Moreover in both organoids nuclear Ar staining is observed indicating an intact signaling pathway. Showing both CD24+ve and CD49f+ve *Tnfrsf19*+ve cells are bipotential in culture. Scale bars represent 50  $\mu$ M (IHC) or 100  $\mu$ M (Brightfield).

## Materials & Methods:

### Mouse work:

All mice work was done in accordance with rules and regulations of the animal welfare laws of the Netherlands. *Tnfrsf19<sup>Kl</sup>* mice were crossed to *Rosa26YFP Cre* reporter strain in a C57BL/6 background. To activate the CreERT2 recombinase mice were injected 5 times using 5mg/kg tamoxifen. Castration/Regeneration assay was performed as described previously<sup>21</sup>. In short, mice were castrated using standard techniques and left for 3 weeks for complete involution of prostate. Prostates were regenerated for 3 weeks by implantation of Alzet minipumps containing 7.5 mg/ml testosterone in PEG-400 (Diluted from 25 mg/ml stock in ethanol), releasing 1,875  $\mu$ g testosterone / hour resulting in serum testosterone levels that resemble physiological levels<sup>21</sup>.

### IHC & IF:

Prostates were isolated from mice and fixed with 4% PFA for one hour on ice. For IHC prostates were embedded into paraffin using standard techniques. IF was performed on 90  $\mu$ m sections of tissue embedded in low melting point agarose on vibratome sections, which were generated as described previously<sup>25</sup>. Sections were blocked and permeabilized using 2% BSA and 1% Triton X-100 in PBS for 10 minutes at RT. Stainings were performed in 0.05% BSA 0.3% Triton X-100 overnight at 4 °C using the following antibodies Ck5 (1:500 AF-138 Covance), CD24 (1:200, 30-F1, eBioscience), Cd49f (1:250, GoH3, BD bioscience),

AR (1:200, N-20 Santa Cruz). Secondary antibodies used were Donkey anti mouse IgG and Donkey anti Rabbit IgG conjugated with alexa fluor 568 or 647 (Invitrogen). Stainings were analyzed using a Leica SP5 confocal microscope.

### **FACS sorting:**

Prostates were isolated from *Tnfrsf19<sup>Kl</sup>* mice, subdivided in three lobe pairs (Anterior Prostate, Dorsolateral Prostate and Ventral Prostate) and subsequently digested in 5 mg/ml collagenase type II (Gibco) in ADMEM/F12 for 60-90 minutes at 37 °C. Digested tissue was washed once using cold ADMEM/F12 and trypsinized for 10-15 minutes. Cells were washed and cells were forced over 42 µm filter to ensure a single cell suspension. Cells were blocked for 10 min with 2% FCS in ADMEM/F12 and stained using Cd49f-PE conjugated antibody (1:200, GoH3, BD Biosciences) and CD24-alexa 647 conjugated antibody (1:200, 30-F1, eBioscience) in 0.05% FCS in ADMEM/F12. Cells were sorted using MoFlo (Dako).

### **RNA, cDNA, PCR:**

RNA was isolated using RNeasy minikit (Qiagen) according to manufacturers protocol. cDNA synthesis was performed with 50-1000 ng RNA using GoScript (Promega) according to manufacturers protocol. qPCR was performed using Sybr green (Bio-Rad) according to manufacturers protocol with primers listed in supplementary table 1.

### **Cell culture:**

Organoid culture was performed as described previously (Karthaus et al.) In short Murine prostate epithelial cells were cultured in ADMEM/F12 containing growth factors EGF 5-50 ng ml<sup>-1</sup> (Peprotech), R-spondin 1 conditioned medium (Reference ABO) or 500 ng ml<sup>-1</sup> recombinant R-spondin 1, Noggin conditioned medium or 100 ng ml<sup>-1</sup> recombinant Noggin (Peprotech) and the tgfbeta/alk inhibitor a33-01 (Tocris) to Dihydrotestosterone (Sigma) was added at 0.1-1 nM final concentration.

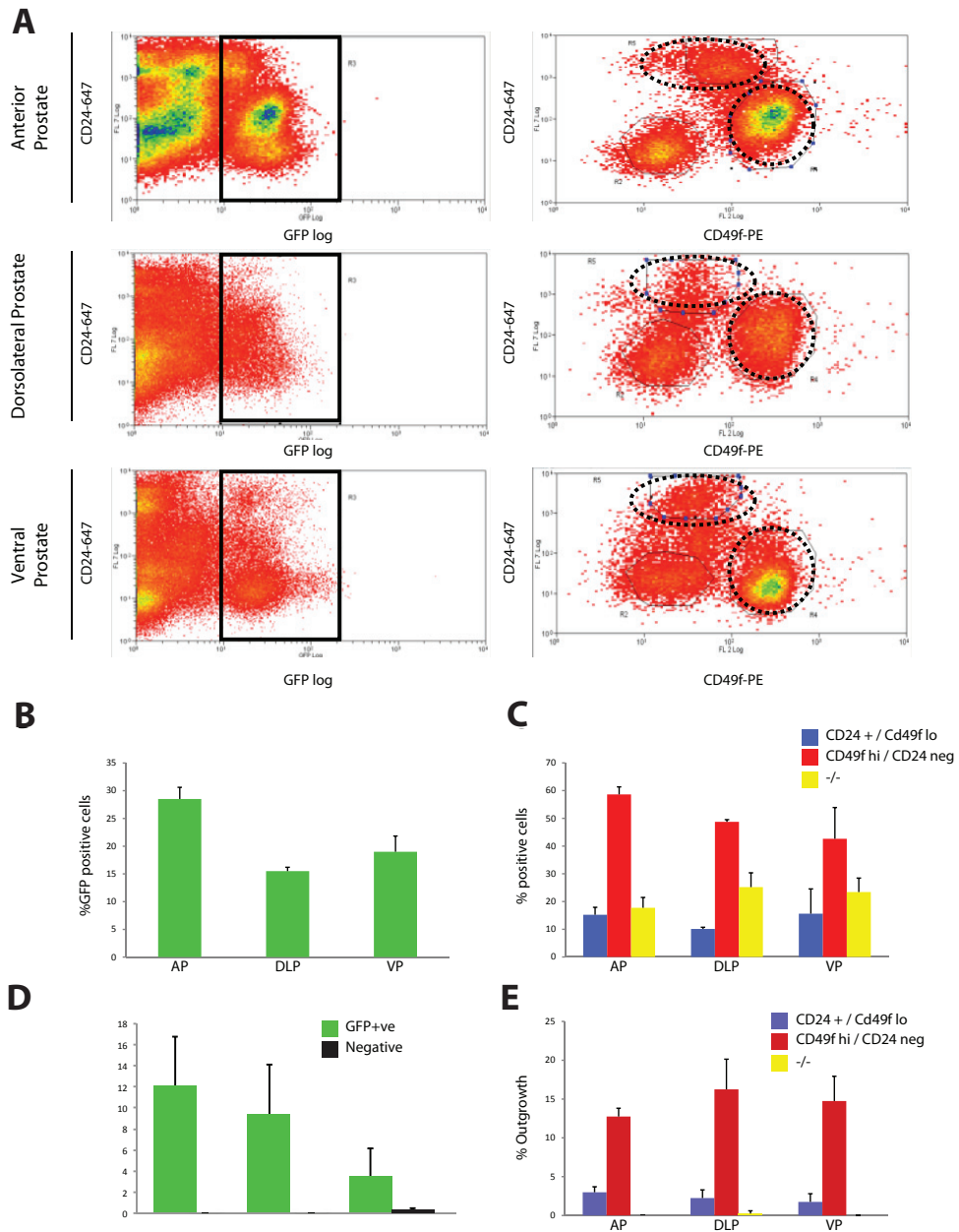
## References:

- 1 McNeal, J. Normal histology of the prostate. *The American journal of surgical pathology* 12, 619-633 (1988).
- 2 Marker, P., Donjacour, A., Dahiya, R. & Cunha, G. Hormonal, cellular, and molecular control of prostatic development. *Developmental biology* 253, 165-174, doi:10.1016/S0012-1606(02)00031-3 (2003).
- 3 Shen, M. & Abate-Shen, C. Molecular genetics of prostate cancer: new prospects for old challenges. *Genes & development* 24, 1967-2000, doi:10.1101/gad.1965810 (2010).
- 4 Xue, Y., Smedts, F., Debruyne, F., de la Rosette, J. & Schalken, J. Identification of intermediate cell types by keratin expression in the developing human prostate. *The Prostate* 34, 292-301, doi:10.1002/(SICI)1097-0045(19980301)34:4<292::AID-PROS7>3.0.CO;2-J (1998).
- 5 Hudson, D. et al. Epithelial cell differentiation pathways in the human prostate: identification of intermediate phenotypes by keratin expression. *The journal of histochemistry and cytochemistry : official journal of the Histochemistry Society* 49, 271-278, doi:10.1177/002215540104900214 (2001).
- 6 Goldstein, A., Huang, J., Guo, C., Garraway, I. & Witte, O. Identification of a cell of origin for human prostate cancer. *Science (New York, N.Y.)* 329, 568-571, doi:10.1126/science.1189992 (2010).
- 7 Lawson, D. et al. Basal epithelial stem cells are efficient targets for prostate cancer initiation. *Proceedings of the National Academy of Sciences of the United States of America* 107, 2610-2615, doi:10.1073/pnas.0913873107 (2010).
- 8 Mulholland, D. et al. Lin-Sca-1+CD49<sup>high</sup> stem/progenitors are tumor-initiating cells in the Pten-null prostate cancer model. *Cancer research* 69, 8555-8562, doi:10.1158/0008-5472.CAN-08-4673 (2009).
- 9 Wang, X. et al. A luminal epithelial stem cell that is a cell of origin for prostate cancer. *Nature* 461, 495-500, doi:10.1038/nature08361 (2009).
- 10 Choi, N., Zhang, B., Zhang, L., Ittmann, M. & Xin, L. Adult murine prostate basal and luminal cells are self-sustained lineages that can both serve as targets for prostate cancer initiation. *Cancer cell* 21, 253-265, doi:10.1016/j.ccr.2012.01.005 (2012).
- 11 Wang, Z. et al. Lineage analysis of basal epithelial cells reveals their unexpected plasticity and supports a cell-of-origin model for prostate cancer heterogeneity. *Nature cell biology* 15, 274-283, doi:10.1038/ncb2697 (2013).
- 12 Barker, N. et al. Crypt stem cells as the cells-of-origin of intestinal cancer. *Nature* 457, 608-611, doi:10.1038/nature07602 (2009).
- 13 Ousset, M. et al. Multipotent and unipotent progenitors contribute to prostate postnatal development. *Nature cell biology* 14, 1131-1138, doi:10.1038/ncb2600 (2012).
- 14 Cunha, G. & Lung, B. The possible influence of temporal factors in androgenic responsiveness of urogenital tissue recombinants from wild-type and androgen-insensitive (Tfm) mice. *The Journal of experimental zoology* 205, 181-193, doi:10.1002/jez.1402050203 (1978).
- 15 Leong, K., Wang, B.-E., Johnson, L. & Gao, W.-Q. Generation of a prostate from a single adult stem cell. *Nature* 456, 804-808, doi:10.1038/nature07427 (2008).
- 16 Goldstein, A. et al. Trop2 identifies a subpopulation of murine and human prostate basal cells with stem cell characteristics. *Proceedings of the National Academy*

- of Sciences of the United States of America 105, 20882-20887, doi:10.1073/pnas.0811411106 (2008).
- 17 English, H., Santen, R. & Isaacs, J. Response of glandular versus basal rat ventral prostatic epithelial cells to androgen withdrawal and replacement. *The Prostate* 11, 229-242 (1987).
- 18 Fafilek, B. et al. Troy, a Tumor Necrosis Factor Receptor Family Member, Interacts With Lgr5 to Inhibit Wnt Signaling in Intestinal Stem Cells. *Gastroenterology*, doi:10.1053/j.gastro.2012.10.048 (2012).
- 19 Tsujimura, A. et al. Proximal location of mouse prostate epithelial stem cells: a model of prostatic homeostasis. *The Journal of cell biology* 157, 1257-1265, doi:10.1083/jcb.200202067 (2002).
- 20 Srinivas, S. et al. Cre reporter strains produced by targeted insertion of EYFP and ECFP into the ROSA26 locus. *BMC developmental biology* 1, 4, doi:10.1186/1471-213X-1-4 (2001).
- 21 Banach-Petrosky, W. et al. Prolonged exposure to reduced levels of androgen accelerates prostate cancer progression in Nkx3.1; Pten mutant mice. *Cancer research* 67, 9089-9096, doi:10.1158/0008-5472.CAN-07-2887 (2007).
- 22 Berman, D. et al. Roles for Hedgehog signaling in androgen production and prostatic ductal morphogenesis. *Developmental biology* 267, 387-398, doi:10.1016/j.ydbio.2003.11.018 (2004).
- 23 Jiao, J. et al. Identification of CD166 as a surface marker for enriching prostate stem/progenitor and cancer initiating cells. *PloS one* 7, doi:10.1371/journal.pone.0042564 (2012).
- 24 Van Keymeulen, A. et al. Distinct stem cells contribute to mammary gland development and maintenance. *Nature* 479, 189-193, doi:10.1038/nature10573 (2011).
- 25 Snippert, H., Schepers, A., Delconte, G., Siersema, P. & Clevers, H. Slide preparation for single-cell-resolution imaging of fluorescent proteins in their three-dimensional near-native environment. *Nature protocols* 6, 1221-1228, doi:10.1038/nprot.2011.365 (2011).

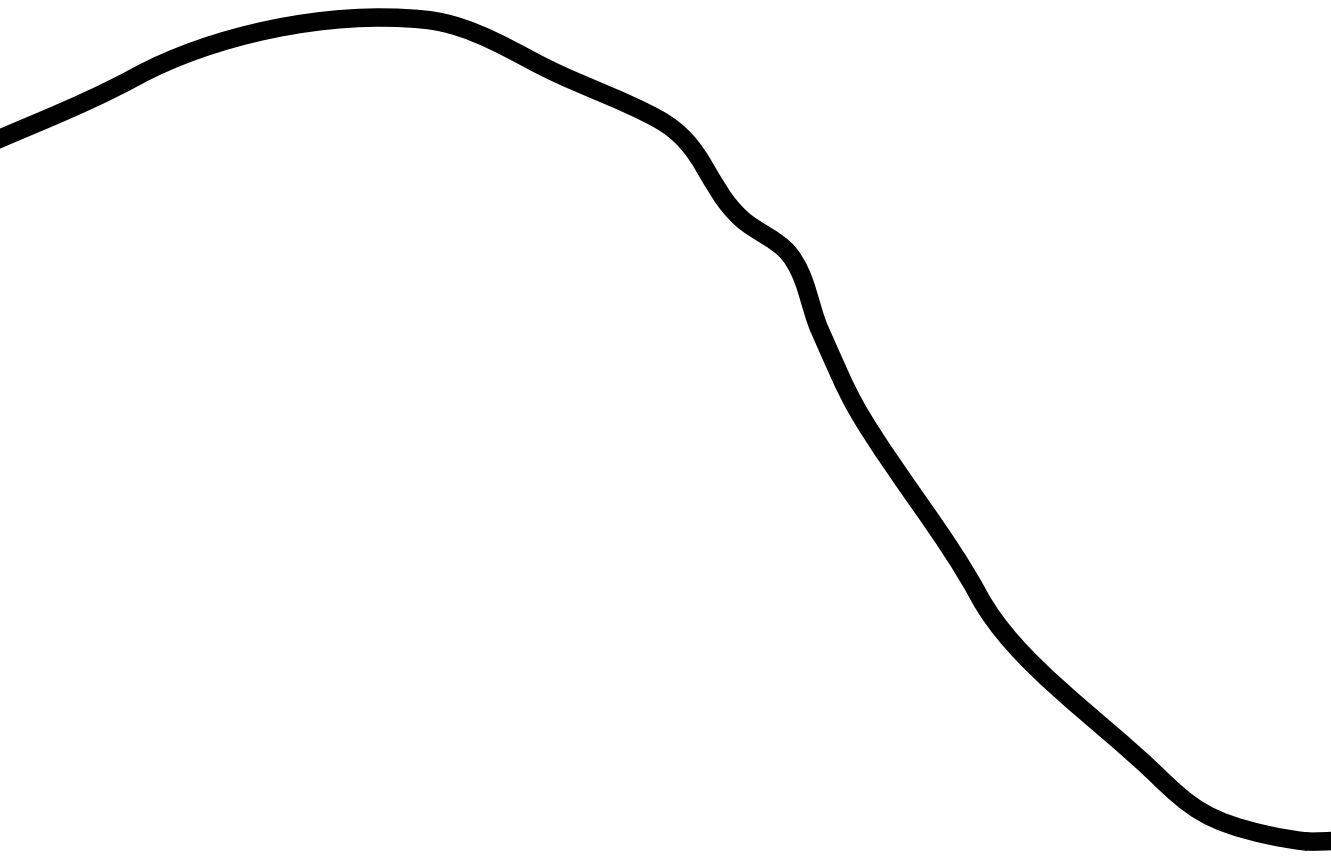
### Supplementary Table S1

Species	Gene	Sequence (5'→3')	Template strand
Mouse	Ck5	Forward primer	GTGGGGGCGAGCCGCTCTTTC
		Reverse primer	TCCAGGAACCGCACCTTGTCG
		Product length	520
Mouse	p63	Forward primer	AGCAGAAAAGAGGAGAGCAGC
		Reverse primer	GGTTCGTGTACTGTGGCTCAC
		Product length	250
Mouse	Probasin	Forward primer	TGACGGGCCTTGGCAAACAA
		Reverse primer	TGCTTGACAGTTGTCCGTGTCC
		Product length	434
Mouse	Nkx3.1	Forward primer	ACGCAGTCCAAGCGGCTCAC
		Reverse primer	TGTGCATCAGACTCGGGTTTCAGTC
		Product length	661



### Supplementary figure 4: Luminal and basal *Tnfrsf19*+ve cells both have organoid forming capacity.

A: FACS profiles of the AP, DLP and VP showing similar populations of eGFP cells and subpopulations in the lobes. B: Total number of eGFP+ve cells is higher in the AP compared to the DLP and VP. (C) eGFP subpopulations from different lobes are similar. (N=3) Results are presented as mean  $\pm$  standard deviation. D: Only *Tnfrsf19*+ve/eGFP+ve cells are capable of organoid formation. (N=3) Results are presented as mean  $\pm$  standard deviation. E: Organoids forming capacities of eGFP subpopulations from different lobes are similar. (N=3) Results are presented as mean  $\pm$  standard deviation.



# Chapter 7: Summarizing discussion



## Summarizing discussion:

*Wouter R. Karthaus*

In adult tissues homeostasis and regeneration are dependent on resident stem cells. Moreover stem cells have also been implied as the initiating cells of diseases like cancer. Therefore insight in stem cell biology is crucial.

The two key-defining features of a stem cell are 1) pluripotency, i.e. the capacity of giving rise to all cell types and 2) longevity. The gold standard for experimentally identifying stem cells *in vivo* makes use of these properties and is named lineage tracing. During lineage tracing a cell is genetically marked and followed over time. If a genetically marked stem cell divides, two daughter cells are also genetically labeled, enabling tracing of the offspring. If overtime all cell types are genetically labeled, it means the first genetically labeled cell is a stem cell. For genetic labeling the Cre-loxP system is commonly used. The Cre-recombinase enzyme recognizes a defined DNA sequence, the loxP site, which is cleaved and subsequently the DNA is recombined, thus genetically labeled.

Using a mouse model where eGFP and CreERT2 (an inducible form of Cre-Recombinase) are knocked in the *Lgr5* genomic locus by homologous recombination, Barker et al. showed that *Lgr5* expressing (*Lgr5*+ve) cells in the small intestinal- and colonic epithelium are long-lived and give rise to all cell types in the intestinal epithelium (Stem cells, Paneth cells, Goblet cells, Enteroendocrine cells and tuft cells) <sup>1,2</sup>. Thus *Lgr5* marks the stem cells of the intestine. In follow-up studies *Lgr5* was found to mark stem cell populations in the hair follicle, stomach and liver <sup>3-5</sup>.

Following the identification of *Lgr5* as a stem cell marker, transcriptional profiles were established using microarray technology. The expression of the nuclear receptor, *Nr2e3* was found to be specific in the ISC. Originally *Nr2e3* expression was thought to be exclusive in the retina <sup>6</sup>, where it functions in specification of cone and rod photoreceptor- progenitors. Mutations in the *Nr2e3* locus are responsible several congenital disorders of the retina <sup>7</sup>. Therefore we postulated that *Nr2e3* might mark novel stem cell populations in different organs and play a role in stem cell maintenance. In chapter 2 we describe a mouse model to study the function of *Nr2e3*, where eGFP and the recombinase CreERT2 are knocked in the locus of *Nr2e3* by homologous recombination. This allows for the detection of *Nr2e3*+ve cells by the expression of eGFP and the CreERT2 allows lineage-tracing studies cells



when crossed with a *Rosa26LacZ Cre reporter* mouse. In contrast to prior reports we found several restricted eGFP/Nr2e3+ve cell populations in a variety of organs, including the retina, small intestine, stomach and lung. Lineage tracing revealed that none of the novel Nr2e3+ve populations represent a stem cell population during homeostasis. However we show that in the stomach Nr2e3 expression was confined to neck mucus cells. We show via lineage tracing that these cells have a lifespan of 2-4 weeks.

Stem cells are also influenced by extrinsic factors. Therefore insight into the stem cell niche or milieu is a vital for understanding stem cells. In chapter 3 we describe the generation of a mouse model where the whole regenerating gene family is knocked-out. The regenerating (Reg) gene family is composed of highly homologous, secreted proteins that contain a c-type lectin-binding domain. We show that several members of the regenerating gene family are expressed in the small intestine. One of the members, Reg3g plays a role in innate immunity of the small intestine<sup>8-10</sup>. Future studies of the complete Reg knockout mice will add to the understanding of the role of these proteins in the intestine and their influence on homeostasis and stem cell function.

With the knowledge attained from Lgr5+ve ISC, an in vitro culture system of the small intestine called organoid culture was developed<sup>11</sup>. In a protein gel (Matrigel®) single ISC are able to form mini-guts, which are composed of a defined crypt and villus region and contain all intestinal epithelial cell types that exist in vivo (Stem cells, Paneth cells, Goblet cells, Enteroendocrine cells and tuft cells). The absence of other cell lineages, allows for the study if the epithelium in an isolated fashion, which could lead to novel insights into diseases with a complex etiology like inflammatory bowel disease. In chapter 4 we study the effects of a key inflammatory cytokine interferon gamma (Ifn $\gamma$ ) on the intestinal epithelium. We find that Ifn $\gamma$  acts as a potent degranulation agent for the Paneth cells. Paneth cells are loaded with anti-microbial proteins, and play a vital role in intestinal homeostasis<sup>12</sup>. We postulate that Ifn $\gamma$ -induced degranulation during an inflammatory situation might serve as a defense strategy to limit microbial growth. Interestingly we find that Paneth cell degranulation is not induced by recognition of pathogen associated molecular patterns (PAMPs). We show that recognition of PAMPs by immune cells and subsequent production of Ifn $\gamma$  is critical for Paneth cell degranulation. Moreover we show that in Ifn $\gamma$ -knockout mice no Paneth cell degranulation is seen upon activation of CD3+ve T-cells confirming our in vitro observations with the organoid culture.

Based on the small intestinal organoid system, similar culture methods have been developed for the epithelium other gastrointestinal organs<sup>4,5,13</sup>. In chapter 5 the development of an organoid culture for both murine and human prostatic epithelium is described.

The prostate is composed of a pseudo-stratified epithelium. Within the epithelium there are 3 lineages recognized 1) Luminal epithelium 2) Basal epithelium and 3) Rare Neuroendocrine cells<sup>14</sup>. The prostate is heavily dependent on androgens and the androgen receptor for its development and function<sup>15-17</sup>. Moreover the treatment of choice of prostate cancer (PCa) is anti-androgen therapy, suggesting a pivotal role of androgens in cancer survival<sup>18,19</sup>. Strangely none of the other culture methods that have been developed for the primary prostate epithelium<sup>20-23</sup> contain androgens at physiological levels<sup>24</sup>. In contrast prostate organoid cultures do contain androgens, allowing full differentiation to all epithelial lineages and function of the prostate organoids. This system allows the murine genetic models of PCa, which resemble *in vivo* phenotypes. Moreover easy genetic manipulation of prostate organoids, allows quick and efficient study of genes involved in PCa. Finally we show that prostate organoids can be treated with clinically approved anti-androgens. Considering almost 100% of patients treated with anti-androgen relapse and develop androgen independent disease or castration resistant prostate cancer (CRPC)<sup>25</sup>, prostate organoids might offer a platform to study the development of CRPC and eventually lead to the development of novel therapies.

As proof that organoids can lead to novel insights into biology we find that in the absence of androgens, anti-androgen treatment still had a growth inhibitory effect, suggesting a ligand independent function of the Androgen Receptor. How the AR functions without a ligand and in which cell type this function is fulfilled remains to be determined.

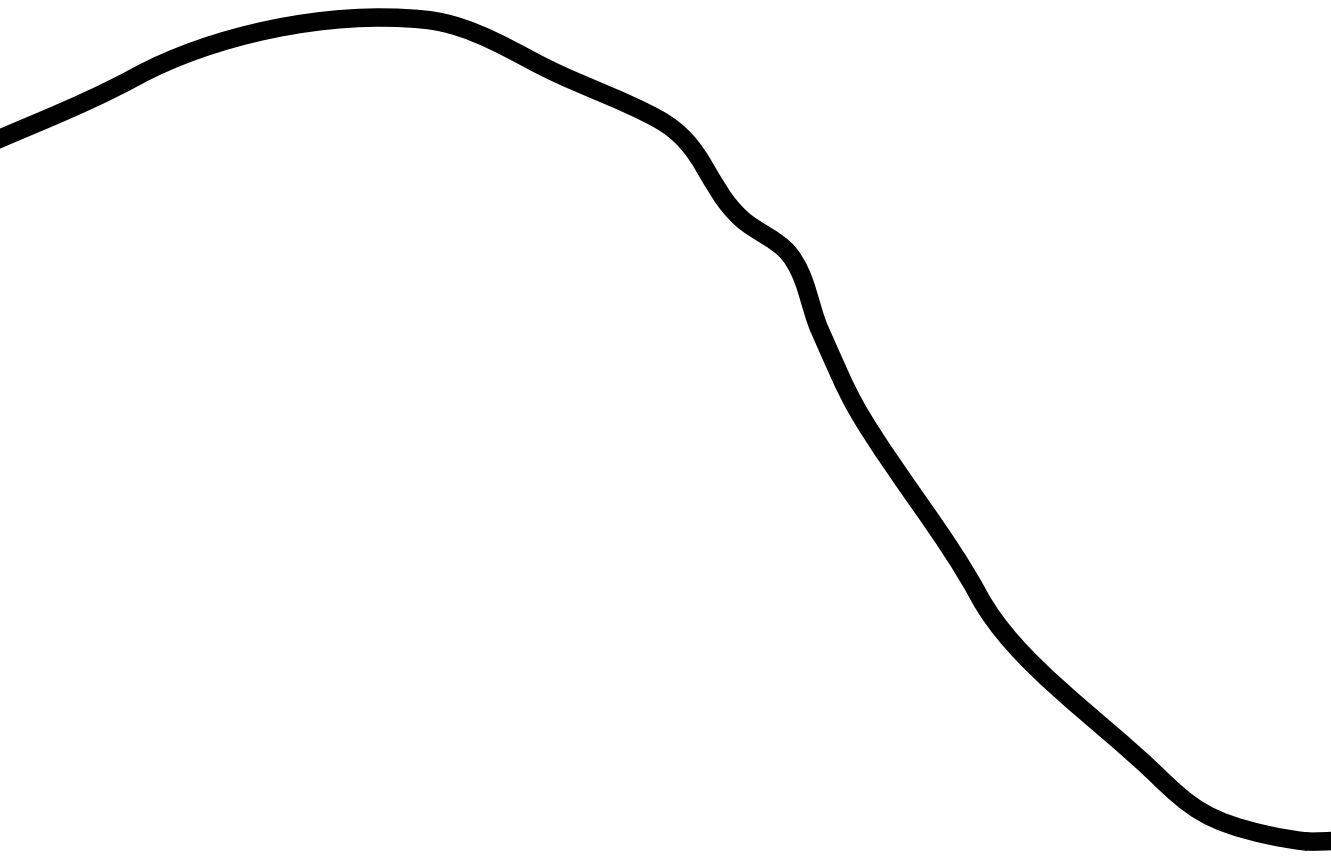
Possibly the ligand independent function of the androgen receptor is in the progenitor cells of the prostate. In chapter 6 we describe the identification of a luminal progenitor cell via the marker *Tnfrsf19*. *Tnfrsf19* expression is specific to *Lgr5*+ve intestinal stem cells but not other *Lgr5*+ve stem cell populations, therefore we postulated that *Tnfrsf19* might mark other stem cell populations. Using the *Tnfrsf19*<sup>KI</sup> mouse model, where eGFP and CreERT2 are knocked in the locus of *Tnfrsf19*, we found both luminal and basal *Tnfrsf19*+ve populations in the prostate. We show via lineage tracing that luminal *Tnfrsf19*+ve cells function as progenitor cells of the luminal lineage during homeostasis and regeneration. Interestingly when placed in organoid

culture conditions both luminal and basal Tnfrsf19+ve cells are bipotent (i.e. capable of generating both luminal and basal lineage), showing a degree of plasticity in the Tnfrsf19+ve populations. What regulates this switch from unipotency *in vivo* to bipotency *in vitro* remains undetermined. Interestingly in hyperactivation of the PI3-Kinase pathway in basal cells results in hyperplasia of cells with a luminal phenotype <sup>26-28</sup>. Possibly the processes regulating this unipotent-bipotent switch, overlap with the processes initiating PCa. The organoid system could play a vital role in unraveling these processes.

## References:

- 1 Barker, N. *et al.* Very long-term self-renewal of small intestine, colon, and hair follicles from cycling Lgr5+ve stem cells. *Cold Spring Harbor symposia on quantitative biology* **73**, 351-356, doi:10.1101/sqb.2008.72.003 (2008).
- 2 Barker, N. *et al.* Identification of stem cells in small intestine and colon by marker gene Lgr5. *Nature* **449**, 1003-1007, doi:10.1038/nature06196 (2007).
- 3 Jaks, V. *et al.* Lgr5 marks cycling, yet long-lived, hair follicle stem cells. *Nature genetics* **40**, 1291-1299, doi:10.1038/ng.239 (2008).
- 4 Barker, N. *et al.* Lgr5(+ve) stem cells drive self-renewal in the stomach and build long-lived gastric units in vitro. *Cell stem cell* **6**, 25-36, doi:10.1016/j.stem.2009.11.013 (2010).
- 5 Huch, M. *et al.* In vitro expansion of single Lgr5+ liver stem cells induced by Wnt-driven regeneration. *Nature* **494**, 247-250, doi:10.1038/nature11826 (2013).
- 6 Kobayashi, M. *et al.* Identification of a photoreceptor cell-specific nuclear receptor. *Proceedings of the National Academy of Sciences of the United States of America* **96**, 4814-4819, doi:10.1073/pnas.96.9.4814 (1999).
- 7 Schorderet, D. & Escher, P. NR2E3 mutations in enhanced S-cone sensitivity syndrome (ESCS), Goldmann-Favre syndrome (GFS), clumped pigmented retinal degeneration (CPRD), and retinitis pigmentosa (RP). *Human mutation* **30**, 1475-1485, doi:10.1002/humu.21096 (2009).
- 8 Cash, H., Whitham, C., Behrendt, C. & Hooper, L. Symbiotic bacteria direct expression of an intestinal bactericidal lectin. *Science (New York, N.Y.)* **313**, 1126-1130, doi:10.1126/science.1127119 (2006).
- 9 Mukherjee, S. *et al.* Regulation of C-type lectin antimicrobial activity by a flexible N-terminal prosegment. *The Journal of biological chemistry* **284**, 4881-4888, doi:10.1074/jbc.M808077200 (2009).
- 10 Vaishnav, S. *et al.* The antibacterial lectin RegIIIgamma promotes the spatial segregation of microbiota and host in the intestine. *Science (New York, N.Y.)* **334**, 255-258, doi:10.1126/science.1209791 (2011).
- 11 Sato, T. *et al.* Single Lgr5 stem cells build crypt-villus structures in vitro without a mesenchymal niche. *Nature* **459**, 262-265, doi:10.1038/nature07935 (2009).
- 12 Clevers, H. & Bevens, C. Paneth cells: maestros of the small intestinal crypts. *Annual review of physiology* **75**, 289-311, doi:10.1146/annurev-physiol-030212-183744 (2013).
- 13 Sato, T. *et al.* Long-term expansion of epithelial organoids from human colon, adenoma, adenocarcinoma, and Barrett's epithelium. *Gastroenterology* **141**, 1762-1772, doi:10.1053/j.gastro.2011.07.050 (2011).
- 14 Shen, M. & Abate-Shen, C. Molecular genetics of prostate cancer: new prospects for old challenges. *Genes & development* **24**, 1967-2000, doi:10.1101/gad.1965810 (2010).
- 15 Paul, C. M., Annemarie, A. D., Rajvir, D. & Gerald, R. C. Hormonal, cellular, and molecular control of prostatic development. *Developmental Biology* **253**, doi:10.1016/S0012-1606(02)00031-3 (2003).
- 16 Cunha, G. *et al.* Hormonal, cellular, and molecular regulation of normal and neoplastic prostatic development. *The Journal of steroid biochemistry and molecular biology* **92**, 221-236, doi:10.1016/j.jsbmb.2004.10.017 (2004).
- 17 Cunha, G. The role of androgens in the epithelio-mesenchymal interactions

- involved in prostatic morphogenesis in embryonic mice. *The Anatomical record* **175**, 87-96, doi:10.1002/ar.1091750108 (1973).
- 18 Huggins, C. & Hodges, C. Studies on prostatic cancer. I. The effect of castration, of estrogen and androgen injection on serum phosphatases in metastatic carcinoma of the prostate. *CA: a cancer journal for clinicians* **22**, 232-240, doi:10.3322/canjclin.22.4.232 (1972).
- 19 Denmeade, S. & Isaacs, J. A history of prostate cancer treatment. *Nature reviews. Cancer* **2**, 389-396, doi:10.1038/nrc801 (2002).
- 20 Xin, L., Lukacs, R., Lawson, D., Cheng, D. & Witte, O. Self-renewal and multilineage differentiation in vitro from murine prostate stem cells. *Stem cells (Dayton, Ohio)* **25**, 2760-2769, doi:10.1634/stemcells.2007-0355 (2007).
- 21 Garraway, I. *et al.* Human prostate sphere-forming cells represent a subset of basal epithelial cells capable of glandular regeneration in vivo. *The Prostate* **70**, 491-501, doi:10.1002/pros.21083 (2010).
- 22 Ohnuki, Y., Marnell, M., Babcock, M., Lechner, J. & Kaighn, M. Chromosomal analysis of human prostatic adenocarcinoma cell lines. *Cancer research* **40**, 524-534 (1980).
- 23 Niranjana, B. *et al.* Primary culture and propagation of human prostate epithelial cells. *Methods in molecular biology (Clifton, N.J.)* **945**, 365-382, doi:10.1007/978-1-62703-125-7\_22 (2013).
- 24 Sedelaar, J. & Isaacs, J. Tissue culture media supplemented with 10% fetal calf serum contains a castrate level of testosterone. *The Prostate* **69**, 1724-1729, doi:10.1002/pros.21028 (2009).
- 25 Singh, P., Yam, M., Russell, P. & Khatri, A. Molecular and traditional chemotherapy: a united front against prostate cancer. *Cancer letters* **293**, 1-14, doi:10.1016/j.canlet.2009.11.019 (2010).
- 26 Goldstein, A., Huang, J., Guo, C., Garraway, I. & Witte, O. Identification of a cell of origin for human prostate cancer. *Science (New York, N.Y.)* **329**, 568-571, doi:10.1126/science.1189992 (2010).
- 27 Wang, Z. *et al.* Lineage analysis of basal epithelial cells reveals their unexpected plasticity and supports a cell-of-origin model for prostate cancer heterogeneity. *Nature cell biology* **15**, 274-283, doi:10.1038/ncb2697 (2013).
- 28 Choi, N., Zhang, B., Zhang, L., Ittmann, M. & Xin, L. Adult murine prostate basal and luminal cells are self-sustained lineages that can both serve as targets for prostate cancer initiation. *Cancer cell* **21**, 253-265, doi:10.1016/j.ccr.2012.01.005 (2012).



# Addendum



## Samenvatting:

Organen zijn opgebouwd uit individuele cellen, die elk hun eigen functie vervullen binnen het weefsel. In volwassenen zijn homeostase (natuurlijk evenwicht) en regeneratie van cellen/organen afhankelijk van weefsel specifieke stamcellen. Bovendien zijn ontregelde stamcellen geïmpliceerd als beginpunt van verscheidene ziekten zoals kanker. Daarom is inzicht in het functioneren van stamcellen cruciaal.

De definitie van een stamcel is 1) pluripotentie, wat betekent dat een cel de capaciteit heeft om alle celtypen te maken, en 2) onsterfelijkheid. Van deze twee eigenschappen wordt gebruik gemaakt om stamcellen experimenteel aan te tonen. Een van deze technieken is lineage tracing. Voor lineage tracing wordt dikwijls het zogenaamde Cre-loxP systeem gebruikt. Cre is een eiwit wat DNA kan knippen op specifieke locaties, de loxP-sequentie. DNA codeert het erfelijk materiaal. Na het knippen is het DNA van de cel veranderd, dus ook de erfelijke code. Hierdoor is een cel waar Cre het DNA heeft geknipt herkenbaar ten opzichte van andere cellen, de cel heeft een soort moleculaire vlag. Door het Cre eiwit specifiek in stamcellen tot expressie te laten komen, is het mogelijk om stamcellen te voorzien van een moleculaire vlag. Als een stamcel deelt, wordt de dochtercel ook voorzien van dezelfde moleculaire vlag. Als in de loop van de tijd alle cellen en celtypes dezelfde moleculaire vlag hebben, kan men concluderen dat de eerste cel een stamcel was.

Met behulp van een muismodel waar een groen fluorescent eiwit (Green Fluorescent Protein ,GFP), een groen eiwit waarmee cellen herkenbaar zijn, en het Cre eiwit specifiek aanstaan in Lgr5 (Lgr5+ve) cellen, is eerder aangetoond door middel van lineage tracing dat Lgr5+ve cellen de stamcellen zijn van het epitheel (de functionele deklaag) van de dunne darm en dikke darm. In vervolgstudies is aangetoond dat ook de stamcellen van de haren, maag en lever Lgr5 tot expressie brengen.

Na de identificatie van de Lgr5+ve stamcellen is met behulp van moleculaire technieken bepaald welke genen specifiek tot expressie komen in deze verschillende Lgr5+ve stamcellen. Een van de genen die specifiek tot expressie komt in stamcellen van de dunne darm is *Nr2e3*. Dit gen was eerst ontdekt in het oog, waar het een essentiële rol speelt in de stamcellen het netvlies. Mutaties in het *Nr2e3* gen hebben tot gevolg dat het netvlies zich niet goed ontwikkelt wat resulteert in blindheid.



Omdat Nr2e3 specifiek tot expressie komt in twee onafhankelijke stamcel populaties stelden wij de hypothese dat Nr2e3 nieuwe stamcel populaties zou markeren in andere organen. Hiervoor hebben wij een muismodel gegenereerd waar GFP en het Cre eiwit specifiek tot expressie komt in cellen die Nr2e3 tot expressie brengen (Nr2e3+ve cellen), de resultaten worden beschreven in hoofdstuk 2. Met behulp van dit muismodel hebben we verscheidene Nr2e3+ve celpopulaties gevonden, onder andere in de dunne darm, het netvlies, maag en long. De analyse van de lineage tracing toonde aan dat geen van deze Nr2e3+ve celpopulaties stamcellen vertegenwoordigen. Echter tonen wij wel aan dat de Nr2e3+ve cellen in de maag, zogeheten neck mucus cells zijn en dat deze een levensspanne van 2-4 weken hebben.

Stamcellen worden ook beïnvloedt door extrinsieke factoren, daarom is inzicht in de niche of milieu van de stamcel ook van belang. In hoofdstuk 3 beschrijven wij een muis model, waarbij de eiwit familie van de Reg proteïnen is uitgeschakeld. Reg proteïnen hebben antibacteriële kwaliteiten, die van belang zijn om de bacteriegroei in de darm te beheersen. Toekomstige studies van dit muismodel zal de functie van deze eiwit familie in de darm en de invloed op stamcellen verder ontrafelen.

Recentelijk is er een kweekstelsel ontwikkeld voor het epitheel van de dunne darm, genaamd de organoid cultuur. In een petrischaal worden alle celtypes van het darmepitheel gemaakt door de Lgr5+ve stamcellen. Deze kweekmethode biedt een nieuw platform voor het onderzoek naar de darm en zou nieuwe inzichten kunnen geven in complexe ziekten van de darm, waar veel verschillende celtypes betrokken zijn.

In ontstekingsziekten van de darm, zoals de ziekte van Crohn en ulcerative colitis zijn naast het darmepitheel ook immuun/afweercellen betrokken, deze communiceren door middel van een grote verscheidenheid proteïnen met elkaar. In hoofdstuk 4 bestuderen wij de invloed van een proteïne uitgescheiden door immuuncellen, interferon gamma ( $\text{Ifn}\gamma$ ), op het darmepitheel. Verassend genoeg heeft  $\text{Ifn}\gamma$  sterke effecten op Paneth cellen, een gespecialiseerd celtype in het darmepitheel. Paneth cellen zijn gevuld met antibacteriële eiwitten, die onder invloed van  $\text{Ifn}\gamma$  allemaal worden uitgescheiden. Vervolgens laten wij zien dat als wij in een muis afweercellen activeren zodat deze  $\text{Ifn}\gamma$  aanmaken, de Paneth cellen ook de antibacteriële proteïnen uitscheiden, als bewijs dat organoid cultuur vertaald kan worden naar processen in een levend individu.

Gebaseerd op dit kweekstelsel van de dunne darm zijn er andere kweekstelsels ontwikkeld voor verteringsorganen zoals de lever, maag en alvleesklier. In hoofdstuk 5 beschrijven we een organoid cultuur voor het prostaatepitheel, de functionele deklaag van de prostaat. In het prostaat epitheel worden 3 celtypen onderscheiden 1) basaal epitheel, 2) lumaal epitheel en 3) zeldzame neuroendocriene cellen. Het prostaat epitheel is voor zijn functie en overleving sterk afhankelijk van het hormoon testosteron en de testosteron/androgeen receptor of AR. Prostaatkanker, wat ontstaat in het epitheel, is tevens sterk afhankelijk van testosteron voor de overleving. De behandeling van prostaatkanker is dan ook gericht op het inhiberen van testosteron signalering, door het verlagen van de testosteronspiegel in het bloed en het blokkeren van de AR functie.

Alhoewel er al kweekstelsels zijn ontwikkeld voor het prostaatepitheel, is in geen van deze testosteron aanwezig, waardoor deze niet de functionele prostaat nabootsen. Het stelsel wat wij hebben ontwikkeld bevat wel testosteron. Hierdoor ontwikkelen in onze kweekmethode prostaatorganoids zich tot volwaardige miniprostaatjes. Bovendien laat deze kweekmethode het toe om voor het eerst prostaatkanker te kweken. Ook kunnen prostaatorganoids behandeld worden met chemokuren die ook in de kliniek worden toegepast. Wanneer men in acht neemt dat in bijna 100% van alle prostaatkankerpatienten de kanker resistent wordt voor de therapie, dan zouden prostaatorganoids nieuwe inzichten kunnen geven in deze resistentie.

Als bewijs dat prostaatorganoids ook nieuwe inzichten kunnen geven in de biologie, laten wij zien dat de AR ook zonder testosteron actief kan zijn. Hoe de AR deze functie wordt vervuld en in welk celtype is nog onduidelijk.

Mogelijk wordt deze functie vervuld in de stamcellen van de prostaat. De identiteit van de stamcellen van de prostaat is echter onbekend. Er wordt gedacht dat de 2 verschillende celtypen, de basale cel en lumaal cel hun eigen stamcel hebben.

In hoofdstuk 6 beschrijven wij met behulp van een muismodel, de Tnfrsf19KI muis, een lumaal stamcel gemarkeerd door expressie van het gen Tnfrsf19, die *in vivo* (in het levende wezen) exclusief lumaal cellen maakt. Echter wanneer deze lumaal cellen in de organoid kweek worden geplaatst, kunnen deze cellen lumaal en basale cellen maken. Wanneer basale cellen in de organoid cultuur worden geplaatst, kunnen deze ook basale en lumaal cellen maken. Hoe deze wissel van unipotent

(de capaciteit om maar een celtype te maken) naar multipotentie (de capaciteit om meerdere cellen te maken) werkt is nog onduidelijk. Interessant genoeg gebeurt er ook een soortgelijk proces van luminale cel generatie, bij de initiatie van kanker. Als er in een basale cel een tumor mutatie ontstaat, resulteert dit in een overgroei van luminale cellen. Mogelijk is een overlap tussen de processen die kankerinitiatie reguleren en degene die organoidformatie reguleren. De organoidkweken zouden een belangrijke rol kunnen spelen bij het ontrafelen van de ze processen.

## Dankwoord

Alhoewel ik iedereen in het lab dankbaar ben voor zijn hulp en bijdrages wil ik graag een paar mensen in het speciaal bedanken.

Beste Hans, groen als gras, maar vol met enthousiasme voor de wetenschap ben ik begonnen als OIO in jouw lab. Na een tijd heb ik mijn draai (en leuke projecten) kunnen vinden. Naast alle mogelijkheden die ik heb gehad, heb ik in jouw lab ontzettend veel kunnen leren over wetenschap in al zijn facetten, daarnaast heb ik mij als persoon kunnen ontwikkelen. Hiervoor ben ik ontzettend dankbaar.

Stieneke bedankt voor alle hulp bij de celkweek, zonder jou hadden de cellen niet zo goed gegroeid. Johan, Carla en Maaïke ontzettend bedankt voor al het huiswerk, ik ben erg onder de indruk van al jullie kunde. Harry en Jeroen, de histo-ruimte vond ik altijd zeer prettig om te zijn en bedankt voor alle kleuringen, praatjes en drop. Nestor Wim, bedankt voor alle boeiende conversaties en meer. Lieve Ana, enigszins verbaasd was ik toen ik terug kwam uit NYC en jij opeens met mij mee ging werken. Dankjewel voor alle kweken die je hebt ingevroren, gesplit, gefixeerd en wat niet! Ik hoop dat jij er ook plezier aan hebt gehad. Beste Jarno, voor jou geldt hetzelfde, ik hoop dat de prostaatorganoids je nog veel zullen brengen. Gerald en Valentina, thanks for all the rides. Although it must have been great fun and a privilege to have me in the car all the way to Amsterdam. Femke, Joyce, Karel bedankt dat jullie mijn grapjes niet zat zijn geworden, het was voor mij een prettige uitlaatklep. Dear Henner, thank you so much for all your help, guidance and patience. I've learned a lot from you. Beste Marc, bedankt voor alle adviezen over zaken zowel binnen als buiten het lab, alle prachtige filosofische discussies en grappen. Nog een speciaal woord voor de OIO's waar ik ruime tijd mee samen op het lab heb gezeten. Hugo bedankt voor alle "kleine" gesprekken, vooral na je Clevers periode. Arnout, het was altijd lachen om met jou op te trekken. Ik heb genoten van o.a. de Clevers ski-trip en een weekendje Barcelona. Een ding weet ik zeker, jij mag nooit meer cola drinken. Jurian, na 5 jaar zijn we echt naar elkaar toegegroeid en hebben we bijna alles met elkaar gedeeld. Ik hoop dat wij elkaar nog geregeld zien in de toekomst. Paul, you're the last one, make us proud.

I also want to give a special thanks to the Sawyers lab at Memorial Sloan Kettering in New York. Dear Charles, thank you for your enthusiasm for the organoid system and having me in your lab, I really enjoyed it. Same goes for Yu. Phil, thanks for all the help with

the prostate organoids and making my stay in NYC a great experience.

Ik wil ook graag mijn oude stage begeleiders bedanken, die mijn interesse voor de wetenschap hebben aangewakkerd. Guido, bedankt voor fantastische stage in Groningen, dankzij jou heb ik de eerste stappen in de wetenschap kunnen zetten. John, thank you so much for having me in your lab at Hopkins, you are one of the most inspiring men I've ever met. I could not have done all the prostate research without everything you've thought me. Don thanks for taking me under your wing and showing me the ropes in the lab.

Naast de mensen op de werkvloer, hebben ook veel anderen een belangrijke rol gespeeld in bij het maken van dit boek. Yokozuna, bedankt voor alle mooie tijden die we hebben gehad en die nog gaan komen. Ik heb veel frustratie door/bij jullie kwijt gekund. Heren van de S.S.A.M. ik ben er altijd zeer trots op geweest op lid te zijn en me zeer welkom gevoeld, ook al ben ik als bioloog een wat vreemde eend in de bijt.

Lieve Mam, bedankt voor al je enthousiasme en liefde. Beste Pap, qua interesses valt de appel blijkbaar niet ver van de boom, bedankt voor alle steun. Eric, ik vind het erg mooi dat het allemaal samen kan gaan op deze manier en naar mijn mening speel jij hier een grote rol in, ik vind je een wereldvent. Barbara, voor jou geldt eigenlijk hetzelfde. Lieve Dirk, Sophie en Joost, de feestdagen en vakanties vind ik altijd erg gezellig, top dat jullie ook mijn familie zijn. Dan al mijn zussen, Fre, Suus, Kartien en Marleen. Ik hoop dat ik voor een keer niet jullie pesterige grote/kleine broer ben en dat jullie misschien zelfs een beetje trots op mij zijn. Stuk voor stuk zijn jullie allemaal wereldmeiden en ik hoop dat we altijd zo met elkaar om kunnen gaan.

Gijs, al 10 jaar vrienden door dik en dun en ook met het proefschrift kan ik op je rekenen. Dankjewel voor alles.

Lieve Sophie (Pi), dankjewel voor al je liefde, geduld en ondersteuning. Ik vind het altijd het leuk om jou weer te zien na een lange dag op het lab. Binnenkort zullen we samen doctor zijn en weer tijd hebben voor andere dingen.

Wouter

## **Curriculum Vitae**

Wouter Richard Karthaus is geboren op 31 mei 1985 te Nijmegen, Nederland. In 2003 behaalde hij zijn VWO diploma aan het Stedelijk Gymnasium Nijmegen, vervolgens begon hij met de studie Biologie aan de Rijksuniversiteit Groningen. In 2006 werd de bachelor succesvol afgesloten met specialisatie in de medische en moleculaire biologie. Aansluitend begon hij de Master Medische Biologie aan dezelfde universiteit die in 2008 succesvol werd afgerond. Tijdens de masterfase liep hij stage in de onderzoeksgroep van Dr. Marco Harmsen en Prof.dr. Marja van Luyn onder begeleiding van Dr. Guido Krenning, waar hij onderzoek deed naar de bijdrage van monocyten aan bloedvatregeneratie. Daaropvolgend heeft hij onderzoek gedaan naar de stamcellen van de prostaat in relatie met prostaat kanker in de onderzoeksgroep van Prof.dr. John Isaacs aan de Johns Hopkins medical school in Baltimore, USA. In september 2008 startte hij als onderzoeker in opleiding in de onderzoeksgroep van Prof.dr. Hans Clevers in het Hubrecht instituut te Utrecht. De resultaten van dit onderzoek zijn in dit proefschrift beschreven.

## List of publications:

### **Wnt signaling through inhibition of $\beta$ -catenin degradation in an intact Axin1 complex.**

Li VS, Ng SS, Boersema PJ, Low TY, **Karthaus WR**, Gerlach JP, Mohammed S, Heck AJ, Maurice MM, Mahmoudi T, Clevers H.

Cell. 2012 Jun 8;149(6):1245-56. doi: 10.1016/j.cell.2012.05.002.

PMID: 22682247

### **Controlled gene expression in primary Lgr5 organoid cultures.**

Koo BK, Stange DE, Sato T, **Karthaus W**, Farin HF, Huch M, van Es JH, Clevers H.

Nat Methods. 2011 Dec 4;9(1):81-3. doi: 10.1038/nmeth.1802.

PMID: 22138822

### **The role of CD133 in normal human prostate stem cells and malignant cancer-initiating cells.**

Vander Griend DJ, **Karthaus W**, Dalrymple S, Meeker A, DeMarzo AM, Isaacs JT.

Cancer Res. 2008 Dec 1;68(23):9703-11. doi: 10.1158/0008-5472.CAN-08-3084.

PMID: 19047148

## ***Unpublished work:***

### **Generation and characterization of Nr2e3 eGFP/CreERT2 reporter mice.**

**Wouter R. Karthaus**, Johan H. van Es, Maaïke van den Born and Hans C. Clevers.

*Submitted*

### **Secretion of antimicrobial Paneth cell products is directly controlled by immune cell-derived Interferon- $\gamma$**

Henner F. Farin<sup>1\*</sup>, **Wouter R. Karthaus**<sup>1\*</sup>, Pekka Kujala<sup>2</sup>, Maryam Rakhshandehroo<sup>3</sup>, Robert Vries<sup>1</sup>, Eric Kalkhoven<sup>3,4</sup>, Edward E. S. Nieuwenhuis<sup>5</sup> and Hans Clevers<sup>1,6</sup>

\* Contributed equally. *Submitted*

### **A novel epithelial culture system reveals ligand-independent Androgen Receptor signaling in prostate**

Wouter R. Karthaus<sup>1</sup>, Phil J. Iaquinta<sup>2\*</sup>, Ana Gracanin<sup>1</sup>, Jarno Drost<sup>1</sup>, John Whongvipat<sup>2</sup>, Vivian S.W. Li<sup>1</sup>, Norman Sachs<sup>1</sup>, Yu Chen<sup>2\*</sup>, Robert G.J. Vries, Charles L. Sawyers<sup>2,3,4\*</sup> and Hans C. Clevers<sup>1</sup>

*Manuscript in preparation*

### **Tnfrs19 marks luminal progenitor cells in the prostate**

Wouter R. Karthaus, Jarno Drost, Marc L. van de Wetering, Daniel E. Stange, Johan H. van Es, Maaïke van den Born and Hans C. Clevers.

*Manuscript in preparation*

